

The Texas Medical Center Library

DigitalCommons@TMC

---

The University of Texas MD Anderson Cancer  
Center UTHealth Graduate School of  
Biomedical Sciences Dissertations and Theses  
(Open Access)

The University of Texas MD Anderson Cancer  
Center UTHealth Graduate School of  
Biomedical Sciences


---

8-2011

## Mechanisms of Adenovirus-Mediated Autophagy

Erin White

Follow this and additional works at: [https://digitalcommons.library.tmc.edu/utgsbs\\_dissertations](https://digitalcommons.library.tmc.edu/utgsbs_dissertations)

 Part of the [Cancer Biology Commons](#), [Cell Biology Commons](#), [Molecular Biology Commons](#), and the [Virology Commons](#)

---

### Recommended Citation

White, Erin, "Mechanisms of Adenovirus-Mediated Autophagy" (2011). *The University of Texas MD Anderson Cancer Center UTHealth Graduate School of Biomedical Sciences Dissertations and Theses (Open Access)*. 183.

[https://digitalcommons.library.tmc.edu/utgsbs\\_dissertations/183](https://digitalcommons.library.tmc.edu/utgsbs_dissertations/183)

This Dissertation (PhD) is brought to you for free and open access by the The University of Texas MD Anderson Cancer Center UTHealth Graduate School of Biomedical Sciences at DigitalCommons@TMC. It has been accepted for inclusion in The University of Texas MD Anderson Cancer Center UTHealth Graduate School of Biomedical Sciences Dissertations and Theses (Open Access) by an authorized administrator of DigitalCommons@TMC. For more information, please contact [digitalcommons@library.tmc.edu](mailto:digitalcommons@library.tmc.edu).



## **Mechanisms of Adenovirus-Mediated Autophagy**

**Erin White, B.S.**

Approved:

---

Juan Fueyo-Margareto, M.D.  
Supervisory Professor

---

Andreas Bergmann, Ph.D.

---

Chinnaswamy Jagannath, Ph.D.

---

Bingliang Fang, Ph.D.

---

Candelaria Gomez-Manzano, M.D.

---

Dean, The University of Texas Health  
Science Center at Houston Graduate  
School of Biomedical Sciences

**Mechanisms of Adenovirus-Mediated Autophagy**

**A**

**DISSERTATION**

**Presented to the Faculty of**

**The University of Texas**

**Health Science Center at Houston**

**and**

**The University of Texas**

**M. D. Anderson Cancer Center**

**Graduate School of Biomedical Sciences**

**in Partial Fulfillment**

**of the Requirements**

**for the Degree of**

**DOCTOR OF PHILOSOPHY**

**by**

**Erin White, B.S.**

**Houston, Texas**

**August 2011**





## **Dedication**

**To my mother, Janet Jordan White,  
Thank you for being more than just a mother, but for being my best friend.  
You taught me everything you needed to in the short time we had together.  
I will cherish you forever.**

## **Acknowledgements**

First off, I would like to thank my mentor and co-mentor Dr. Juan Fueyo and Dr. Candelaria Gomez-Manzano. I know I had more things happen to me during my PhD program than most people have in a lifetime. You were both very supportive of me. I have learned so much from you, not just scientifically but on how to be a responsible adult and well-rounded member of society. Thank you so much for believing in me and having faith that I could pursue my dreams.

Secondly, I would like to thank Dr. Hong Jiang (Helsinki). I would have never been as successful in my Ph.D. program if I did not have you so hold my hand along the way. You were always patient with me and never got upset when I messed something up. You taught me all of the techniques I know, and not just the techniques but you always made sure I understood the theory behind them as well. I am forever indebted to you.

Thirdly, I would like to thank past and present lab mates Dr. Marta Alonso, Dr. Jing Xu, Dr. Sujana Piya, Dr. Albert Lee, Dr. Yuji Piao, Dr. Lili Dan, Dr. Sudheer Pabbisetty, Dr. Nahir Cortes Santiago, Dr. Frank Roche, Dr. Belayat Hossain, and Sarah Klein. Marta, you were always so willing to troubleshoot with me. I also enjoyed all of our conversations at our desks, you were always there when I needed someone to talk to. Jing, thank you for being perfect! You were always so tolerant while you were teaching me all the adenovirus techniques. Thanks for sharing stories about your family and then taking the time to hear about mine. You're a sweetheart. Sujana, thanks for being the western blot king.

I probably would have spent an extra 2 years doing my Ph.D. if you had not helped me fix all of my western blot problems. Nahir, thank you so much for teaching me all of my immunohistochemistry and immunofluorescence techniques. I never would have been able to graduate on time if it wasn't for you!

I would like to thank my husband, Scott, for always coming up to lab with me whenever I asked you to. You really helped the weekend work go by quickly. Thank you for supporting me through everything the past four years. I couldn't have done it without you.

## **Mechanisms of Adenovirus-Mediated Autophagy**

**Publication No.\_\_\_\_\_**

**Erin White**

**Supervisory Professor: Juan Fueyo-Margareto, M.D.**

A patient diagnosed with a glioma generally has an average of 14 months to live after implementation of conventional therapies such as surgery, chemotherapy, and radiation. Glioblastomas are highly lethal because of their aggressive nature and resistance to conventional therapies and apoptosis. Thus other avenues of cell death urgently need to be explored. Autophagy, which is also known as programmed cell death type II, has recently been identified as an alternative mechanism to kill apoptosis-resistant cancer cells. Traditionally, researchers have studied how cells undergo autophagy during viral infection as an immune response mechanism, but recently researchers have discovered how viruses have evolved to manipulate autophagy for their benefit. Extensive studies of viral-induced autophagy provide a rationale to investigate other viruses, such as the adenovirus, which may be developed as part of a therapy against cancers resistant to apoptosis. Despite the present and relatively poor understanding of the mechanisms behind adenoviral-induced autophagy, adenovirus is a promising candidate, because of its ability to efficiently eradicate tumors. A better understanding of how the adenovirus induces autophagy will allow for the development of viruses with increased oncolytic potency. We hypothesized that adenovirus induces autophagy in order to aid in lysis. We found that replication,

not infection, was required for adenovirus-mediated autophagy. Loss of function analysis of early genes revealed that, of the early genes tested, no single gene alone was sufficient to induce autophagy. Examination of cellular pathways for their role in autophagy during adenovirus infection revealed a function for the eIF2 $\alpha$  pathway and more specifically the GCN2 kinase. Cells lacking GCN2 are more resistant to adenovirus-mediated autophagy *in vitro*; *in vivo* we also found these cells fail to undergo autophagy, but display more cell death. We believe that autophagy is a protective mechanism the cell employs during adenoviral infection, and in the *in vivo* environment, cells cannot recover from virus infection and are more susceptible to death. Congruently, infected cells deficient for autophagy through deletion of ATG5 are not able to undergo productive cell lysis, providing evidence that the destruction of the cytoplasm and cell membrane through autophagy is crucial to the viral life cycle. This project is the first to describe a gene, other than a named autophagy gene, to be required for adenovirus-mediated autophagy. It is also the first to examine autophagic cell death as a means to aid in viral-induced cell lysis.

## Table of Contents

Approval Sheet.....	i
Title Page.....	ii
Dedication.....	iii
Acknowledgments.....	iv
Abstract.....	vi
List of Tables.....	xii
List of Figures.....	xvii
<b>Chapter 1: Introduction.....</b>	<b>1</b>
Tribulations of glioma therapy.....	1
Autophagy.....	2
Autophagy and the Viral Life Cycle.....	3
Adenovirus.....	4
The Delta-24-RGD voyage from bench to bedside.....	5
Potential Interactions of Adenoviral Early Genes in the Role of Autophagy.....	6
Bioenergy Sensing Pathways and Autophagy.....	7

LKB1 Regulation of AMPK.....	8
AMPK.....	8
TSC1/2.....	9
mTOR.....	10
eIF2 $\alpha$ pathway in Autophagy.....	11
PERK.....	12
GCN2.....	12
 <b>Chapter 2: Materials and Methods.....</b>	 <b>13</b>
Cell Culture.....	13
Viruses and Virus Propagation.....	14
Acidic Vesicular Organelles Analysis with Flow Cytometry.....	15
Transfection.....	15
Immunoblotting.....	16
Electron Microscopy.....	17
Crystal Violet Staining.....	18
Quantitative Real Time-PCR.....	18

Antibody Kinase Array.....	19
siRNA and shRNA Technologies.....	19
Replication Assays.....	20
Infectious Viral Particle Quantification.....	20
Quantification of Cell Lysis.....	21
Plaque Forming Assays.....	21
Animal Experiments.....	22
Immunofluorescence.....	22
Immunohistochemistry.....	23
 <b>Chapter 3: Results</b> .....	 25
Rationale and Significance.....	25
Examination of the Role Infection and Early Genes Play in Adenovirus-Mediated Autophagy.....	26
Overexpression of E1A Failed to Induce Autophagy.....	36
Examining the Role of Adenoviral Early Genes on Autophagy Induction.....	36
Intracellular ATP Levels Decreased After Adenovirus Infection.....	53
Intracellular Sensors for ATP as Effectors of Autophagy Induction.....	53



Adenovirus Activated the AKT Pathways During Late Stage Viral Infection.....	56
Downregulation of TSC2 Failed to Prevent Adenovirus-Mediated Autophagy....	57
eIF2 $\alpha$ Phosphorylation Increases After Viral Infection.....	59
Examination of PERK.....	60
Examination of GCN2.....	62
<i>In vivo</i> Analysis of GCN2.....	71
Examination of Cell Lysis After Adenovirus Infection.....	76
Autophagy Inducers and Inhibitors Regulated Viral Plaque Area.....	78
3-MA Decreased Cell Lysis.....	86
Knockdown or Downmodulation of ATG5 Impaired Cell Lysis.....	89
 <b>Chapter 4: Conclusions</b> .....	 98
 <b>Chapter 5: Discussion</b> .....	 102
 <b>References</b> .....	 110
 <b>Vita</b> .....	 130

## List of Tables

Table 1. Viruses and Virus Propagation.....	14
Table 2. Antibody List.....	17

## List of Figures

Figure 1: Proposed Interactions of Adenovirus Early Proteins and Their Potential Interaction with Proteins/Pathways Involved in Autophagy.....	6
Figure 2: Upstream Kinases That Regulated eIF2 $\alpha$ Activity.....	11
Figure 3: A replication-deficient virus fails to induce GFP-LC3 punctata.....	28
Figure 4: A replication-deficient virus does not increase lysosomal vacuoles....	29
Figure 5: Electron micrographs revealed no ultra-structural morphological changes after infection with Delta-E1.....	32
Figure 6: Only replication competent viruses induce cleavage of LC3-I and degradation of p62.....	34
Figure 7: Exogenous expression of E1A does not result in the induction of autophagy.....	35
Figure 8: Schematic representing the generation of an E1B19K mutant adenovirus.....	37
Figure 9: Mutant Virus Fails to Express E1B19K, with No Effect on E1B55K.....	38

Figure 10: Delta-E1B19K increases the volume of acidic compartments after virus infection.....	38
Figure 11: E1B19K Binds to Beclin 1 <i>in vivo</i> .....	41
Figure 12: A time course experiment revealed that PI3KCIII associates in a complex with E1B19K and Beclin 1 while BCL2 does not.....	42
Figure 13: Infection with Delta-E1B19K leads to increased cleavage of PARP...42	
Figure 14: Delta-24-RGD revealed impaired replication.....	43
Figure 15: Ultrastructure studies of MRC-5 infected with adenovirus mutants reveals the presence of autophagosomes.....	45
Figure 16: All mutant viruses, induced GFP-LC3 punctate staining.....	52
Figure 17: Infection with Ad300 decreases the levels of intracellular ATP.....	54
Figure 18: shLKB1 knockdown cells revealed no difference in acridine orange staining compared to wild-type cells. ....	55
Figure 19: AMPK $\alpha$ 1 $\alpha$ 2 null MEFs revealed no difference in acridine orange Sstaining compared to wild-type cells. ....	55
Figure 20: AMPK $\alpha$ 1 $\alpha$ 2 knockout cells underwent autophagy after virus infection.....	56
Figure 21: Activation of the AKT pathway after adenovirus infection.....	58

shTSC2 knockout cells revealed no difference in acridine orange staining compared to wild-type. ....	58
Figure 23: shTSC2 cells undergo autophagy after virus infection.....	59
Figure 24: Translation initiation factor eIF2 $\alpha$ is phosphorylated during adenovirus infection.....	60
Figure 25: ER Stress proteins are degraded during virus infection.....	61
Figure 26: GCN2 Null Mefs are resistant to virus infection.....	64
Figure 27: GCN2 knockout MEFs have increased viability after adenovirus infection.....	65
Figure 28: Loss of GCN2 renders cells resistant to adenovirus infection.....	66
Figure 29: Even at high multiplicities of infection, GCN2 KO cells are resistant to virus infection.....	67
Figure 30: GCN2 knockout MEFs have decreased levels of autophagy after infection.....	68
Figure 31: GCN2 null MEFs failed to cleave LC3 or degrade p62 after virus infection.....	68
Figure 32: Ultrastructure analysis revealed a lack of autophagosome induction after virus infection in GCN2 knockout MEFs.....	69

Figure 33: GCN2 null mice undergo large amounts of necrosis and hemorrhage after infection with extremely high viral doses.....	73
Figure 34: GCN2 wild-type and null mice both express E1A.....	74
Figure 35: Cell death in mouse livers in congruent with E1A expression.....	75
Figure 36: Autophagic analysis of livers from GCN2 wild-type and knockout mice.....	76
Figure 37: Bafilomycin inhibits autophagosomal degradation during adenovirus infection.....	79
Figure 38: Treatment with Bafilomycin A1 does not have an effect on viral replication.....	81
Figure 39: U251 Cells infected with Ad300 display increased membrane degradation over time.....	81
Figure 40: Rapamycin increase the number of plaques and the size.....	84
Figure 41: Rapamycin increases viral titer.....	85
Figure 42: 2-Deoxyglucose increases the number of plaques and the size of plaques.....	87
Figure 43: 3-Methyladenine decreased plaque number and overall plaque size.....	88

Figure 44: 3-MA inhibits AVO formation and cell lysis.....	89
Figure 45: Infection of ATG5 Knockout MEFs did not induce autophagic vacuole formation.....	92
Figure 46: Infection of ATG5 Knockout MEFs did not induce LC3 cleavage.....	93
Figure 47: Membrane degradation was decreased in Atg5 null cells compared to wild-type.....	94
Figure 48: Generation of an ATG5 downregulated cell line.....	94
Figure 49: Cells with downregulated ATG5 failed to cleave LC-3 after adenovirus infection.....	95
Figure 50: Downregulation of ATG5 led to a decrease in acidic compartment volume.....	95
Figure 51: Downregulation of ATG5 decreased cell lysis.....	96
Figure 52: Downregulation of Atg5 did not affect viral replication.....	97

## List of Abbreviations

AMPK- AMP-Activated Protein Kinase

ATG- Autophagy Gene

ATP- Adenosine Triphosphate

ATF4- Activated Transcription Factor 4

AVO- Acidic Vacuole Organelles

Becn1- Beclin 1

DE1- delta E1

DE1B19K- delta early gene 19K

DE1B55K- delta early gene 55K

DVA RNA- Delta viral associated ribonucleic acid

DNA- Deoxyribonucleic Acid

E1- early gene 2

E1A- early gene 1A

E1B19K-early gene 1B19K

E1B55K- early gene 1B55K

E2- early gene 2

E3- early gene 3

E4- early gene 4

E4-ORF-1- early gene open reading frame 1

E4-ORF-4- early gene open reading frame 4

eIF2 $\alpha$ - eukaryotic translation initiation factor 2  $\alpha$

EM- Electron Microscope

ER- Endoplasmic Reticulum

GCN2- General Control Non-Derepressible 2

HIV- Human Immunodeficiency Virus

HRI- Heme-regulated eIF2 $\alpha$  Kinase

KO- knock out

LC3- Microtubule associated protein light chain-3

MG- Malignant Glioma

MOI- multiplicity of infection

mTOR- mammalian Target of Rapamycin

PI3K-CIII- Phosphatidylinositol 3-kinase class III

PERK- PKR-like ER localized Kinase

PKR- RNA activated protein kinase

Rheb- Ras homolog enriched in brain

RNA- ribonucleic acid

TSC- tuberous sclerosis complex

TSC1- Hamartin

TSC2- Tuberin

tRNA-transfer ribonucleic acid

ULK1- Unc-51-like kinase, also known as the mammalian homolog of yeast Atg1

VA RNA- viral associated ribonucleic acid

WT- wild-type



# **Chapter One: Introduction**

## **The tribulations of glioma therapy**

While there have been many advancements in some cancers, no such exciting discoveries have been made for glioma therapy in the past 25 years (1). Glioblastomas are infamous because of their aggressive nature and resistance to conventional cytotoxic injuries, such as radiation and chemotherapy (2). Survival data on glioma patients reveals that after chemotherapy, radiation, and surgical resection, the patient only has a life expectancy of fourteen months, and most succumb to their illness within two years (1). In fact, due to the high rates of mortality, malignant gliomas are the first leading cause of cancer death in children, the third leading cause of cancer-related death among men 15-54 and the fourth for women 15-34 years of age. Gliomas are resistant to apoptosis; thus new modes of cell death must be explored.

## **Autophagy**

Autophagy is a basal process that is essential to normal function of life. Autophagy is a cellular process the cell undergoes in response to stresses, such as starvation and pathogen infection (reviewed by (3)). The cell digests proteins and organelles to provide energy for homeostatic function and catabolic processes (reviewed by (3)). The cell has internal sensors for monitoring energy and nutrient levels and, in turn, regulates protein translation and autophagy in response to any changes.

Autophagy is a crucial process in order to function properly. Defective autophagy has been demonstrated to have detrimental effects for multiple species, such as *Saccharomyces cerevisiae* (4) *Dictyostelium discoideum* (5), *Drosophila melanogaster* (6, 7), and *Caenorhabditis elegans* (8) . Two autophagy genes have been extensively studied for their role in embryogenesis, *Atg5* and *Becn1*. Mice null for an essential gene, *Atg5*, die within 12 hours of birth, if starved, versus around 21 hours for the wild-type mice (9). However, homozygous deletion of Beclin 1 causes mice to die at embryonic day 7.5 (10).

There are two main biochemical markers that scientists can use to monitor autophagy in higher eukaryotes: LC3, and p62 (11, 12). ATG5 has been shown to be an indicator of autophagy during adenovirus infection (13). ATG5 almost exclusively exists in a covalently bound complex to ATG12 (14). ATG12 is bound to ATG5 through the actions of the ubiquitin E1 and E2-like ligases, ATG7 and ATG10, respectively (14, 15). ATG5/12 then associates with ATG16 in an 800kDa complex and localizes to the phagophore (16). The localization of the complex is required for the recruitment of LC3 to the phagophore.

LC3 is the most common protein used to monitor autophagy. LC3 exists primarily in two forms: LC3-I and LC3-II. The LC3-I, and is cleaved by ATG4 to the mature form LC3-II. LC3-II is subsequently lipidated to a phosphatidylethanoamine by an E2-like enzyme Atg7 and incorporated into the phagophore (17). Scientists can monitor the cleavage of LC3-I to LC3-II through western blotting or by analyzing cellular localization of fluorescent tagged LC3 (11). p62, along with LC-3, binds poly-ubiquinated proteins and directs them to

the autophagosome to be degraded (18, 19). p62 is then subsequently degraded by the autophagolysosome.

### **Autophagy during the viral life cycle**

Autophagy during virus infection has largely been associated with viral clearance and major histocompatibility complex type II antigen presentation (20). Recently, the viral-associated autophagy field has diverged to also explore how viruses have hijacked this evolutionarily conserved process in order to aid in replication. (+) RNA viruses, which replicate in the cytoplasm, manipulate intracellular membrane structures to form replication complexes (reviewed by (21)). Dengue virus, equine arteritis virus, and mouse hepatitis virus all colocalize at sites of DNA replication with double-membrane vesicles in the cytoplasm ((22-24) reviewed by (21)). LC3 was shown to colocalize with virus-induced vesicles leading researchers to agree that these were, in fact, autophagosomes (23, 24). Mouse hepatitis virus yields fall by a factor of 1000 in the absence of ATG5 (23). On the other hand, human cytomegalovirus, HIV Type I and herpes simplex virus must thwart autophagy in order to have a productive viral life cycle (20, 25, 26). Five labs, including ours, have demonstrated that adenovirus is associated with autophagy (13, 27-31). We propose that in contrast to the RNA viruses, adenovirus is a DNA virus that replicates in the nucleus; therefore it should not utilize cytoplasmic located autophagosomes for replication scaffolds; furthermore suggesting that the adenovirus-induced autophagy serves a distinct justification and constitutes a

separate regulatory mechanism. Since autophagy is associated with adenoviral replication, we believe that autophagy is beneficial for adenovirus and must serve some purpose. Our theory suggests that adenovirus replication leads to excessive consumption of ATP and amino acids, generating a potential deficit of energy resulting in the triggering of autophagy to generate materials for adenovirus replication. Autophagy has been speculated as a mechanism to provide the cell with ATP during stressful times (32).

## **Adenovirus**

Adenovirus is a common virus that most humans develop immunity to by the time they reach adolescence. Adenovirus causes acute upper respiratory infections and conjunctivitis (33-35). There are 51 different human adenovirus serotypes (36-38). The studies here are based upon Class C Adenovirus type 5, a non-oncogenic adenovirus. Adenovirus is an encapsidated, double-stranded DNA virus (38). Adenovirus encodes 34 proteins from both strands of DNA. The genome holds three transcription groups: early transcription genes, delayed transcription genes, and late transcription (38). Replication is broken down into three stages. The first 2-4 hours of after infection is deemed the immediate-early infection. This is when E1 (E1A, E1B55K, and E1B19K) is expressed. From hours 4-12 is early infection. E2, E3, and E4 are expressed. After 12 hours is considered late infection. The transcription and translation is focused on capsid proteins.

## **The Delta-24-RGD voyage from bench to bedside**

Delta-24 has a 24-nucleotide deletion that renders it unable to bind to E1A (39). This virus cannot replicate in cells with a competent Rb pathway, which makes it cancer specific. Second generation Delta-24, Delta-24-RGD, has a RGD-4C sequence inserted in the HI loop of the fiber knob (40). Glioma cells are known to have increased amounts of RGD-binding integrins on their surface, an observation exploited by Delta-24-RGD, whose RGD domain increases its binding efficiency to gliomas. Delta-24-RGD has been a successful anticancer therapy in osteosarcoma, lung, prostate, cervical, and ovarian cancer cell lines (31, 41-44). Delta-24-RGD has recently been administered to patients in Phase I clinical trials in M. D. Anderson Cancer Center, and furthermore, it is being tested in the University of Alabama-Birmingham for ovarian cancer (45). Previous studies focused on the ability of Delta-24-RGD to kill cancer cells (13, 28, 29), and this study is unique because it will focus on mechanistic studies underlying Delta-24-RGD and wild-type adenovirus-mediated autophagy by manipulating and enhancing cell death to increase the antiglioma effect.

## **Potential Interactions of Adenoviral Early Genes in the Role of Autophagy**

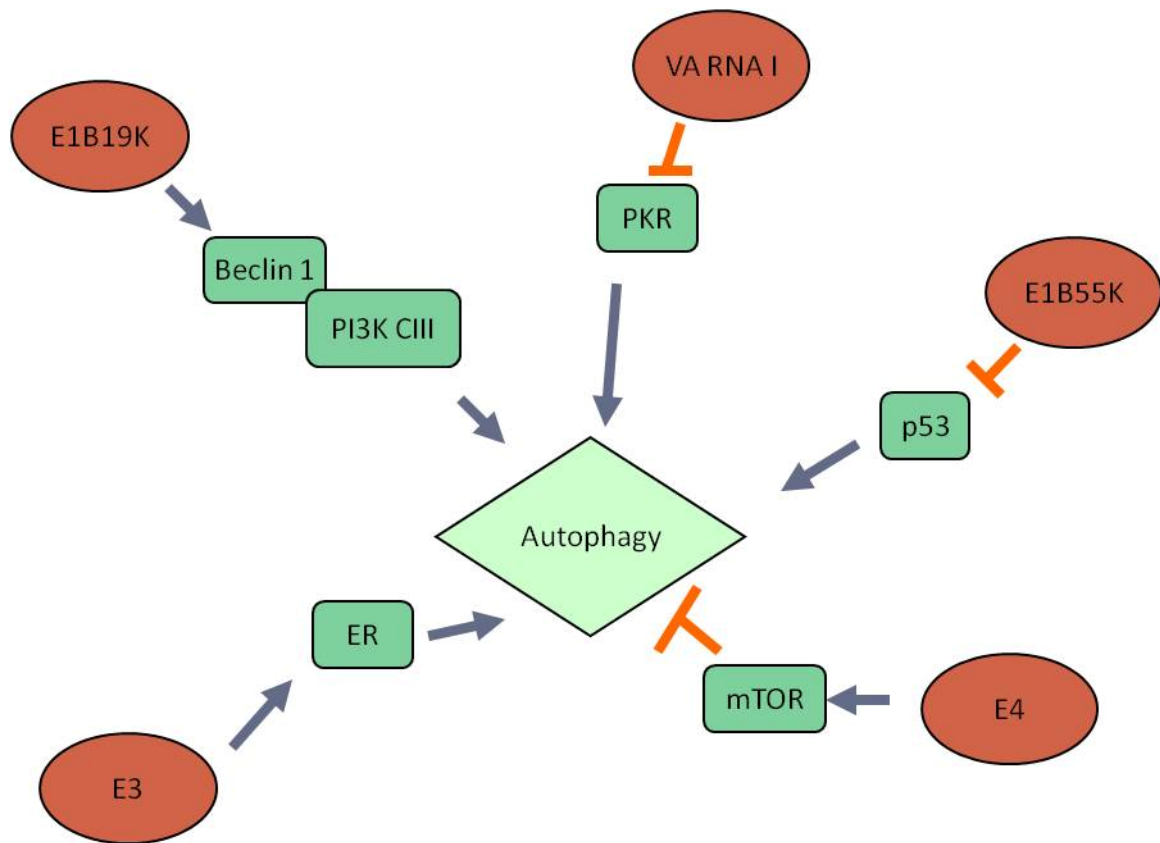


Figure 1: Proposed interactions of adenovirus early proteins and their potential interaction with proteins/pathways involved in autophagy.

Adenovirus has many potential genes that may be responsible for inducing autophagy (figure 1). Primarily, adenoviral proteins are expressed either as early genes or late genes. Early gene E1A binds to the retinoblastoma protein and is necessary for the virus to replicate (46). Loss of E1 renders the virus unable to replicate. Early gene E1B19K is a Bcl-2 homolog responsible for the inhibition of apoptosis (47). We hypothesize that E1B19K disrupts the balance of Bcl-2 binding to Beclin 1, thus favoring autophagy. Early gene E1B55K binds to p53 to inhibit apoptosis and p53 is a known upstream regulator

of DRAM (48) (49). E3 is associated with cell death (50, 51). E4 is necessary for host cell shutoff, late gene expression, and DNA replication (52). E4 is also associated with mTOR activation (53). It has been shown that E4-ORF-1 and E4-ORF-4 from adenovirus are able to mimic the growth factor signals by activating PI3-kinase, thus activation of mTOR (53). mTOR is an important regulator of cell growth. It serves as the cells' sensor for nutrient and growth factor signals (53). Adenoviral VA RNA binds to and blocks the activation PKR (54) which is also a regulator of autophagy (55). Our goal is to elucidate the mechanism in which adenovirus triggers autophagy in the host cell.

### **Bioenergy Sensing pathways and Autophagy**

“Whole-body energy metabolism” is an extremely delicate process with multiple checks and balances (Steinberg, G., et al., 2009). The body uses different cytokine signals to communicate energy needs in each tissue. On a cellular level, AMP-activated protein kinase (AMPK) has been identified as the translator of these extracellular signals (reviewed by (56)). AMPK is charged with regulating metabolism based on energy demand and supply within the cell. In times of nutrient deficiency, AMPK inhibits growth primarily by exerting inhibition over the master growth regulating kinase mTOR (57). AMPK is involved in other equally valuable functions of the cell, such as regulating polarity, cell structure, and fatty-acid production (reviewed by (58)).

### **LKB1 regulation of AMPK**

On the road to discovering the genetic principle behind the familial disease, Peutz-Jeghers syndrome, researchers in Finland found the gene *LKB1* to be inactively mutated in most patients (59). This was the first description of a cancer-susceptibility syndrome caused by inactivation of a protein kinase (59). LKB1 is classically known as the sensor of metabolic energy and maintaining homeostasis in the cell by activating AMPK (60), but it is also responsible for positively regulating 13 other proteins in the AMPK-related family of kinases also essential in regulating cellular polarity and structure (61). LKB1 distinguishes between these responsibilities by delegating AMPK $\alpha$  and SIK in regulating energy homeostasis and eliciting MARK proteins, SAD proteins, and AMPK $\alpha$ 2 to regulate cell polarity and structure. LKB1 activates the downstream kinases via direct phosphorylation in their activation loops (reviewed by (58)). LKB1 activates AMPK by phosphorylation of Threonine 172 (Thr172). AMPK propagates the signal through phosphorylation of downstream substrates (reviewed by (62)).

## **AMPK**

AMPK is a heterotrimeric protein consisting of a catalytic  $\alpha$  domain and regulatory  $\beta$  and  $\gamma$  subunits (63). AMPK binds to AMP and ATP in the cystathionine- $\beta$ -synthase domain of the  $\gamma$  domain. The  $\alpha$  and  $\gamma$  subunits are tethered together via the  $\beta$  subunit (63). Upon binding AMP, AMPK undergoes a conformational change allowing phosphorylation of Thr172 by an upstream



kinase; however, binding ATP does not produce a conformational change, subsequently inhibiting upstream kinase-mediated phosphorylation (64).

Of many responsibilities, AMPK specifically regulates autophagy, cell growth, and protein translation through inhibition of mTOR. Specifically, AMPK inhibits mTOR by phosphorylation of the upstream inhibitor of mTOR, TSC1/2. AMPK can also directly inhibit mTOR by phosphorylating raptor, a subunit of the mTORC1 complex (reviewed by Hezel (58)). A more robust description of mTOR regulation is discussed below.

## **TSC1/2**

TSC1 and TSC2 were identified as tumor suppressors in the 90s after isolating the genetic loci frequently mutated in the autosomal dominant syndrome TSC that causes multiple benign tumors (65). TSC1/2 exists in a heterodimeric complex essential to prevent ubiquitin-mediated degradation. While, TSC2 contains the enzymatic GAP activity, TSC1 is required to stabilize TSC2. The TSC1/2 complex often has mutations in the GAP domain of TSC2 or mutations in TSC1 that lead to destabilization, and both of which are regularly causes of the TSC disease (reviewed by (65)). TSC1/2 are activated by numerous pathways, including the PI3K-AKT, ERK-RSK, and LKB1-AMPK pathways. After activation through LKB1, AMPK propagates its signal through TSC1/2 via phosphorylation of TSC2 on Serine 1387 and Threonine 1271, subsequently stimulating TSC2 GAP activity (66). The complex mode of action during the phosphorylation of TSC2 is

not entirely known, however, it is known that TSC2 mediates its effects through negatively regulating the GAP activity of Rheb (reviewed by (65)). When the GAP activity of TSC2 is stimulated, it converts the GTP-bound form of Rheb to the GDP-bound form, however Akt activation is opposite. Akt phosphorylates TSC2 at a different site from AMPK phosphorylation to inhibit the GAP activity of Rheb, therefore stimulating mTOR activity.

### **mammalian Target of Rapamycin**

mTOR is a 240kDa protein that can exist in two complexes: mTORC1 and mTORC2. mTORC1 consists of mTOR, raptor, mLST8, PRAS40 while mTORC2 consists of mTOR, rictor, mLST8, and SIN1 (67, 68). mTORC2, is primarily associated with actin organization and feedback inhibition of Akt and is not relevant, with respect to AMPK regulation. mTORC1 is responsible for the regulation of protein translation in response to growth factors and nutrient availability, and autophagy as well. In order for mTORC1 to have maximal catalytic activity it must be associated with GTP-bound Rheb. Rheb is only in the GTP-bound state when TSC2 GAP activity is suppressed, such as Akt activation. When Rheb binds to mTOR, mTORC1 positively regulates the phosphorylation of two effectors, S6K (p70S6 kinase) and 4E-BP1 (eukaryotic initiation factor 4E binding protein 1), which allow protein translation under favorable conditions (67). On the other hand, mTOR is also responsible for the phosphorylation of ULK-1 and Atg13 to promote autophagy (69). Under normal growth conditions, mTOR

is activated through the PI3K/Akt pathway resulting in cell growth. However, when nutrients are withdrawn, or AMPK is stimulated, mTOR is inhibited through activation of TSC1/2 which inhibits Rheb binding to mTOR eventually halting protein synthesis and inducing autophagy.

### eIF2 $\alpha$ pathway in Autophagy

eIF2 $\alpha$  is a translation factor that is responsible for halting translation in response to cellular stresses. There are four kinases that regulate eIF2 $\alpha$  (figure 2). PERK (70), GCN2 (71, 72), HRI (73), and PKR (74)(reviewed in (75)). eIF2 $\alpha$  can selectively translate certain mRNAs based on which stressor it is responding to (reviewed in (76)). Our focuses were mainly on GCN2 and PERK as HRI is mainly a tissue specific protein, primarily erythroid-specific and PKR is inactivated by adenovirus (77, 78).

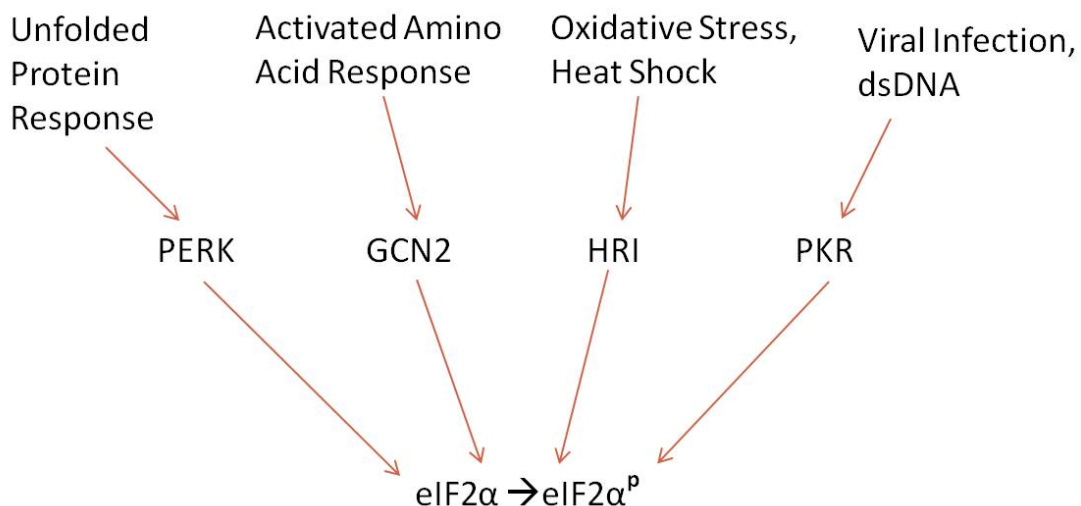


Figure 2: Upstream kinases that regulate eIF2 $\alpha$  activity.

## **PERK**

PERK is activated upon ER stress, such as the unfolded protein response (70). PERK then phosphorylates eIF2 $\alpha$  to reduce global protein synthesis (79). However, during ER stress there is preferential translation of mRNA, such as ATF4 (80-83). ATF4 is known to be upregulated by the unfolded protein response, oxidative stress and amino acid starvation (79). Continued ER stress can lead to the induction of autophagy (84, 85). Induction of autophagy is thought to help clear the unfolded protein aggregates and aid in cell survival (85).

## **GCN2**

GCN2 is an evolutionarily conserved kinase that was first identified in yeast (86). GCN2 is primarily a surveyor of intracellular amino acids and has been shown to be required for proper amino acid starvation adaptation in *in vivo* mouse models (72, 87). GCN2 has a domain that binds to uncharged tRNAs that functions as a sensor for available amino acids (88, 89). When there is an abundance of uncharged tRNAs, GCN2 is activated and phosphorylates eIF2 $\alpha$  to halt translation (88, 90). However, GCN2 can regulate protein translation in response to UV irradiation, as well (71). GCN2 has been indicated in autophagy induction during amino acid starvation via an eIF2 $\alpha$  dependent mechanism (55).

## Chapter 2: Material and Methods

### Cell culture

MRC-5 human fibroblasts, U251-MG, U87-MG, and HeLa cells were cultured in Dulbecco's modified Eagle medium/F12 medium (1:1, v/v) supplemented with 10% fetal bovine serum and 1% penicillin/streptomycin/amphotericin B (Invitrogen, Carlsbad, CA). AMPK $\alpha 1^{-/-}\alpha 2^{-/-}$  mouse embryonic fibroblasts (MEFs) (Keith Laderoute, SRI), GCN2 $^{-/-}$  and WT MEFs (Douglas Cavener, PSU), PERK $^{-/-}$  and WT MEFs (David Ron, PSU) were cultured in Dulbecco's modified Eagle medium (1:1, v/v) supplemented with 10% fetal bovine serum and 1% penicillin/streptomycin/amphotericin B. All cells were grown in a humidified atmosphere containing 5% CO<sub>2</sub> at 37°C.

## Viruses and Virus Propagation

Table 1.

Gene Mutation	Virus Name	Source	Original Source
<b>E1-Deleted</b>	AdOLE/1.8	MDACC	Adenoviral Core
<b>E3-Deleted</b>	Ad300		
<b>E1A Mutation</b>	Delta-24	Juan Fueyo	Athanassios P. Kyritsis (39)
<b>Fiber Modification</b>	Delta-24-RGD	Ramon Alemany	Ramon Alemany (42)
<b>E1B55K-Deleted</b>	dl1520/Onyx-O15	Ramon Alemany	Frank McCormick (91)
<b>E1B19K-Deleted</b>	Delta-E1B19K	Our Laboratory	Our Laboratory
<b>E4-Deleted</b>	dl366	Clodagh O'shea	Tom Shenk (92)
<b>Delta-VA RNA</b>	Ad-VAdel	Ramon Alemany	Ramon Alemany (93)

## **Acidic Vesicular Organelles Analysis with Flow Cytometry**

$2 \times 10^5$  cells were seeded in a 6 well plate. The same day cells were treated as indicated and incubated for 48-72 hours. Acridine Orange (Sigma-Aldrich, St Louis, MO) was added to the cells for a final concentration of  $1 \mu\text{g/ml}$  and incubated for 15 minutes in the cell culture incubator. The media was collected and spun at 14,000 RPM for 20 seconds the supernatant was aspirated. Remaining cells were washed once with PBS, trypsinized, collected in PBS, and spun in the same tube as before. Cells were resuspended in 200-500  $\mu\text{l}$  of PBS. Samples were analyzed on a Becton Dickson Flow Cytometer with CellQuest software.

## **Transfection**

U-87 MG cells were transiently transfected using FuGENE6 with either pCDNA3.1 empty vector or pCDNA3.1-12s E1A cDNA expressing vector (gift from Dr. Mein Chie Hung, MD Anderson Cancer Center, Houston, TX) per the vendors instructions. Cells were collected 48-96 hours after transfection and subjected to immunoblotting.

U-87 MG cells were stably transfected using FuGENE6 with an eGFP-LC3 expressing plasmid (Noburu Mizushima, Japan). The cells were selected with G418 at a concentration of  $700 \mu\text{g/ml}$ . After selection the cells were plated at a concentration of  $4 \times 10^4$  cells per well in Lab Tek II chamber slides (Cole-Parmer,

Vernon Hills, Illinois). Cells were infected as indicated and after 48 hours the media was aspirated and the cells were fixed in 4% paraformaldehyde for 30 minutes at -20°C. The cells were washed with PBS and mounted with ProLong Gold Antifade reagent with Dapi (Invitrogen, Carlsbad, CA). Images of the cells were taken and processed on a Zeiss Axiovert Zoom fluorescence microscope (Carl Zeiss, Inc., Thornwood, NY, USA) equipped with AxioCam MRM camera and 40x 1.3 oil EC Plan-NEOFLUAR objective, using Immersol ( $n = 1.518$ ) at room temperature. Acquisition software was AxioVision Release 4.7.1 (Carl Zeiss, Inc.).

### **Immunoblotting**

Cells ( $1 \times 10^6$  in a 10cm dish) were treated as indicated. Samples containing 40µg of protein were subjected to 1.5 mm 12% or 6% SDS-Tris-glycine gel electrophoresis. We also used 4-20% Novex gels (Invitrogen, Carlsbad, CA). Proteins were transferred to Whatmann nitrocellulose membranes or PVDF membranes (Bio-Rad, Hercules, CA ) using a Bio-Rad Semi-Dry transfer machine at 25V for 30 minutes or 20V for 1 hour for larger proteins. Membranes were blocked in 10% Non-fat dry milk solubilized in 1x TBS-0.05% Tween-20. Membranes were incubated overnight in 2% Nonfat dry milk in 1x TBS-0.05% Tween-20 with antibody. Membranes were washed three times (15min, 5 min, 5 min) with 1x TBS-0.05% Tween-20. Antibody complexes were detected using chemiluminescence reagent (GE Amersham, Piscataway, NJ ) in accordance with the manufacturer's instructions.



Table 2.

<b>Antibody</b>	<b>Dilution</b>	<b>Company</b>
<b>Atg5</b>	1:2000	Cosmo Bio, Japan
<b>LC3</b>	1:1000	Cell Signaling, Danvers, MA
<b>p62 (WB)</b>	1:200	Santa Cruz Biotechnology, Santa Cruz, CA
<b>eIF2<math>\alpha</math></b>	1:1000	Cell Signaling, Danvers, MA
<b>Phospho-eIF2<math>\alpha</math></b>	1:1000	Cell Signaling, Danvers, MA
<b>Actin</b>	1:4000	Santa Cruz Biotechnology, Santa Cruz, CA
<b>GCN2</b>	1:1000	Cell Signaling, Danvers, MA
<b>Phospho-GCN2</b>	1:1000	Cell Signaling, Danvers, MA
<b>E1A</b>	1:200	Santa Cruz Biotechnology, Santa Cruz, CA
<b>P62 (IF)</b>	1:600	Sigma Aldrich, St. Louis, MO

### **Electron Microscopy**

Cells were seeded in a ten centimeter dish ( $1-2 \times 10^6$ ) and infected at 100 MOI. If indicated, cells were treated with Bafilomycin A1, a vacuolar ATPase inhibitor, (Sigma Aldrich, St. Louis, MO) at a concentration of 10nM. Cells were collected and pelleted at 300 x g were rinsed with PBS and fixed in a solution containing 3% glutaraldehyde plus 2% paraformaldehyde 1% Millipore-filtered uranyl acetate. Samples were dehydrated in increasing concentrations of ethanol, infiltrated, and embedded in LX-112 medium. Samples were polymerized in a 70°C oven for two days. Ultra thin sections were cut in a Leica

Ultracut microtome (Leica, Deerfield, IL), stained with uranyl acetate and lead citrate in a Leica EM Stainer, and examined in a JEM 1010 transmission electron microscope (JOEL, USA, Inc., Peabody, MA) at an accelerating voltage of 80kV. Digital images were obtained using AMT Imaging System (Advanced Microscopy Techniques Corp, Danvers, MA).

### **Crystal Violet Staining**

$8.0 \times 10^4$  cells were seeded in a 24 well plate and infected with adenovirus as indicated. 96 hours later the media was aspirated, cells were washed with PBS, and stained with 0.05% Crystal Violet (Sigma, St Louis, MA) in 20% methanol for 10 minutes. Cells were washed and crystal violet was solubilized with 1% SDS and read at a wavelength of 570nm.

### **Quantitative Real Time-PCR**

Cells ( $1 \times 10^6$  per well in 10cm plates) were infected with wild type adenovirus type 5, with a MOI of 100. Twenty hours after infection, cells were collected and mRNA was extracted using the RNeasy kit (Qiagen, Valencia, CA). Samples were subjected to the turbo DNA free kit to remove all traces of DNA (Ambion, Austin, TX) and sent to for the autophagy PCR array (SA Biosciences, Frederick, MD).

## **Antibody Kinase Array**

MRC5 cells were either mock infected or infected at a MOI of 100 and collected at 16, 32, or 48 hours post infection. Lysates were subjected to the human phospho-kinase array kit that was purchased from R&D Systems (Minneapolis, MN) and used according to the manufactures instructions.

## **siRNA and shRNA technologies**

The pLKO.1 vector was a generous gift from Robert Weinberg, Whitehead Institute, Boston, MA.  $7 \times 10^5$  HEK-293T cells were plated in 5ml of a 6cm culture dish. 24 hours later pLKO.1, psPAX2, and pMD2.G were cotransfected with FuGENE6 (Roche Diagnostics, Indianapolis, IN) for 15 hours. 48 hours later the media was collected and stored a 4°C and fresh media was added to the remaining cells. 24 hours later the media was collected again and combined with the previous media collected. The media was spun at 1,250 rpm for 5 minutes to pellet cell debris. The media-containing virus was stored at -80°C. The supernatant was used to infect  $0.5 \times 10^6$  U251-MG cells. 8µg/ml of polybrene was added to the cells and 1ml of supernatant was added to the cells. 24 hours after infection 1µg/ml of puromycin was added for selection of infected cells.

To knockdown *ATG5*, we purchased a shRNA-expressing plasmid from Origene (Rockville, MD, USA). We transfected the plasmids into the U87 cells with FuGENE 6. The cells were screened, and stable cell clones were maintained in culture medium plus 0.5 µg/ml puromycin.

## **Replication assays**

Cells were seeded at  $4 \times 10^4$  in a 12 well plate and infected at 100 MOI for 24 hours. The supernatant or cell extract was boiled at 95°C for 10 minutes and used as the DNA template. Platinum SybR Green (Invitrogen, Carlsbad, CA) was used as per manufactures instructions. PCR was performed on a Bio-Rad iCycler with parameters: Cycle 1-95°C 5 mins, Cycle 2-30- 95°C 30s, 60°C 20s, and 70°C 20s. Cycle thresholds were compared to known quantities of the adenoviral genome in order to derive the genome copy number.

## **Infectious Viral Particles**

Viral titer was assessed using the Adeno-X-Rapid Titer kit (BD Biosciences, Palo Alto, CA). Cells were subjected to three freeze thaw cycles to release the virus. The diluted virus was seeded over  $1 \times 10^5$  293 cells in 24 well plates. The cells were fixed with methanol at -20°C for two minutes 48 hours later after infection. Cells were incubated at 37°C for two hours with goat anti-hexon in PBS containing 1% bovine serum albumin. Cells were washed 3 times with PBS+1% bovine serum albumin. Cells were incubated with goat conjugated HRP antibody (Vector Laboratories, Burlingame, CA) for two hours. Cells were washed 3 times with PBS+ 1% BSA. HRP substrate was added per manufactures instructions (Vector Laboratories, Burlingame, CA). Samples were developed using DAB tablets (Sigma-Aldrich, St. Louis, MO). Positive cells were be visualized on a compound light microscope. Mathematical equations are used

to derive the titer were calculated using the equation from the Adeno-X-Rapid Titer kit (BD Biosciences, Palo Alto, CA). Briefly we calculated the number of fields in the objective, multiplied by the number of hexon positive cells, divided by the dilution factor, and multiplied by the volume of virus.

### **Quantification of cell lysis**

The cells were stained with 8  $\mu$ M ethidium homodimer 1 (Molecular Probes, Inc., Eugene, OR) in phosphate-buffered saline solution (PBS) for 15 minutes at room temperature. Stained cells were then analyzed by flow cytometry using a FACScan cytometer and CellQuest software (Becton Dickinson). Red (FL2-H channel) fluorescence emissions from  $10^4$  cells were analyzed.

### **Plaque Forming Assays**

Cells were plated overnight at varying densities in a 6-well plate. The next day the cells were infected at the indicated PFU for 1 hour. The media was removed and the cells were washed. 10% SeaPaque agarose was mixed and melting with ddH<sub>2</sub>O. The agarose was diluted with culture media. Once the agarose had cooled to around 40°C it was added to the cells. After the agarose cooled 1 ml of culture media was added to the cells. Between days 5 and 7 the cells were stained with MTT and the diameter and quantity of the plaques was determined using the UN-SCAN-IT gel version 6.1 software (Silk Scientists, Orem, UT).

## **Animal Experiments**

All animals were purchased through Jackson Laboratory and housed in the MD Anderson BSRB Animal Facility. The GCN2 knockout mice (B6.129S6-Eif2ak4tm1.2Dron/J), originally generated by Dr. David Ron and were back crossed with C57BL/6J mice. C57BL/6J mice served as the wild-type strain. The animals were injected with Ad300, measured in virus particles/mouse, via tail vein injection. Their weight was measured pre-injection and post-mortem. The mice were monitored every day for moribundity. If the mice appeared moribund then they were sacrificed and all of their organs were preserved. The tissues were processed and embedded through the MD Anderson Department of Veterinary Medicine.

## **Immunofluorescence**

The organs were deparaffinized by baking the slides for 1 hour at 65°C. They were subsequently incubated in 3 washes of Xylene, 2 washes of 100% Ethanol, 2 washes in 95% Ethanol, and 1 wash in 70% Ethanol for 3 minutes each. Then they were washed 3 times in PBS+ 0.05% Tween-20, and diH<sub>2</sub>O all for 5 minutes each. The slides were then heated in prewarmed 10mM Sodium Citrate pH 6.0 for 30 minutes in a steamer. The slides were allowed to cool for 20 minutes on the bench top. Slides were then washed three times in PBS+ 0.05% Tween-20 for 5 minutes. The sections were marked using a hydrophobic pen and incubated overnight with the antibody and an IgG control with the same

amount of IgG from the 1° antibodies species. The next day the slides were washed 3 times with PBS+ 0.05% Tween-20 and incubated with the 2° antibody at a 1:400 dilution and incubated for 1 hour. The slides were washed 3 times with PBS+ 0.05% Tween 20 for 5 minutes each. The slides were counterstained with VECTASHIELD mounting medium with Dapi (Vector Laboratories, Burlingame, CA). Images of the tissues were taken and processed on a Zeiss Axiovert Zoom fluorescence microscope (Carl Zeiss, Inc., Thornwood, NY, USA) equipped with AxioCam MRM camera and 40x 1.3 oil EC Plan-NEOFLUAR objective, using Immersol ( $n = 1.518$ ) at room temperature. Acquisition software was AxioVision Release 4.7.1 (Carl Zeiss, Inc.).

### **Immunohistochemistry**

The organs were deparaffinized by baking the slides for 1 hour at 65°C. They were subsequently incubated in 3 washes of Xylene, 2 washes of 100% Ethanol, 2 washes in 95% Ethanol, and 1 wash in 70% Ethanol for 3 minutes each. Then they were washed 3 times in PBS+ 0.05% Tween-20, and diH<sub>2</sub>O all for 5 minutes each. The slides were then heated in prewarmed 100mM Sodium Citrate pH 6.0 for 30 minutes in a steamer. The slides were allowed to cool for 30 minutes on the bench top. Slides were then washed three times in PBS+ 0.05% Tween-20. The sections were marked using a hydrophobic pen and incubated overnight with the antibody and an IgG control with the same amount of IgG from the 1° antibodies species. The next day the slides were washed 3

times with PBS+ 0.05% Tween-20 and incubated with the 2° antibody at a 1:400 dilution and incubated for 1 hour. 30 minutes before use the ABC reagent was prepared (Vector Laboratories). The slides were washed 3 times with PBS+ 0.05% Tween 20. The slides were incubated with the ABC reagent for one hour. Slides were washed 3 times with PBS+ 0.05% Tween-20. DAB+ H<sub>2</sub>O<sub>2</sub> (Sigma Aldrich, St. Louis, MO) tablets were dissolved in tap water and added to the sections. Once the slides were developed, they were washed 3 times in 3 with PBS+ 0.05% Tween-20. Slides were dipped in Hematoxylin for 30 seconds and rinsed in water for five minutes. Slides were incubated in 95% Ethanol, Xylene 3 times each for 3 minutes and mounted with Permount (Sigma Aldrich, St Louis, MO). Pictures were obtained through an Olympus BX41 with Olympus DP71 camera.



## **Chapter 3: Results**

### **Significance and Rationale**

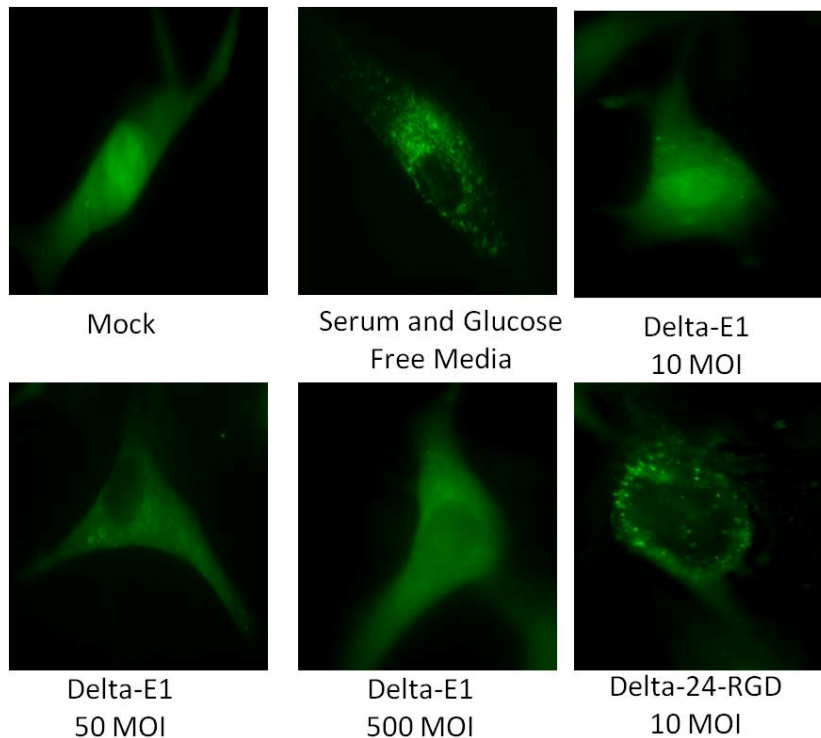
Autophagy was discovered approximately forty years ago as a cellular response to starvation. It has only recently been examined enough to join the ranks of apoptosis as an established form of programmed cell death. In the past decade, many labs have focused on the relationship between viruses and autophagy. Autophagy investigation has become increasingly popular in laboratories studying pathogen infection and immunity (reviewed by (94)), but scientists have also examined how viruses manipulate the autophagy pathway to their advantage (reviewed by (95)). Our collaborator was the first to report that conditionally replicating adenoviruses induce autophagy (29), and, unfortunately, no group until ours has pursued any mechanistic studies. Therefore, it is imperative for the advancement of the area of adenovirus and autophagy that this is explored more in depth because understanding how adenovirus mediates autophagy is crucial translationally as a potential anticancer therapy, because of the many cancers that are highly resistant to conventional pro-apoptotic therapies.

### **3.0 Examination of the Role Infection and Early Genes Play in Adenovirus Mediated Autophagy**

The role of replication during autophagy was carried out through experiments with adenovirus deleted of the E1 gene, rendering it incapable of replication. U87.GFP-LC3 cells were generated by Dr. Hong Jiang at the University of Texas MD Anderson Cancer Center (MDACC). The GFP-LC3 plasmid was originally constructed by Dr. Noboru Mizushima (96). U87.GFP-LC3 cells have a low basal level of autophagy, thus providing an optimum cell line for autophagic studies. Autophagy is identified by punctate GFP staining of the cells versus diffuse cytoplasmic staining in the absence of autophagy. The technique follows the movement of LC3-I to LC3-II incorporation into the autophagosome. U87.GFP-LC3 cells were infected with the AdOLE/1.8 virus (Delta-E1) purchased from the Keck Memorial Adenovirus Core at MDACC (figure 3). At increasing MOI, there was no increase in the GFP-LC3 punctate formation. Uninfected cells were used as a negative control and serum and glucose starved cells were the assay's positive controls. Delta-24-RGD infected cells served as a control for comparison between viruses. There was a 2.5 fold increase in GFP-LC3 punctuation in Delta-24-RGD infected cells over Delta-E1 infected cells. These results provide evidence that infection does not play a role in adenovirus-mediated autophagy.

A second technique to confirm the role of infection on autophagy induction was to assay autophagy is through the accumulation of an acidotropic dye within the autophagosome. Acridine orange emits red fluorescence when localized in

an acidic compartment and fluoresces green when bound to DNA. After infection with Delta-E1, there was no significant increase in the acidic apartments of the cell (figure 4). Mock infection and serum and glucose starvation were used as assay positive controls. Ad300 infection served as an infection control. There was almost a 14-fold increase in acidic vacuoles in Ad300 infected cells over Delta-E1 infected cells. Looking at the scattered population of cells, one sees that under glucose and serum free media starvation the population of cells increase in intracellular complexity. This can be contributed to the vacuolar structures now present in the cytoplasm. Now examining wild-type infected cells the population increases in intracellular complexity but also in DNA content due to virus replication. Acridine orange when bound to DNA fluoresces green and this is monitored through FL1-H. During infection with a Delta-E1 virus there was no population shift in either direction, suggestion no increase in vacuoles or viral replication. Infection does not increase acidic compartments in the cell.



Treatment	Cells With GFP-LC3 Punctata (%)
Mock	9.8±3.6
Serum and Glucose Free Media	23.7±2.9
Delta-E1 10 MOI	8.5±3.0
Delta-E1 50 MOI	10.1±2.2
Delta-E1 500 MOI	9.0±1.2
Delta-24-RGD 10 MOI	26.4±4.0

Figure 3: A Replication-Deficient Virus Failed to Induce GFP-LC3 Punctata. A) U87-MG were stably transfected with a GFP-LC3 construct. Cells were visualized by fluorescence microscopy and cells with more than 5 GFP-LC3 punctata were considered positive for autophagy. Cells were incubated in complete media for 48 hours and infected with dl309 (an E1-deleted virus) at the multiplicity of infection (MOI) indicated. Incubation in

serum and glucose media served as a positive control. B) GFP-LC3 positive cells were quantified. Around 200 cells were counted per well and three wells were counted.

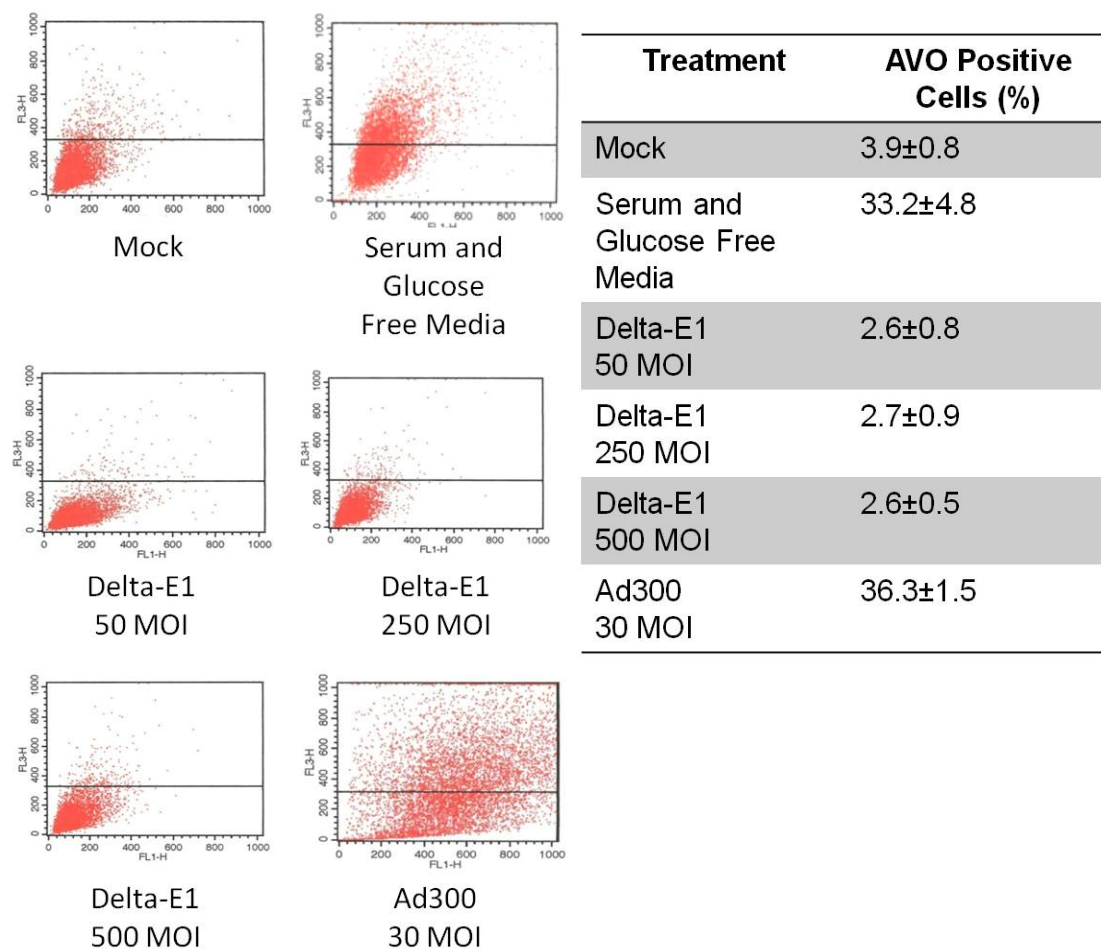
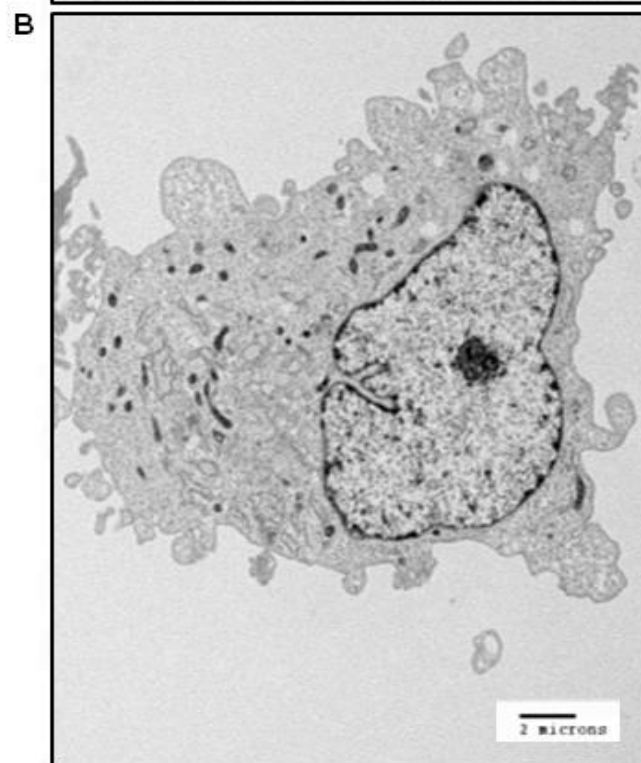
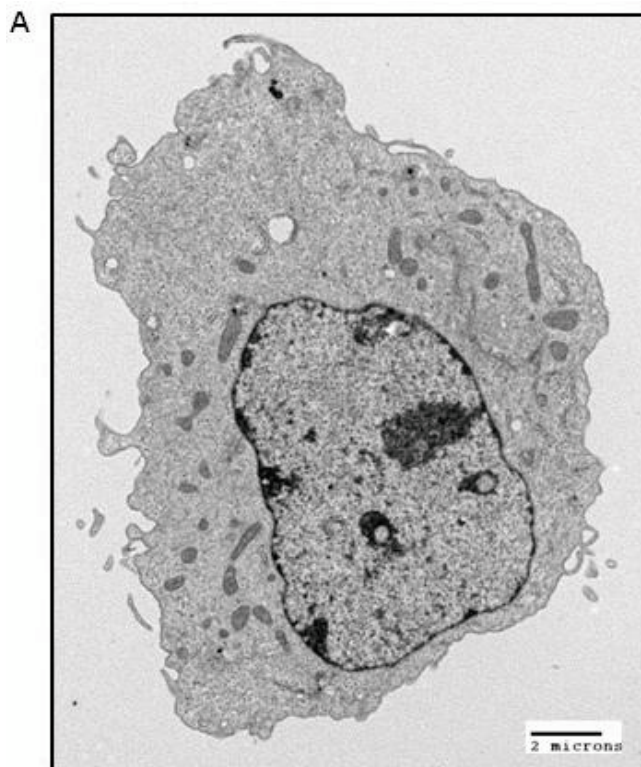


Figure 4: A Replication-Deficient Virus Did Not Increase Lysosomal Vacuoles. A) Cells were treated as indicated. 48 hours after infected cells were incubated for 15 minutes with Acridine Orange (1µg/ml). Cells were trypsinized and collected in PBS and analyzed by a Becton Dickson flow Cytometer. B) Quantification of acridine orange flow cytometry.

Ultrastructure morphology analysis is the gold standard for autophagy identification, therefore to confirm the previous experiments we infected MRC-5 fibroblasts with Delta-E1 or wild-type adenovirus and compared the morphology

to the uninfected control (figure 5). Cells that were uninfected displayed a continuous cytoplasm sprinkled with mitochondria. The morphology for a cell infected with Delta-E1 looked remarkably similar. There was no disruption in the cytoplasm. However, cells infected with wild-type adenovirus displayed a strikingly different morphology. The cytoplasm was littered with vacuoles that appeared empty but upon amplification there are remnants of digested material inside of the vacuoles. In the enlarged inset there are multi-lamellar structures inside of a vacuole to be digested. The nucleus has multiple virions present. Since there was no change in morphology we can interpret that infection does not play a role in autophagy induction.

For biochemical confirmation, we analyzed the proteins p62 and LC3 for changes indicative to autophagy induction. p62 is a long-lived protein that is preferentially digested by autophagy (18). Western blot analysis of the quantity of p62 within the cell is an indicator of autophagy. In accordance with our hypothesis, after infection with Delta-E1 there was no degradation of p62, and there was a decrease after infection with Delta-24-RGD (figure 6). A second biochemical marker of autophagy is the cleavage and subsequent lipidation of MAP-LC3b (LC3). Under basal conditions LC3 is primarily found in the uncleaved state, LC3-I. Monitoring this cleavage from LC3-I to LC3-II is indicative of autophagy. Mock and Delta-E1 cells had a similar ratio of LC3-II/LC3-I. However, upon infection with Delta-24-RGD all of the LC3-I was converted to LC3-II. Therefore, with all of these results we can conclude that infection is not sufficient to induce autophagy.



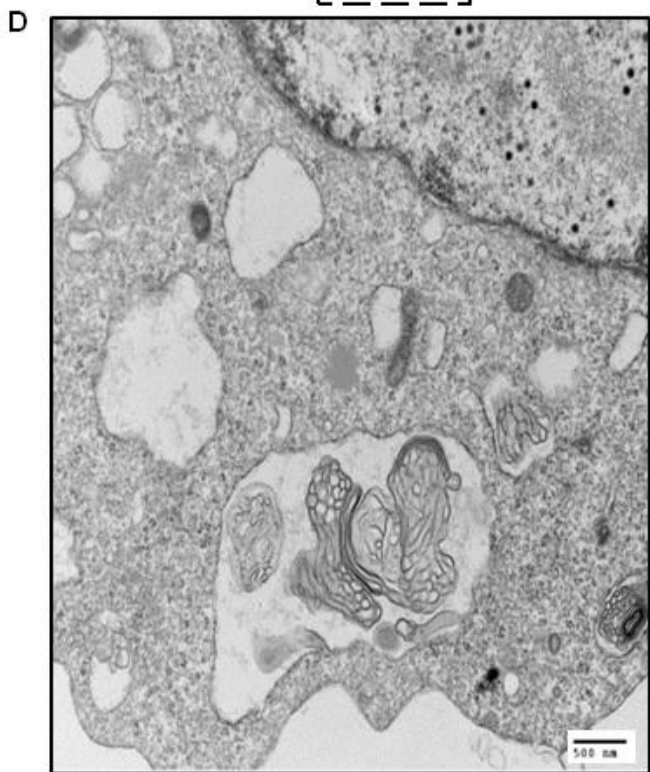
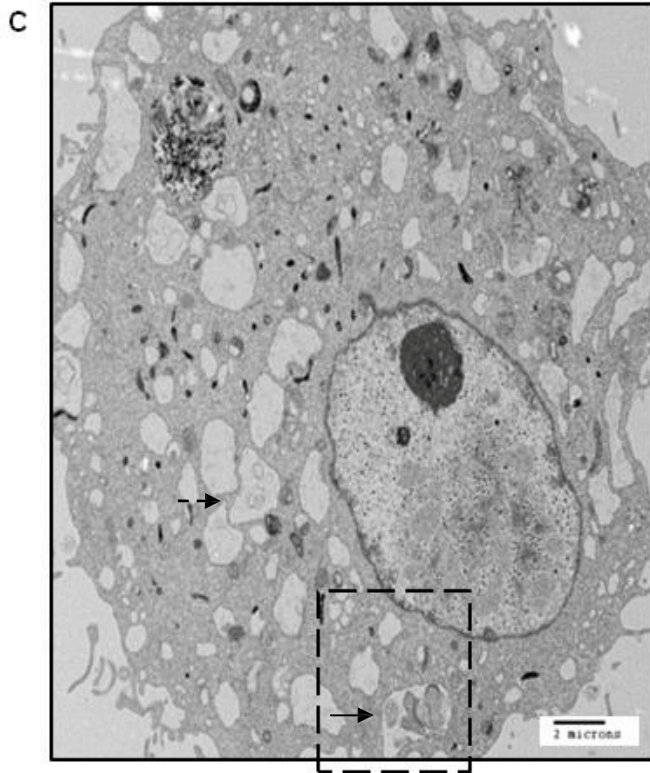




Figure 5: Electron Micrographs Revealed No Ultrastructural Morphological Changes After Infection with Delta-E1. MRC-5 fetal lung fibroblasts were treated for 72 hours and then fixed and processed for electron microscopy. A) Mock Infected Cells, 6000x magnification. B) Delta-E1 infected at 100 MOI, 6000x magnification. C) Ad300 infected at 100 MOI, 6000x magnification. D) Ad300 infected at 100 MOI, 25000x magnification. Dotted arrow: late stage autolysosome. Solid arrow: autophagosome

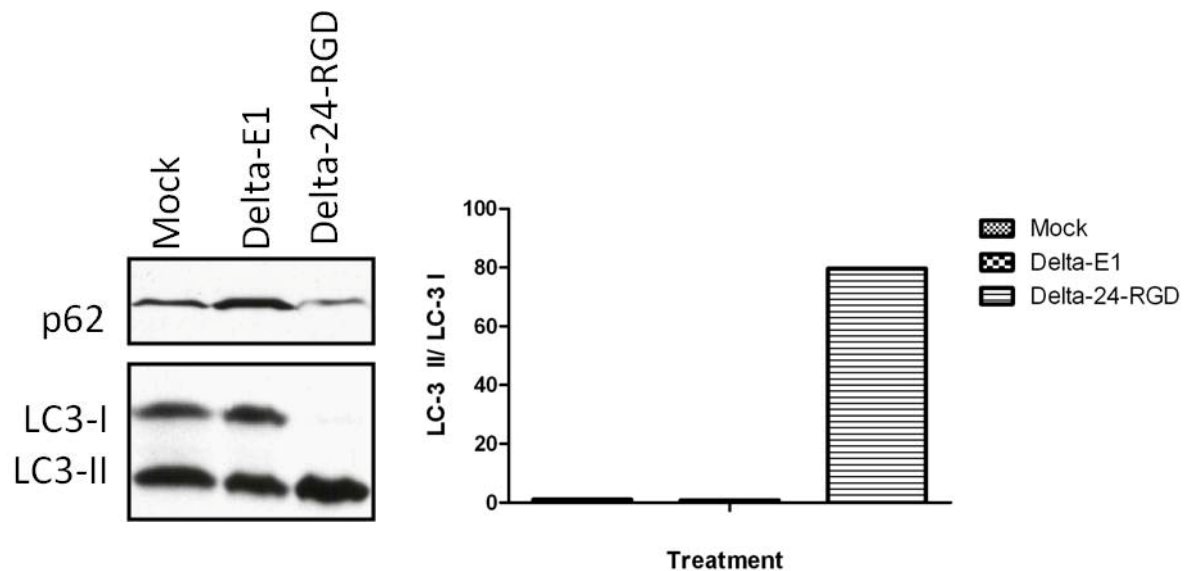


Figure 6: Only Replication Competent Viruses Induced Cleavage of LC3-I and Degradation of p62. MRC-5 fibroblasts were infected at 100 MOI for 72 hours. Cell were collected and subjected to western blotting. A) p62 levels decreased after infection with a replication competent virus (Delta-24-RGD) and fail to decrease with the replication deficient virus. LC3 was cleaved after infection with Delta-24-RGD and not after infected with Delta-E1. B) Densitometry of LC3-I

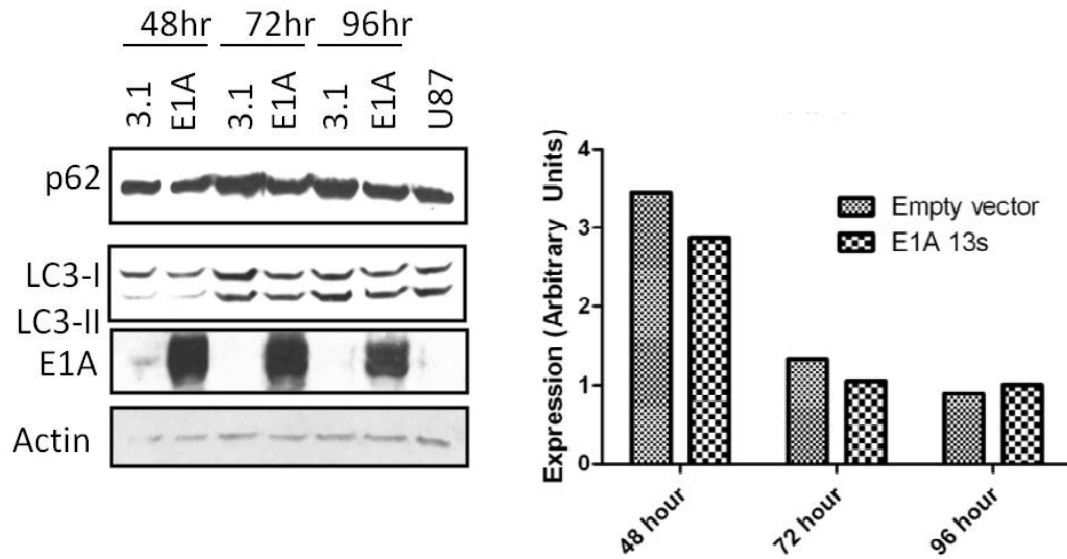


Figure 7: Exogenous Expression of E1A Did Not Result in the Induction of Autophagy. A) U87-MG cells were transfected with pCDNA3.1+ or pCDNA3.1-E1A 12S vectors for 48, 72, or 96 hours and analyzed for autophagy. B) Densitometry of the cleavage of LC3-I to LC3-II.

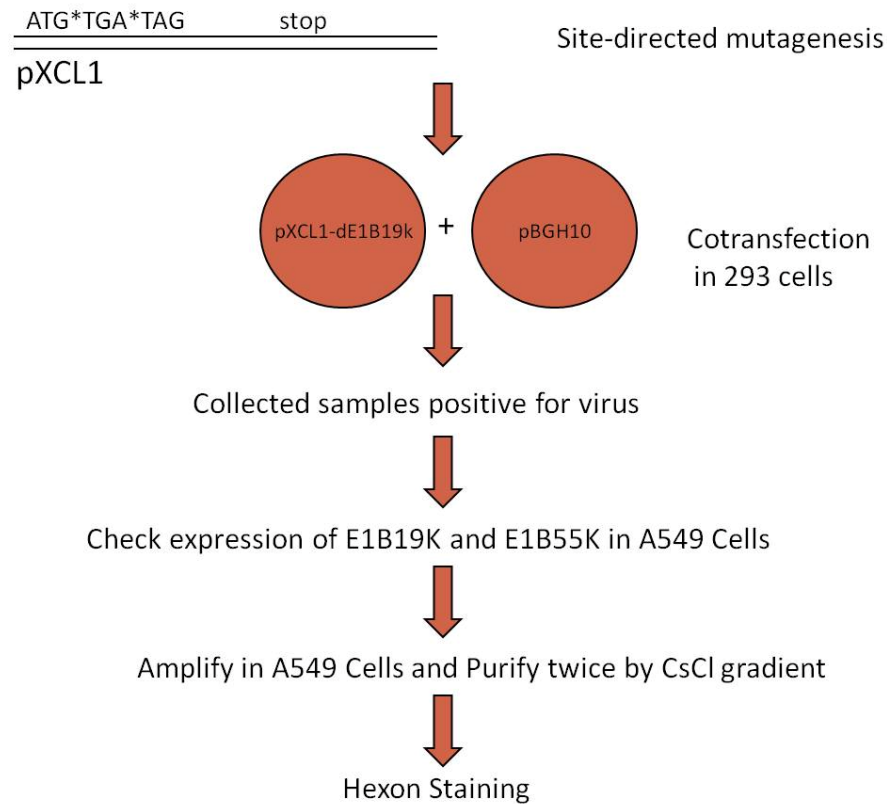
### **3.1 Overexpression of E1A Fails to Induce Autophagy**

We next asked whether E1A, the gene responsible for the replication deficiency in the Delta-E1 virus, was sufficient to induce autophagy when expressed alone. Using a pCDNA3.1-12s E1A expression vector, U87 cells were transiently transfected and subsequently analyzed for autophagy via western blotting (figure 7). Comparing each time point to its own empty vector control there was no difference in the level of p62 despite strong E1A expression. Examination of LC3 in these same samples revealed no difference in the ratio of LC3-II/LC3-I. We can conclude that E1A is required for adenovirus-mediated autophagy, but not sufficient.

### **3.2 Examining the Role of Adenoviral Early Genes on Autophagy Induction**

In order to isolate the function adenoviral early genes play in autophagy induction, we utilized viruses deleted for each early gene separately. We were able to obtain knockout viruses for E1, E3, E1B55K, E4, and VARNA I&II. We constructed the E1B19K deleted virus through the generation of stop codons in the open reading frame using site-directed mutagenesis (figure 8, top). The mutated sequence was confirmed through sequencing (figure 8, bottom). Secondly, we analyzed the virus for expression of E1B19K and E1B55K (figure 9). We chose to amplify the mutant virus that had similar levels of E1B55K expression compared to wild type, while lacking expression of E1B19K. Our first goal was to examine the capability of Delta-E1B19K to induce autophagy. Our

first comparative studies with Delta-E1B19K, were acridine orange staining after infection with Ad300 or Delta-E1B19K. We showed that there were similar levels of AVO positive cells in a dose dependent manner (figure 10). These results indicate that E1B19K plays a partial role in adenovirus-mediated autophagy.



**B**

		(83)	83	90	100	110	120	130	140	150	164	Section 2
E1B19K	(1)	-----	-----	-----	-----	CGCCGTGGGCTAATCTTGGTTACATCTGACCTCATGGAGGCTTGGGAGTGT	TTG					
E1B4.EKU2_D02_010	(83)	TGGGGCGGGGCTTAAAGGGTATATAATG	CGCCGTGGGCTAATCTTGGTTACATCTGACCTCATGGAGGCTTGATAGTGT	TTG								
Consensus	(83)					CGCCGTGGGCTAATCTTGGTTACATCTGACCTCATGGAGGCTTG	AGTGT	TTG				

Figure 8: Schematic Representing the Generation of an E1B19K Mutant Adenovirus.

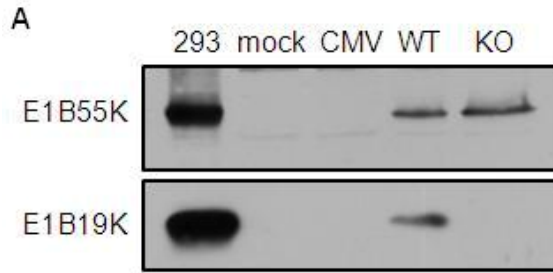


Figure 9: Mutant Virus Failed to Express E1B19K, with No Effect on E1B55K. A) 293 serves as a positive control for E1B55K and E1B19K. U251-MG cells were mock infected, AdCMV (Delta-E1) infected, Ad300 (WT) infected, and E1B19K KO infected.

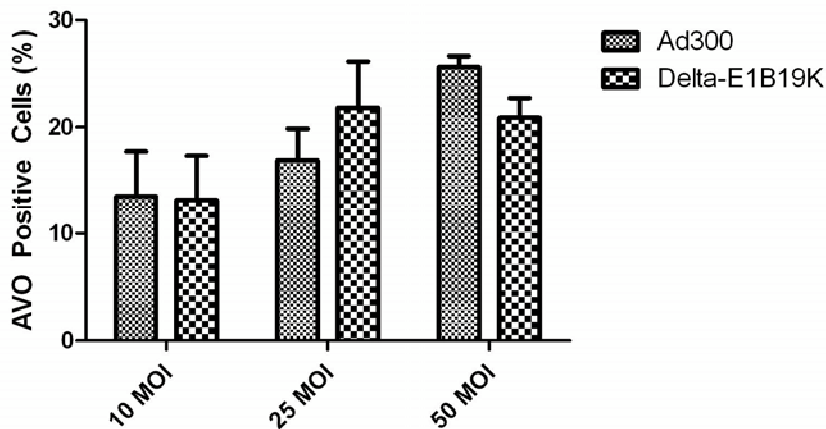


Figure 10: Delta-E1B19K Increased the Volume of Acidic Compartments After Virus Infection. A) U251-MG cells were infected at the MOI indicated and analyzed for acridine orange staining 48 hours post infection.

Acridine orange examination of Delta-E1B19K revealed there was not a complete abolishment of autophagy. We chose to examine this phenomenon more in depth. E1B19K is known to interact with E1B19K interacting Protein (Bnip3) through a BH-like domain. Bcl-2 encompasses a BH3 domain that binds to Beclin 1 to inhibit autophagy. E1B19K is a homologue of BCL-2. We proposed that E1B19K interacted with Beclin 1 to regulate autophagy. The first experiment was immunoprecipitation of E1B19K and examination of Beclin 1. Infection of HeLa cells with Delta-24-RGD or Delta-E1B19K and subsequent co-immunoprecipitation revealed that only an E1B19K expressing adenovirus could co-immunoprecipitate Beclin 1 (figure 11). The converse experiment pulling down Beclin 1 could still precipitate E1B19K. Therefore, we concluded that E1B19K does, in fact, bind to Beclin 1 *in vitro*.

It is relevant to also establish the Beclin 1 binds to PI3K CIII. Beclin 1 must associate with PI3K CIII in order to induce autophagy. A time course experiment revealed that PI3KCIII associated in a complex with E1B19K and Beclin 1 while BCL2 did not (figure 12). Beginning at 6 hours post infection PI3KCIII was detected with co-immunoprecipitation with Beclin 1 while BCL2 detection in the complex decreased. Simultaneously, immunoprecipitation with E1B19K revealed that PI3KCIII co-immunoprecipitated with increased time while BCL2 was never detected. We discovered that E1B19K competes with Bcl-2 to bind Beclin 1 and that Beclin 1, E1B19K, and E1B19K all exist in a complex together.

We noticed through gross microscopic analysis of the cells revealed that at 48 hours 100% of the cells were floating and revealing cytopathic effect. We chose to look at the induction of apoptosis because earlier studies revealed there was not an increase in autophagy induction. Infection with Delta-E1B19K revealed an increase in cleaved PARP while only in the presence of E1B19K PARP remained in the uncleaved form (figure 13). Therefore, deletion of E1B19K fails to induce autophagy, which subsequently leads the cells to undergo apoptosis.

Since there was an increase in apoptosis, we sought to establish whether the replication cycles of these to virus were similar. HeLa cells were infected with Ad300, Delta-E1B19K and Delta-24-RGD (figure 14). 48 hours later the cells and supernatant were collected and analyzed for infectious viral progeny. Delta-E1B19K had a 70% and 64% decrease in replication compared with Ad300 (student's t-test  $p=0.0004$ ) and Delta-24-RGD respectively. Deletion of E1B19K causes the cells to undergo apoptosis causing the cells to die before a full replication cycle has concluded.

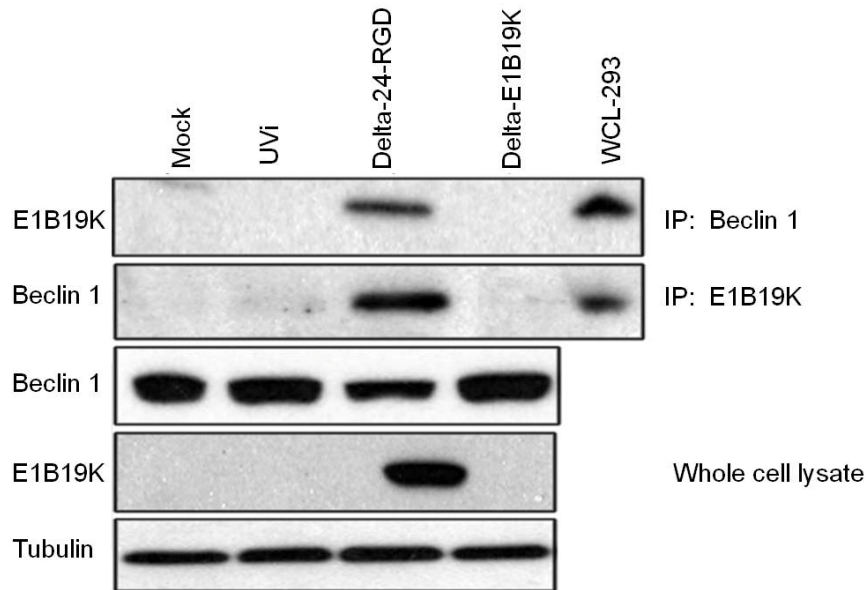
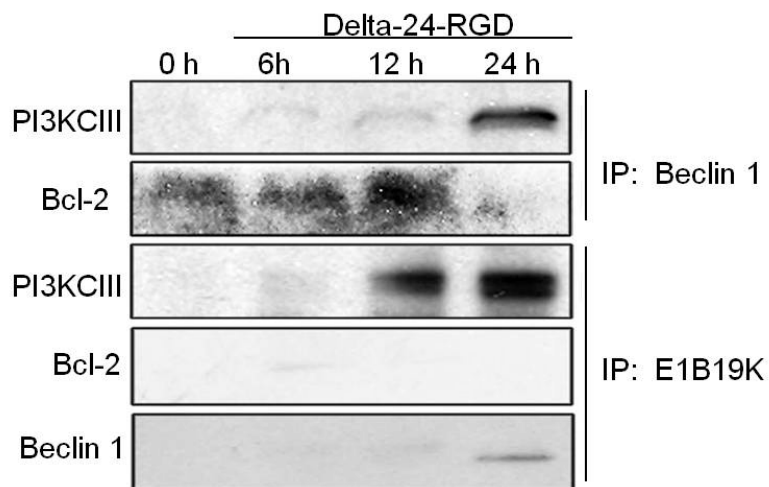


Figure 11: E1B19K Binds to Beclin 1 *in vivo*. Infection with of HeLa cells with Delta-24-RGD or Delta-E1B19K and subsequent co-immunoprecipitation reveals that only an E1B19K expressing adenovirus can co-immunoprecipitate Beclin 1. The converse experiment pulling down Beclin 1 can still precipitate E1B19K.





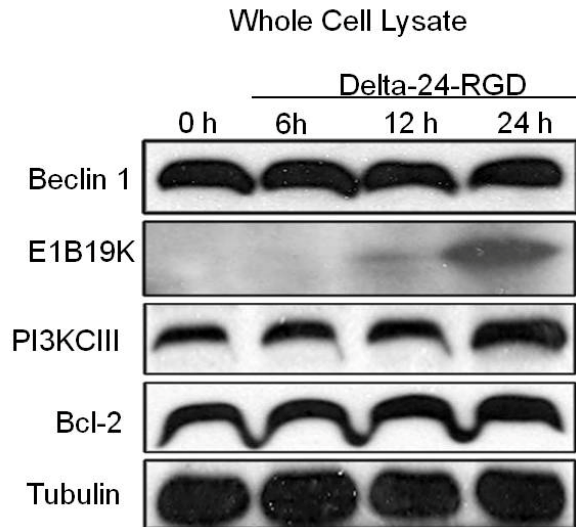


Figure 12: A Time Course Experiment Revealed that PI3KCIII Associates in a Complex with E1B19K and Beclin 1 while BCL2 Does Not. Beginning at 6 hours post infection PI3KCIII was detected with immunoprecipitation with Beclin 1 while BCL2 detection in the complex decreased. Simultaneously, immunoprecipitation with E1B19K revealed that PI3KCIII co-immunoprecipitated with increased time while BCL2 was never detected.

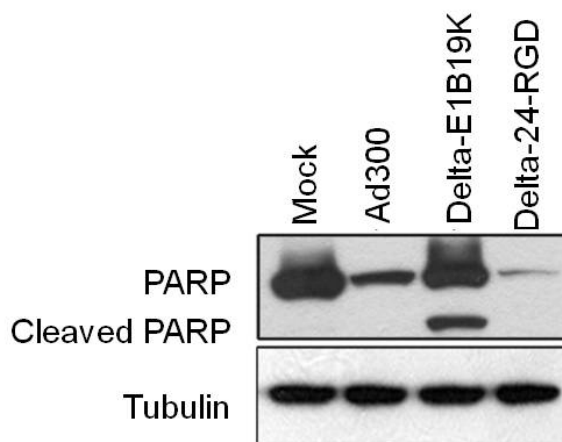


Figure 13: Infection With Delta-E1B19K Led to Increased Cleavage of PARP. Cells were infected with each virus and assayed by Immunoblotting for PARP cleavage.

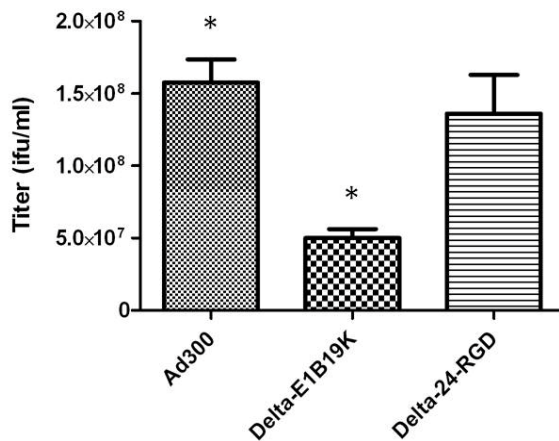
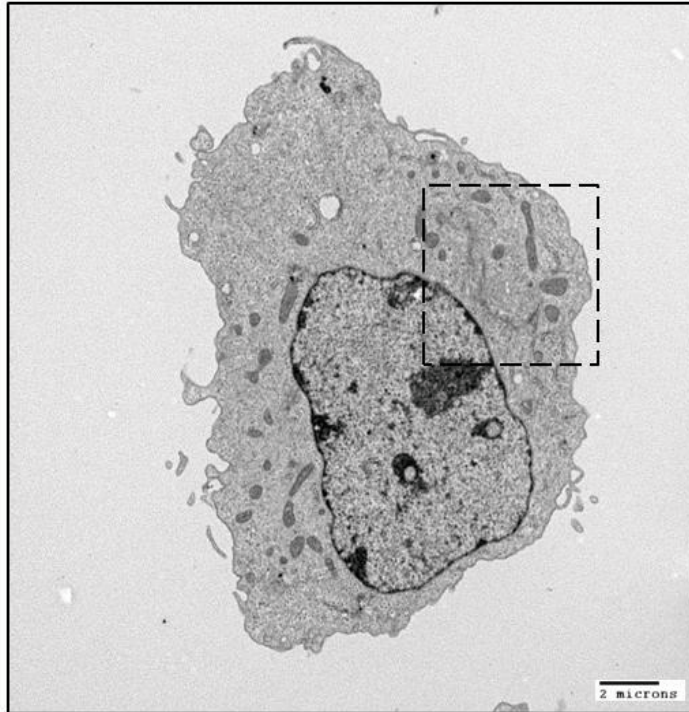


Figure 14: Delta-24-RGD Revealed Impaired Replication. HeLa cells were infected with Ad300, Delta-E1B19K and Delta-24-RGD. 48 hours later the cells and supernatant were collected and analyzed for infectious viral progeny.  $p=0.0004$ .

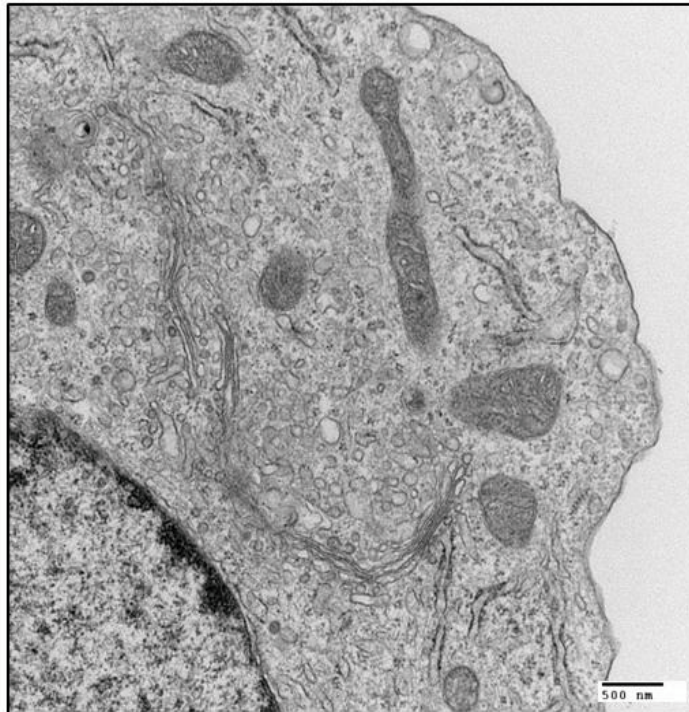
We examined the ability of all of our knockout viruses to induce autophagy. Ultrastructure morphology studies revealed similar results as earlier stated. The Delta-E1 infected control cell displayed a continuous cytoplasm with mitochondria and ER clearly present. The cell infected with Delta-24-RGD adenovirus has a disrupted cytoplasm with autophagic vacuoles. Item D shows a phagosome with multi-lamellar structure present and also vacuoles with digested material inside. The nucleus was spotted with virions. Infection with Delta-E3, Delta-E1B19K, Delta-E4, and Delta-VARNA all exhibited a similar phenotype (figure 15:A-L). None of the genes were required for adenovirus mediated autophagy.

It was also important that we examined LC3 punctuation after infection with the mutants for biochemical confirmation. Cells with more than five GFP-LC3 dots were considered positive for autophagy. Replication competent mutants had a 3-7 fold increase in the number of autophagy positive cells over the mock treated and Delta-E1treated controls (figure 16). This experiment indicated that no single viral gene tested, except E1A, is required for adenovirus-mediated autophagy.

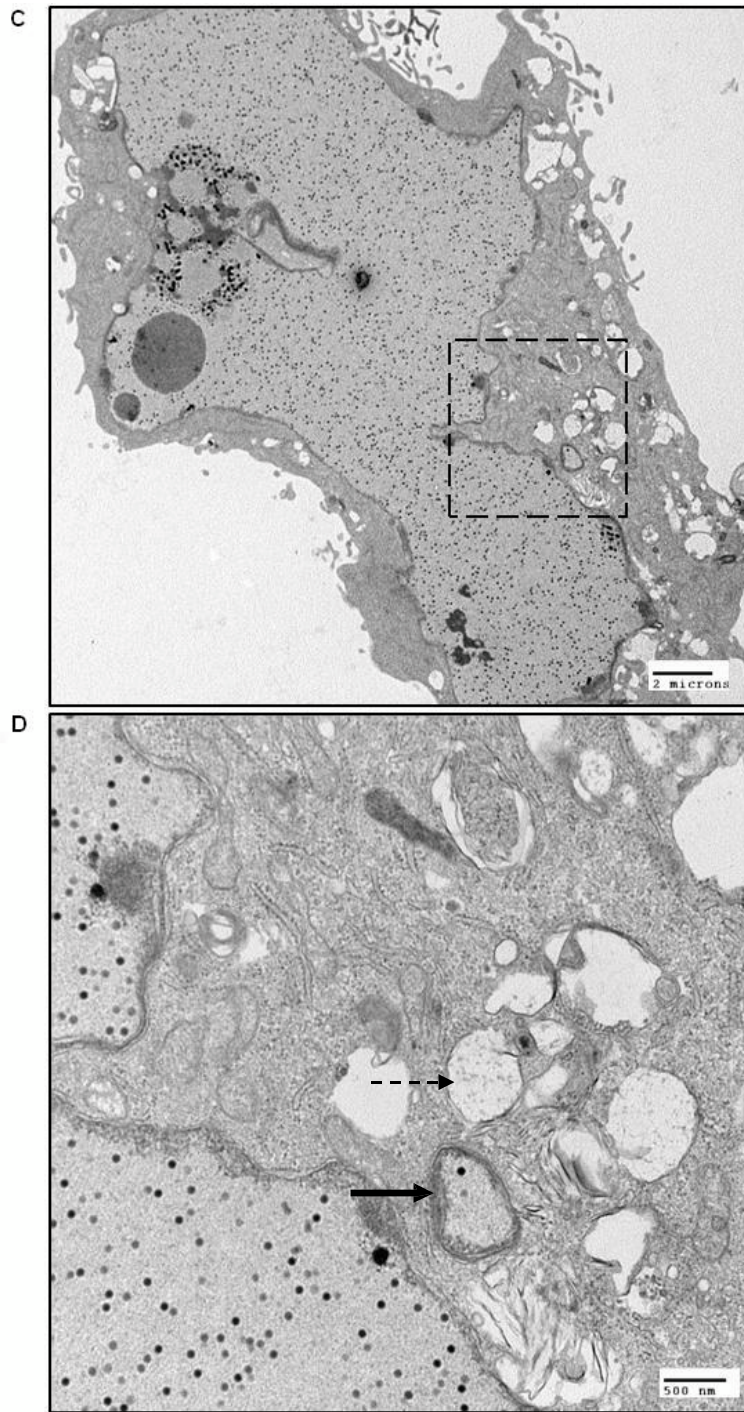
A



B

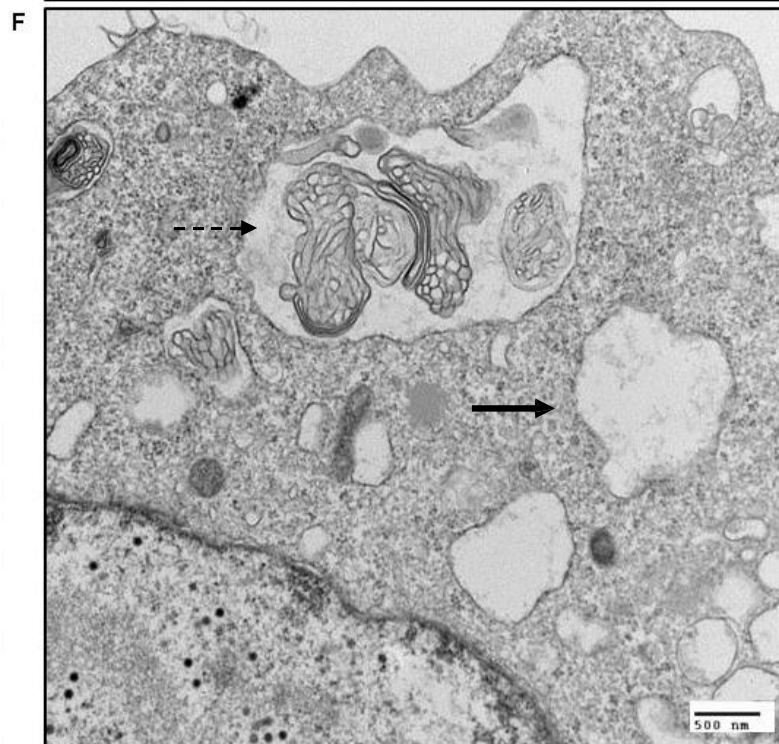
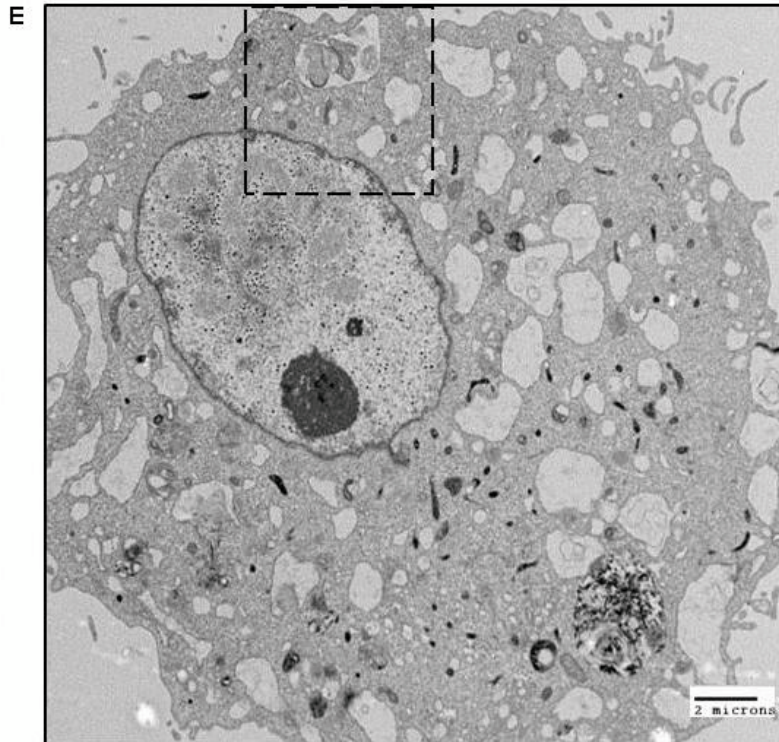


Delta-E1 Infected cell

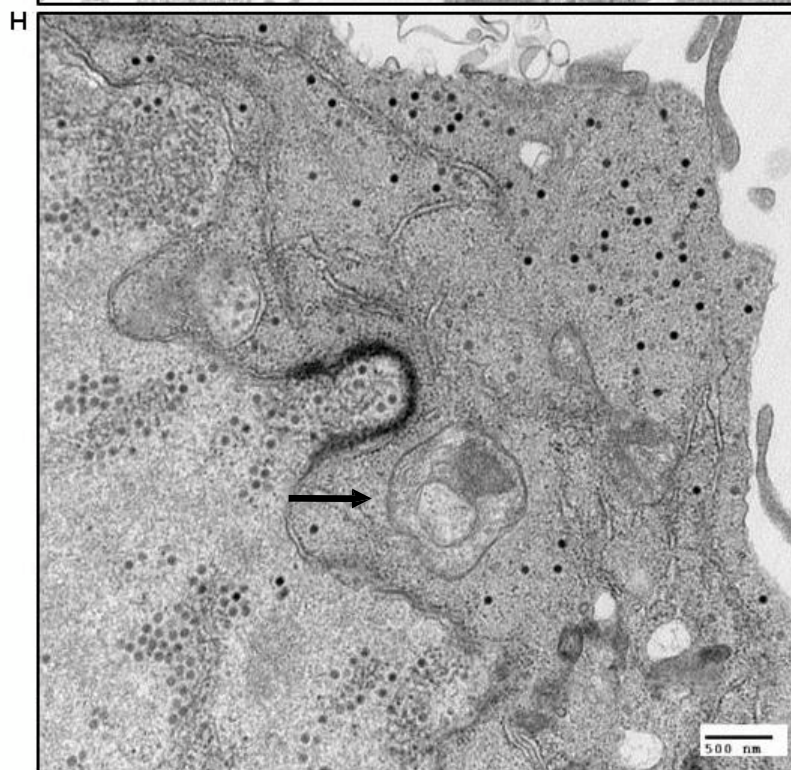
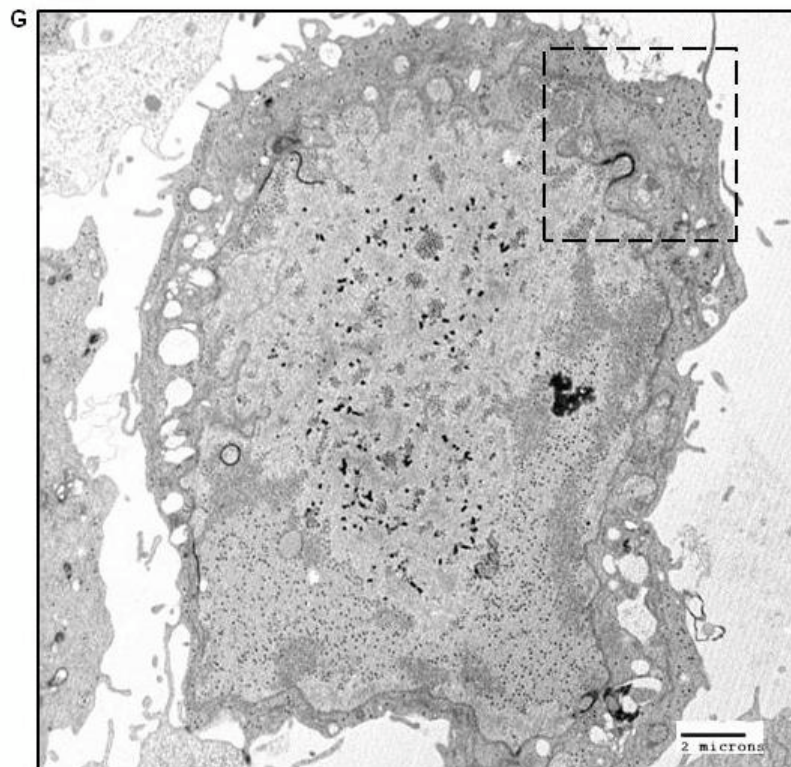


Delta-24-RGD Infected cell



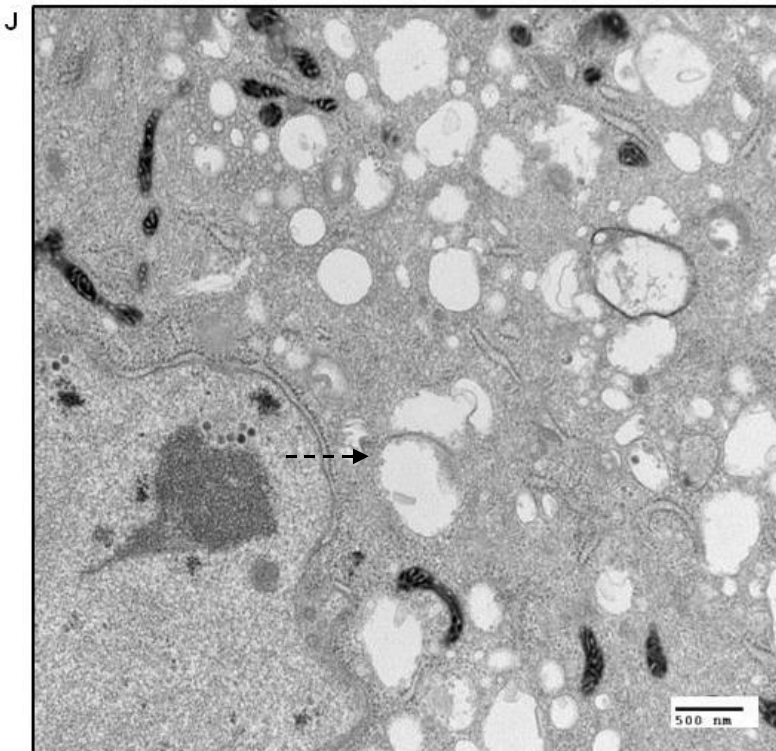
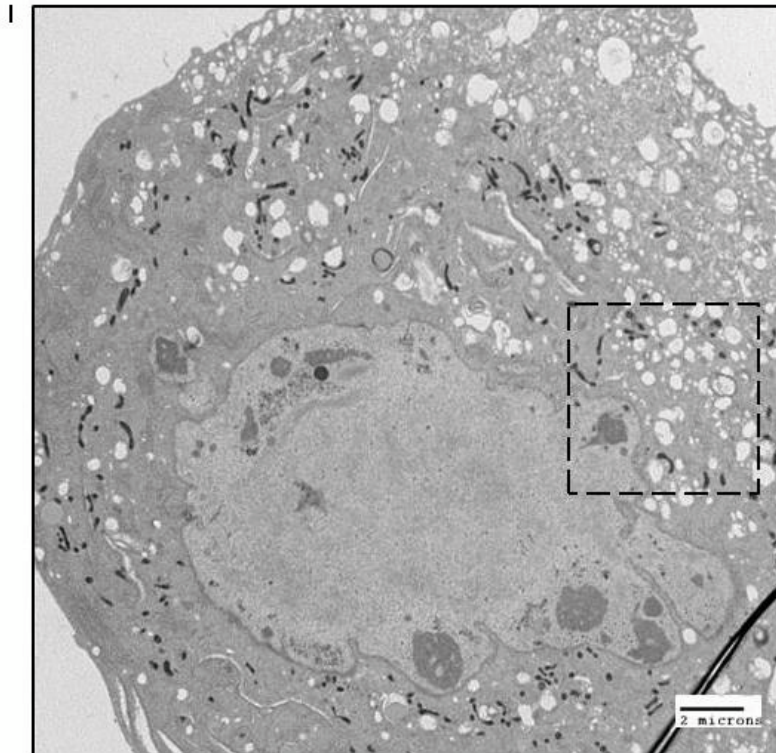


Delta-E3 Infected cell



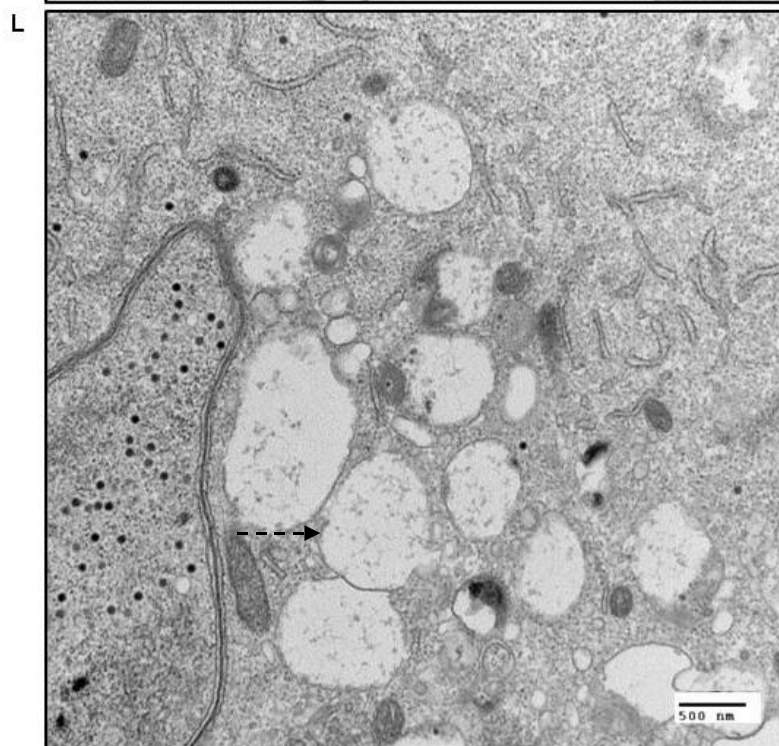
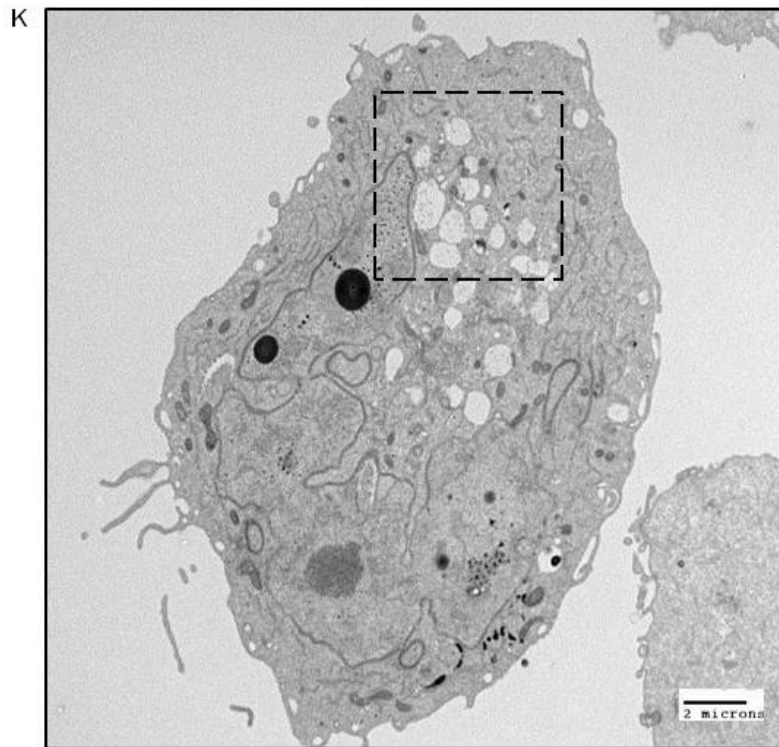
Delta-E1B19K Infected cell





Delta-E4 Infected cell





Delta-Va RNA I Infected cell

Figure 15: Ultrastructure Studies of MRC-5 Infected with Adenovirus Mutants Revealed the Presence of Autophagosomes. A) Delta-E1 virus 100 MOI, 5000x magnification. B) Delta-E1 virus 100 MOI, 25000x, magnification. C) Delta-E3 virus (Delta-24-DGD) 100 MOI, 6000x magnification. D) Delta-E3 virus (Delta-24-DGD) 100 MOI, 25000x, magnification. E) Delta-E3 virus (Ad300) 100 MOI, 6000x magnification. F) Delta-E3 virus (Ad300) 100 MOI, 25000x, magnification. G) Delta-E1B19K virus 100 MOI, 6000x magnification. H) Delta-E1B19K virus 100 MOI, 25000x, magnification. I) Delta-E4 virus (dl366) 100 MOI, 6000x magnification. J) Delta-E4 virus (dl366) 100 MOI, 25000x, magnification. K) Delta-VARNA virus 100 MOI, 6000x magnification. L) Delta-VARNA virus 100 MOI, 25000x, magnification. Dotted arrow: late stage autolysosome. Solid arrow: autophagosome

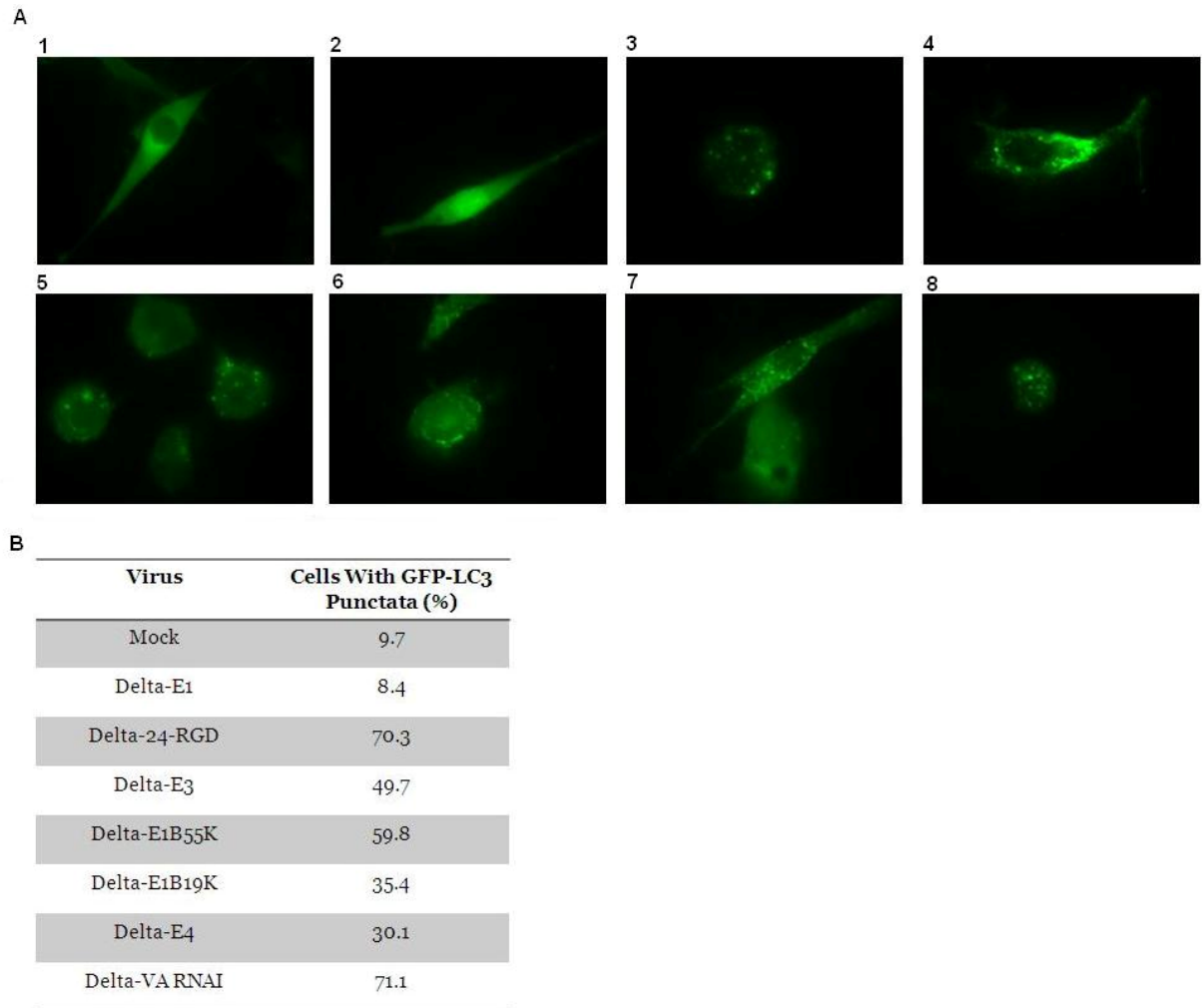


Figure 16: All Mutant Viruses, Induced GFP-LC3 Punctate Staining. U87-MG cells stably transfected with GFP-LC3 and either mock infected or infected with adenovirus mutants at 30 MOI. Cells with greater than five GFP-LC3 punctata were considered positive for autophagy. A) 1.Mock infection. 2. Delta-E1. 3. Delta-24-RGD. 4. Delta-E3. 5. Delta-E1B55K. 6. Delta-E1B19K. 7. Delta-E4. 8. Delta-VARNA-I. B) Quantitation of the wells.

#### **4.0 Intracellular ATP levels decrease after adenovirus infection**

Jiang *et. al.* 2008 proposed that a possible mechanism of adenovirus-mediated autophagy was that the virus induces a hyperanabolic state. Increased energy demands for the production of the virus can stress the cell and deplete ATP stores. We wanted to measure the intracellular levels of ATP after virus infection and we were able to accomplish this by utilizing an Intracellular bioluminescence kit that needs ATP to facilitate the reaction of D-luciferin and O<sub>2</sub> to produce light. We infected U251 cells at 100 MOI for 24-72 hours (figure 17). We collected the cells by lysing them in water and used an aliquot as the ATP source for our bioluminescent reaction. At 24 hours there was a 2.6 fold decrease in ATP levels. That difference increased to 4 and 5 fold at 48 and 72 hours respectively. Therefore, there is a decrease in ATP which could be a trigger for autophagy induction.

#### **4.1 Intracellular sensors for ATP as effectors of autophagy induction**

LKB1 is the kinase that regulates AMPK. AMPK is the sensor for intracellular ATP. In order to study the role that LKB1 and AMPK play in the induction of adenovirus mediated autophagy we obtained shLKB1 U251 cells and AMPK $\alpha$ 1 $\alpha$ 2 null MEFs from our collaborators. U251 cells were transfected with shRNA against LKB1 and clones were picked to analyze the expression level. We chose the clone with the least amount of expression and infected the parental, shControl, and shLKB1 cell lines with 30 MOI of Ad300 (figure 18). Infection of shLKB1 had no bearing on the ability of adenovirus to induce

autophagy. We analyzed acidic vacuoles and LC-3 cleavage and there was no difference between the parental cell lines, control cells lines or the knockout/knockdown cell lines. Infection with AMPK $\alpha$ 1 $\alpha$ 2 null MEFs revealed similar findings (figure 19 and 20). This data indicate that LKB1, and AMPK do not play a role in adenovirus-mediated autophagy.

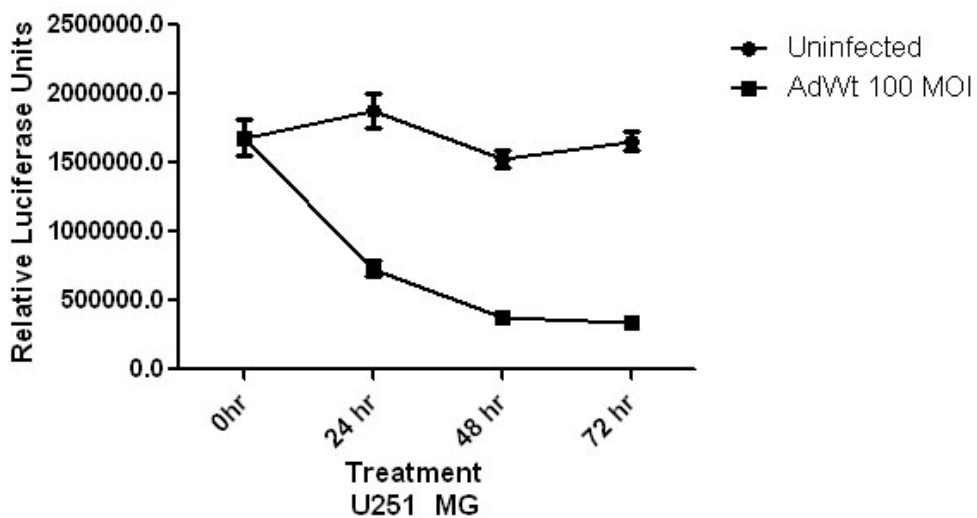


Figure 17: Infection with Ad300 Decreased the Levels of Intracellular ATP. U251 cells were plated in triplicate and infected with Ad300 at 100 MOI. Every 24 hours the cells were collected, lysed in diH<sub>2</sub>O and analyzed using an ATP intracellular bioluminescence assay. ANOVA  $p < 0.0001$ .

	<b>U251.parental</b>	<b>U251.shcont</b>	<b>U251.shLKB1</b>
Mock	4.6±0.6	1.7±0.5	4.1±0.2
Delta-E1	5.4±0.8	1.7±0.7	3.5±0.3
Ad300	30.2±6.5	25.0±1.9	29.0±0.6

Figure 18: shLKB1 Knockdown Cells Revealed No Difference in Acridine Orange Staining Compared to Wild-type Cells. A) U251-MG, shCont and shLKB1 cells were infected at 30 MOI and analyzed for acridine orange staining 48 hours post infection.

	<b>AMPK Wild-type</b>	<b>AMPK Knockout</b>
Mock	4.1±0.4	1.8±0.6
Rapamycin	24.0±0.7	24.5±1.3
Delta-E1	3.5±0.6	1.7±0.4
Ad300	49.6±2.6	48.4±1.8

Figure 19: AMPK $\alpha$ 1 $\alpha$ 2 Null MEFs Revealed No Difference in Acridine Orange Staining Compared to Wild-type Cells. Underwent Autophagy After Virus Infection. A) AMPK wild-type and AMPK $\alpha$ 1 $\alpha$ 2 null MEFs were infected at 50 MOI and analyzed for acridine orange staining 48 hours post infection.

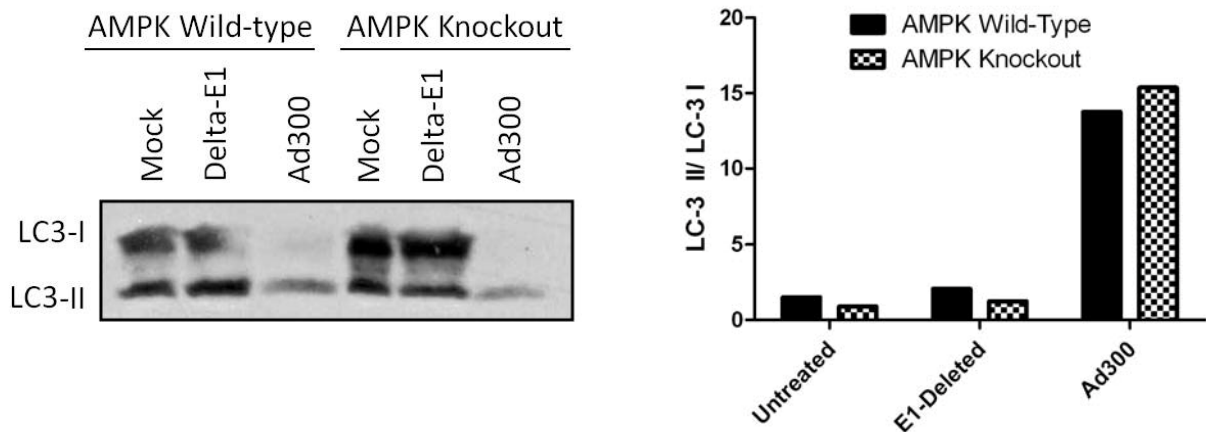


Figure 20: AMPK $\alpha$ 1 $\alpha$ 2 Knockout Cells

Underwent Autophagy After Virus Infection. A) AMPK wild-type and AMPK $\alpha$ 1 $\alpha$ 2 knockout cells were infected at 50 MOI and analyzed for LC3 cleavage 48 hours post infection. B) Densitometric analysis of LC-3 cleavage.

#### 4.2 Adenovirus activates the AKT pathway during late stage viral infection

The current model of starvation-mediated autophagy implies a decrease in the activity level of the AKT/mTOR pathway. Using an antibody array, we found that AKT was phosphorylated in response to adenovirus infection at residue S473 16 hours after infection and at residue T308 36 hours after infection (Figure 21). AKT must be phosphorylated at both residues to be maximally active (97). This indicates that it was only active during the late stage of viral infection, 36 hours. Interestingly levels of phosphorylation on residue S2448 of mTOR were, in most part, unchanged until the late stage of viral infection. Interestingly, one of the most prevalent mTOR targets, p70S6K, was phosphorylated at its active site, T398 despite little or no changes of mTOR phosphorylation at 16 hours. AKT

and mTOR are activated during late hours of infection and therefore we looked further into the pathway.

#### **4.3 Downregulation of TSC2 fails to prevent adenovirus-mediated autophagy.**

To further dissect the role of the AKT/AMPK/mTOR pathway, we obtained TSC2 knockdown cells to examine the role TSC2 played in the induction of autophagy after adenovirus infection. U251 cells were transfected with shRNA against TSC2 and clones were picked to analyze the expression level. We chose the clone with the least amount of expression and infected the parental, shControl, and shTSC2 cell lines with 30 MOI of Ad300 (figure 22). There was no change in the volume of acidic compartments or the number of cells that were positive for acidic compartments. We also analyzed LC-3 cleavage as an indicator of autophagy and found there was no difference between any of the cell lines (figure 23). TSC2 does not play a role in adenovirus mediated autophagy therefore, there with the array data and the lack of involvement of TSC2, we cannot conclude that the AKT/mTOR pathway play a role in adenovirus-mediated autophagy.



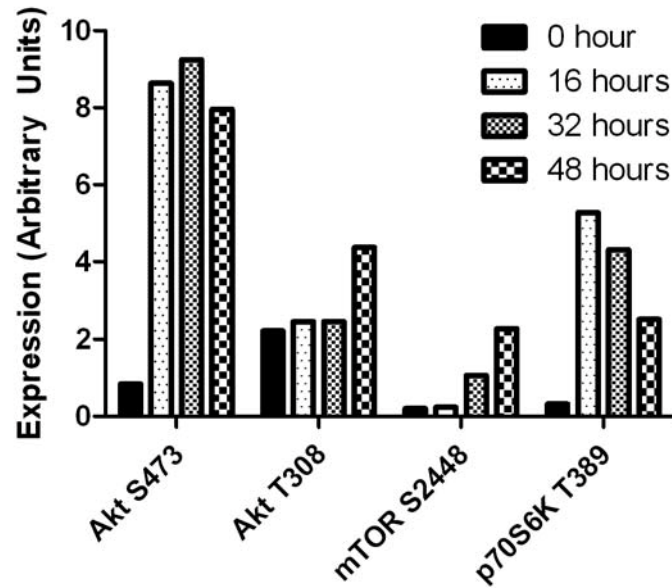


Figure 21: Activation of the AKT Pathway After Adenovirus Infection. A) MRC-5 cells were infected at 100 MOI and collect at 16, 32, and 48 hours. The lysates were subjected to an AKT antibody array from R&D Systems.

	U251.parental	U251.shcont	U251.shTSC2
Mock	4.2±0.4	4.0±0.7	5.8±0.8
Delta-E1	3.9±0.5	3.6±1.0	5.6±1.3
Ad300	52.6±3.5	46.5±2.3	46.4±2.3

Figure 22: shTSC2 Knockout Cells Revealed No Difference in Acridine Orange Staining Compared to Wild-type. A) Generation of TSC2 shRNA downregulated cell line. B) U251 parental, shCont, or shTSC2 cells were infected at 30 MOI and analyzed for acridine orange staining 48 hours post infection.

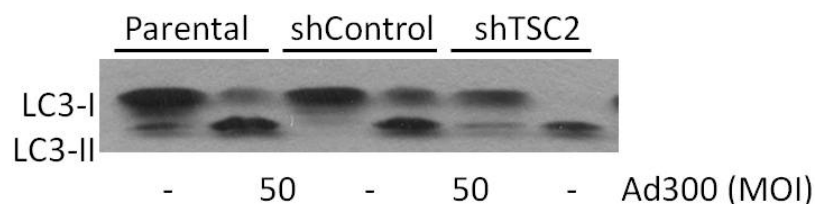


Figure 23: shTSC2 Cells Undergo Autophagy After Virus Infection. A) TSC2 wild-type and TSC2 downregulated cells were infected at 30 MOI and analyzed for LC3 cleavage 48 hours post infection.

#### 4.4 eIF2 $\alpha$ Phosphorylation Increases After Viral Infection

Other pathways besides the AKT pathway are known to induce autophagy. For instance, PKR is known to phosphorylate eIF2 $\alpha$  during viral infections (55). Thus, we monitored eIF2 $\alpha$  phosphorylation levels during adenoviral infection, in our study. MRC-5 cells were infected at 100 MOI, and eIF2 $\alpha$  phosphorylation was monitored every 12 hours. Figure 24 demonstrates that eIF2 $\alpha$  phosphorylation increased starting 36 hours after infection and culminated with a 3-fold total increase at 48 hours, with no change in the total levels of eIF2 $\alpha$ . There was also an inverse correlation with the levels of eIF2 $\alpha$  phosphorylation and the decrease in the levels of p62, suggesting that eIF2 $\alpha$  may be involved in autophagy induction.

## 4.5 Examination of PERK

There are four kinases that are responsible for eIF2 $\alpha$  phosphorylation. Of those four, we chose to examine PERK and GCN2. PERK activation is primarily monitored by investigating its downstream effectors. PERK increases translation of chaperone proteins during ER stress. We infected U251 cells at 100MOI and examined disulfide isomerase (PDI) and BiP (figure 25). Unexpectedly, we saw a disappearance of these proteins after virus infection despite an increase in eIF2 $\alpha$  phosphorylation.

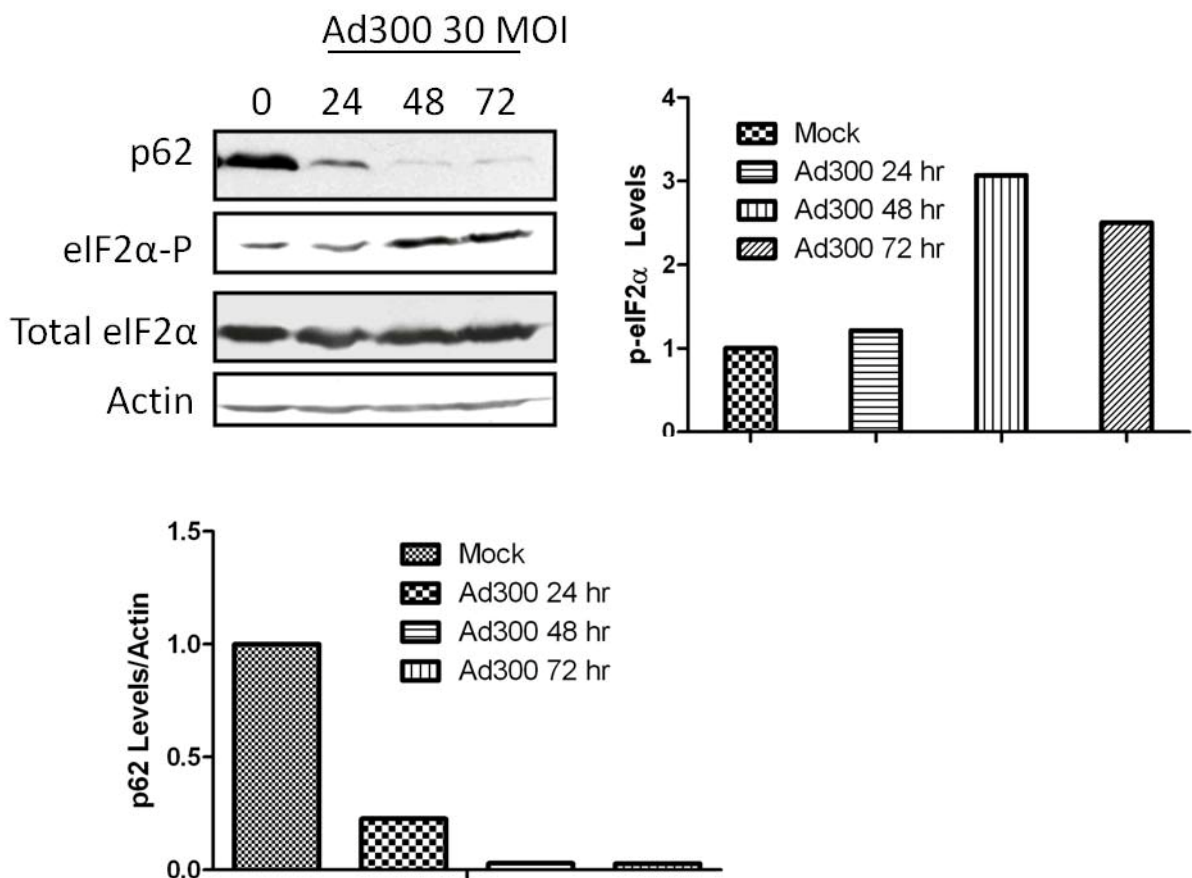


Figure 24: Translation Initiation Factor eIF2 $\alpha$  is Phosphorylated During Adenovirus Infection. U251-MG cells were infected at 100 MOI and the cell lysates were analyzed by western blotting for autophagy and eIF2 $\alpha$  phosphorylation status. A) eIF2 $\alpha$  is phosphorylated between 24 and 48 hours after virus infection without changes in the total levels of eIF2 $\alpha$ . This degradation also correlates with a dramatic p62 degradation. B) Densitometry of phospho-eIF2 $\alpha$ /total eIF2 $\alpha$  and normalized to actin. C) Densitometry of p62 normalized to actin.

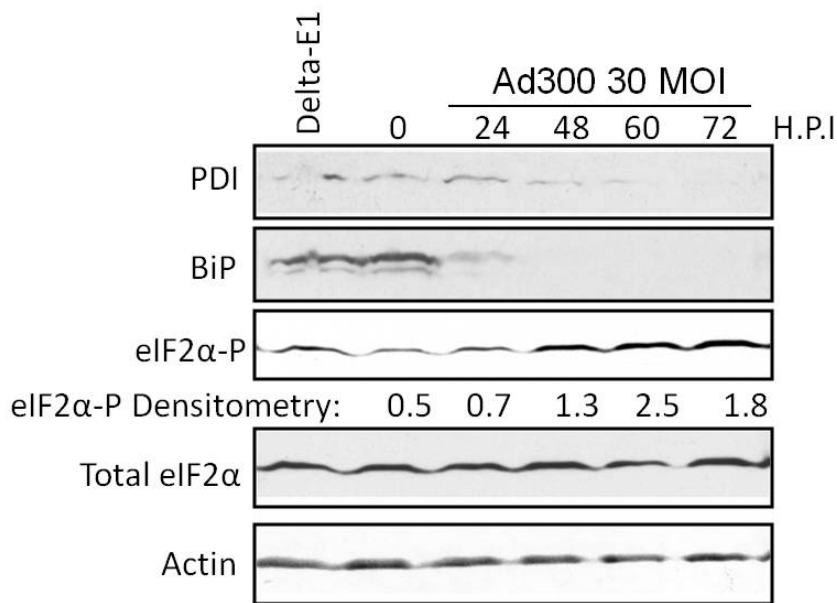


Figure 25: ER Stress Proteins are Degraded During Virus Infection. A) U251 Cells were infected and cell lysates were collected at the time points indicated. PDI and BiP (chaperone proteins) were degraded after virus infection despite eIF2 $\alpha$  phosphorylation.

## 4.6 Examination of GCN2

Next, we obtained GCN2 knockout mouse embryonic fibroblasts to study the role of GCN2 in the induction of autophagy. Upon infection it was abundantly clear that these cells were highly resistant to the cytopathic effect of the virus (figure 26). Trypan blue viability studies confirmed the observation. Mock treated cells were 94% and 96% viable for wild-type and knockout cell lines, respectively (figure 27). Similar levels of viability were seen with Delta-E1 infected cells with 91 and 94% viability, respectively. However, at 50 MOI and 100 MOI viability dropped 64% and 70% for wild-type cells, respectively. The GCN2 knockout cells had relatively no change in viability 50 and 100 MOI yielded 90 and 92% viability, respectively ( student's t-test  $p=0.0001$ ). A second method was used to examine viability of the cells, crystal violet. Cells were seeded in a 12-well plate and infected at increasing MOI (figure 28). 96 hours later cells were stained with the dye crystal violet. Most of the wild-type cells were completely cytopathic and lifted off of the plate at 50 MOI. This supports the lack of change in the trypan blue viability data at 50 and 100 MOI for wild-type cells. However, the amount of crystal violet retained by GCN2 knockout cells remains fairly constant, with only a slight decrease in crystal violet retention at 160 MOI. We repeated the experiment with an MOI up to 300 and we still continued to see a resistance of GCN2 knockout cells to adenovirus induced cytopathic effect (figure 29). We concluded that GCN2 was involved in the cellular response to the virus and decided to examine autophagy induction.

In order to examine autophagy in the GCN2 null cells, we used acridine orange, an acidotropic dye, to quantify the acidic vacuoles in the cell. The cells were infected at 50 MOI and analyzed with acridine orange 72 hours later (figure 30). There was a 3-fold increase in the percent cells positive for acidic vacuoles over the GCN2 null cells. This data implies that the GCN2 cells are impaired for autophagy induction after adenovirus infection.

For further conformation on the presence of autophagy we analyzed the cells for LC3 cleavage. Both cell lines were infected at 50 MOI and analyzed 48 hours post infection (figure 31). LC3-I was completely cleaved into LC3-II and that autophagosome completely degraded LC3-II, where it was not visible via western blotting. On the other hand, there was only slight cleavage of LC3-I to LC3-II in the GCN2 knockout cells. GCN2 cells do not undergo autophagy.

To confirm our biochemical data we analyzed the cells for autophagy through the gold standard for visualization of autophagy, which is electron microscopy. Both cell lines were infected with the same multiplicity of infection and fixed 72 hours post infection. Wild-type cells displayed a similar morphology to human cells infected with virus (figure 32b). The only difference was the lack of virions present in the cell due to the semi-permissive replication status of murine cells. This was expected as these cells are only semi-permissive to adenovirus replication. However, the GCN2 knockout cells appeared extremely similar to the untreated control cells (32a and d). There was no rounding of the cell and no gross vacuolar structures in the cytoplasm. We concluded GCN2 null cells do not undergo autophagy like their wild-type counterparts.

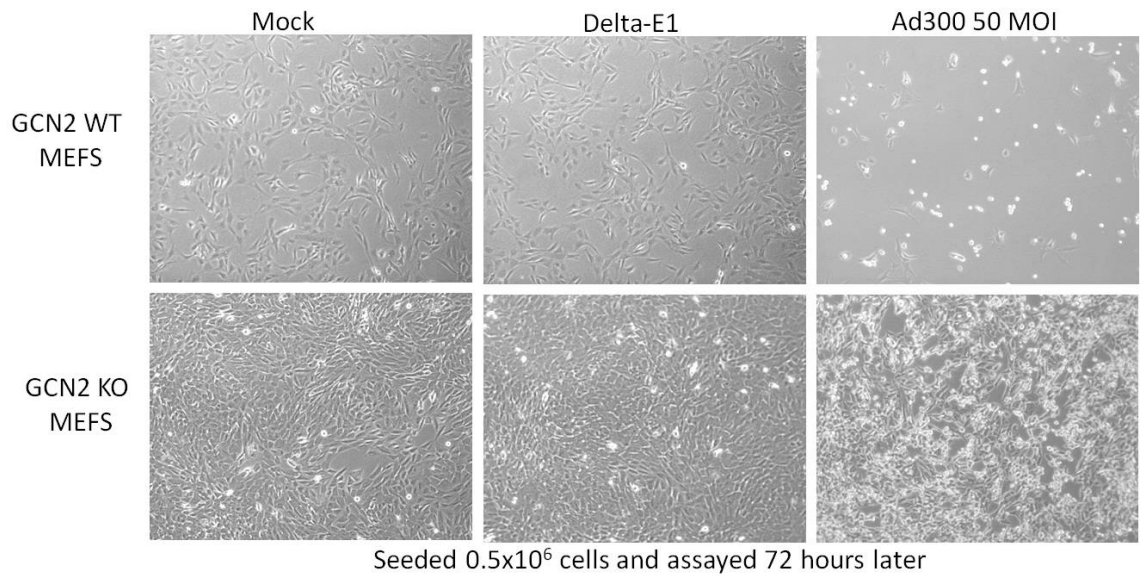


Figure 26: GCN2 Null Mefs are Resistant to Virus Infection. A) Wild-type and knockout MEFS were seeded at  $5 \times 10^5$  cells per well. Cells were infected at 50 MOI and visualized by phase contrast microscopy 72 hours post infection.

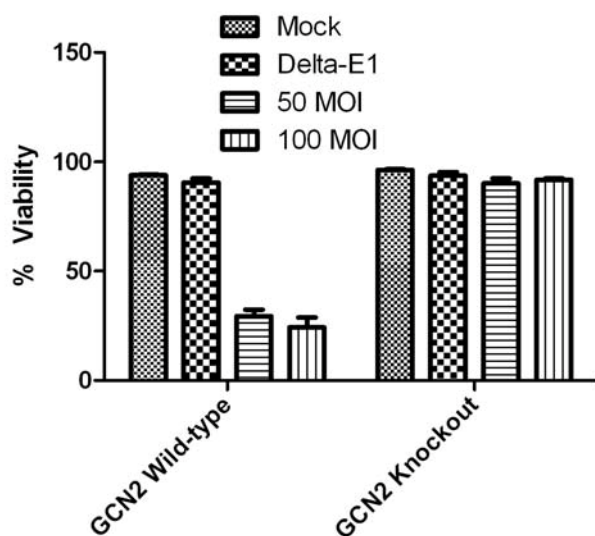


Figure 27: GCN2 Knockout MEFs Have Increased Viability After Adenovirus Infection.  $4 \times 10^4$  cells were seeded in a 12-well plate infected at the indicated MOIs. Floating cells were collected and the remaining cells were rinsed with PBS, trypsinized and combined with the floating cells and analyzed on an automated cell counter.



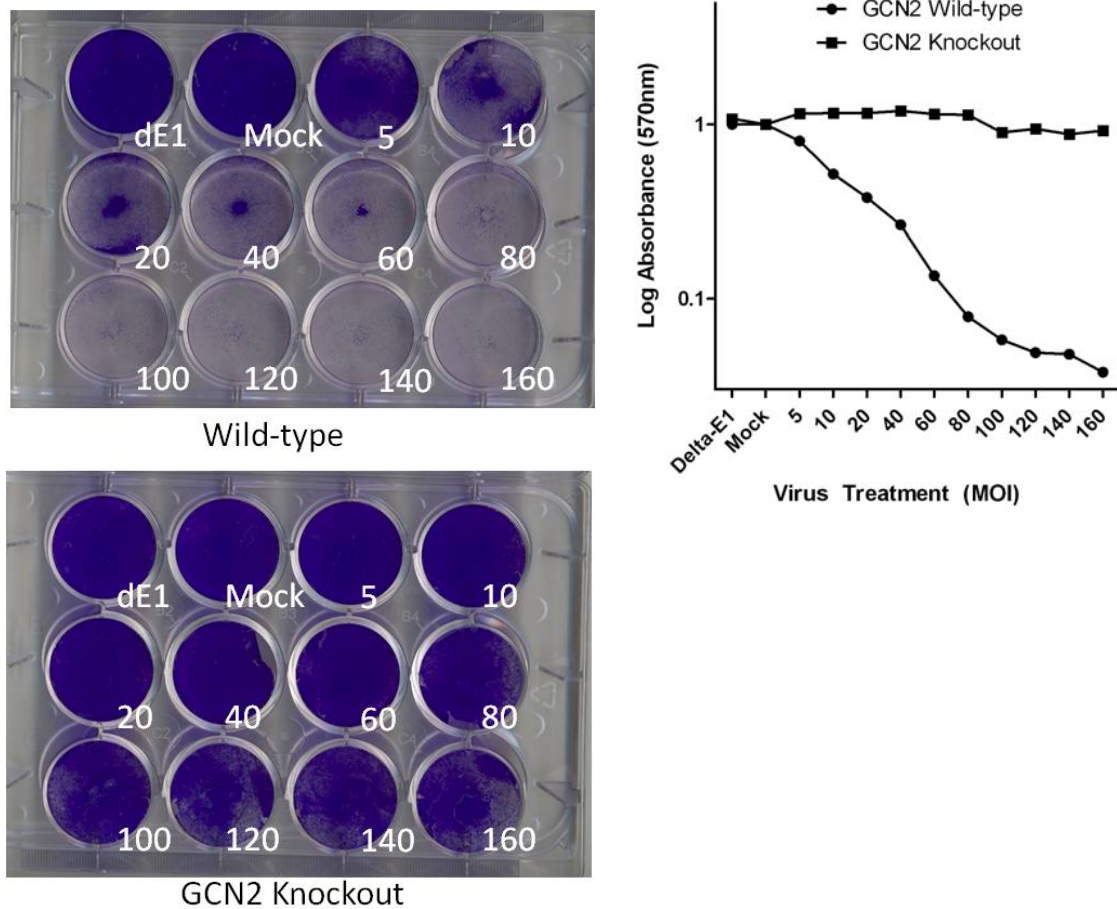


Figure 28: Loss of GCN2 Renders Cells Resistant to Adenovirus Infection.  $8.0 \times 10^4$  cells were seeded in a 24 well plate and infected with adenovirus as indicated. 96 hours later the media was aspirated, cells were washed with PBS, and stained with 0.05% Crystal Violet in 20% methanol for 10 minutes. Cells were washed and crystal violet was solubilized with 1% SDS and read at a wavelength of 570nm in a spectrophotometer. Two way ANOVA,  $p < 0.0001$ .

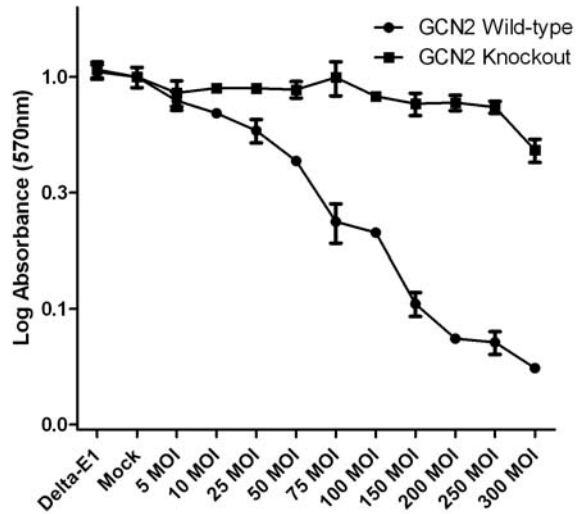


Figure 29: Even at High Multiplicities of Infection, GCN2 KO Cells are Resistant to Virus Infection.  $8.0 \times 10^4$  cells were seeded in a 24 well plate and infected with adenovirus as indicated. 96 hours later the media was aspirated, cells were washed with PBS, and stained with 0.05% Crystal Violet in 20% methanol for 10 minutes. Cells were washed and crystal violet was solubilized with 1% SDS and read at a wavelength of 570nm in a spectrophotometer. Two way ANOVA,  $p < 0.0001$ .

AVO Positive Cells (%)		
	GCN2 Wild-type	GCN2 Knockout
Mock	6.3±1.7	3.9±0.5
Serum and Glucose Free Media	54.4±0.7	59.6±0.6
Delta-E1	7.3±0.4	5.4±1.3
Ad300	77.9±2.8*	25.8±1.8*

Figure 30: GCN2 Knockout MEFs Have Decreased Levels of Autophagy After Infection. A)  $2 \times 10^5$  cells were seeded per well in a six-well plate and treated as indicated. Cells were analyzed 48 hours post infection. Students t-test,  $p < 0.001$

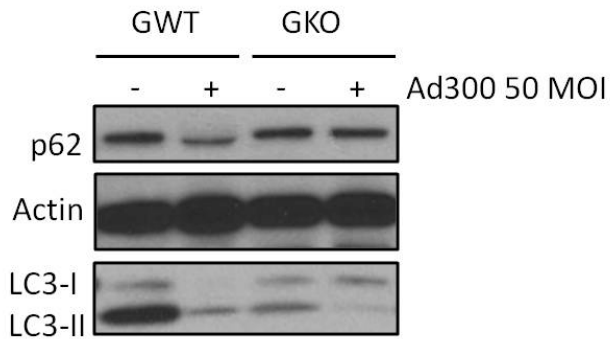
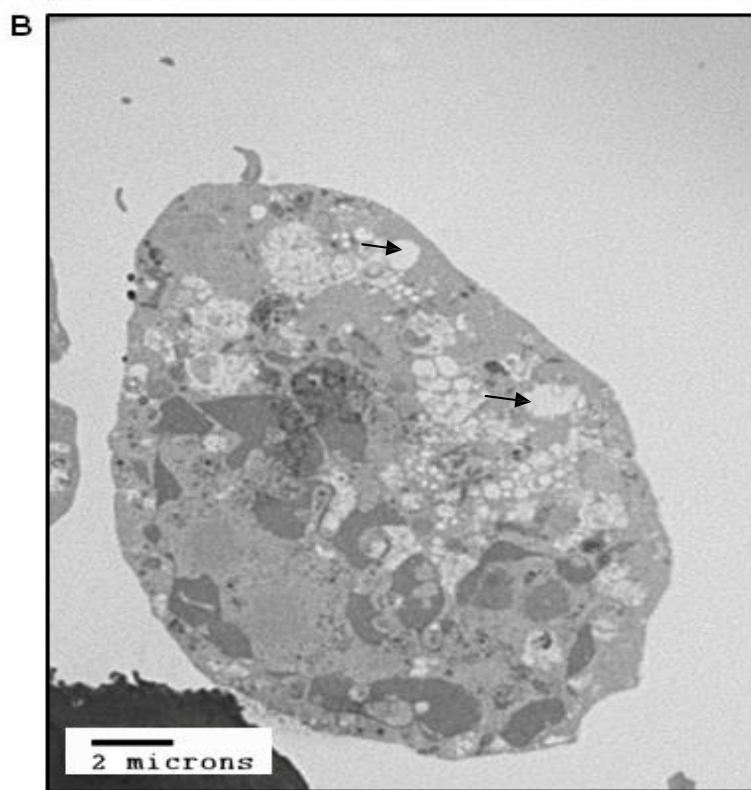
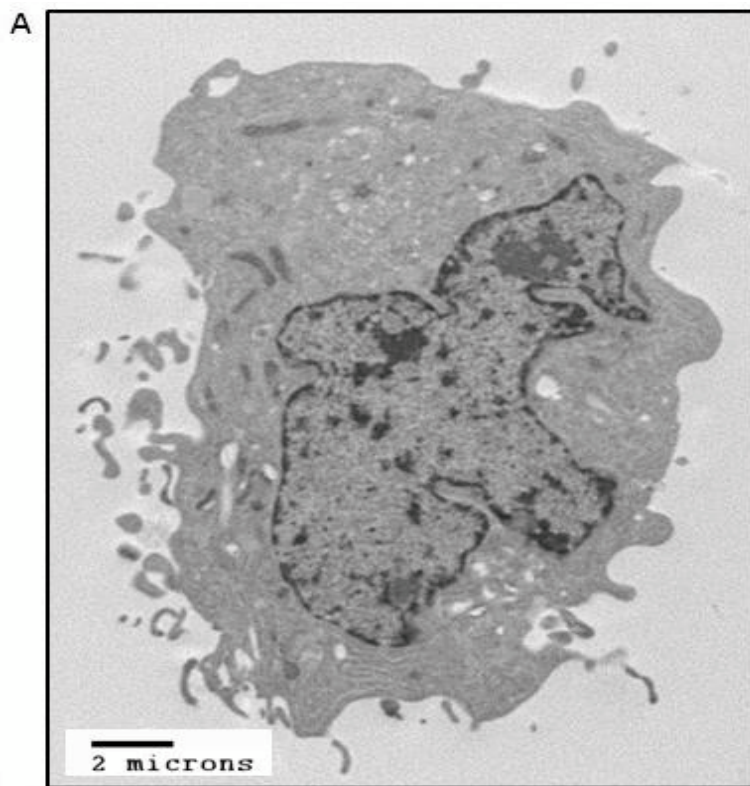
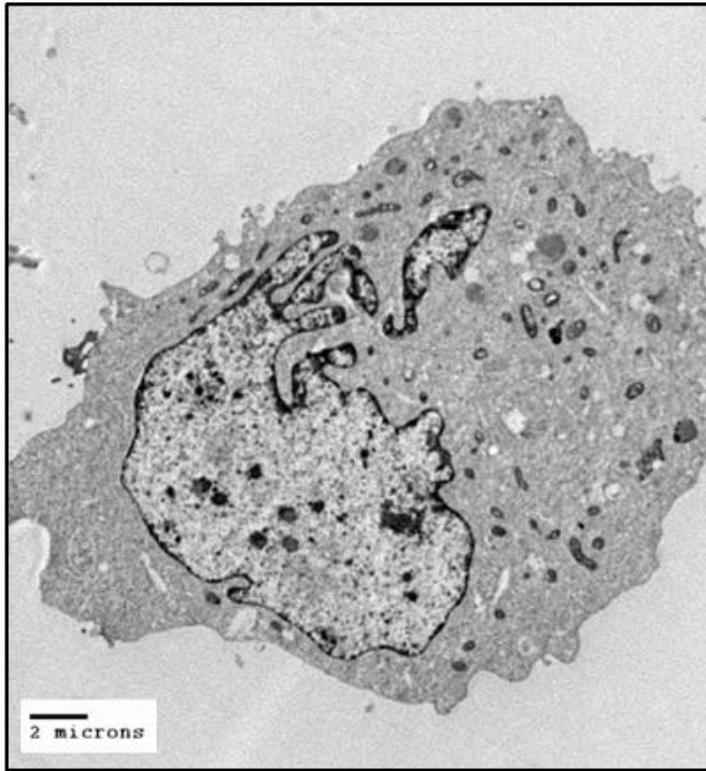


Figure 31: GCN2 Null MEFs Failed to Cleave LC3 or Degrade p62 After Virus Infection.  $1 \times 10^6$  GCN2 Wild-type and GCN2 Knockout MEFs were seeded in a 10cm dish and infected at 50 MOI. Cells were harvested 72 hours post infection and subjected to immunoblotting.



C



D

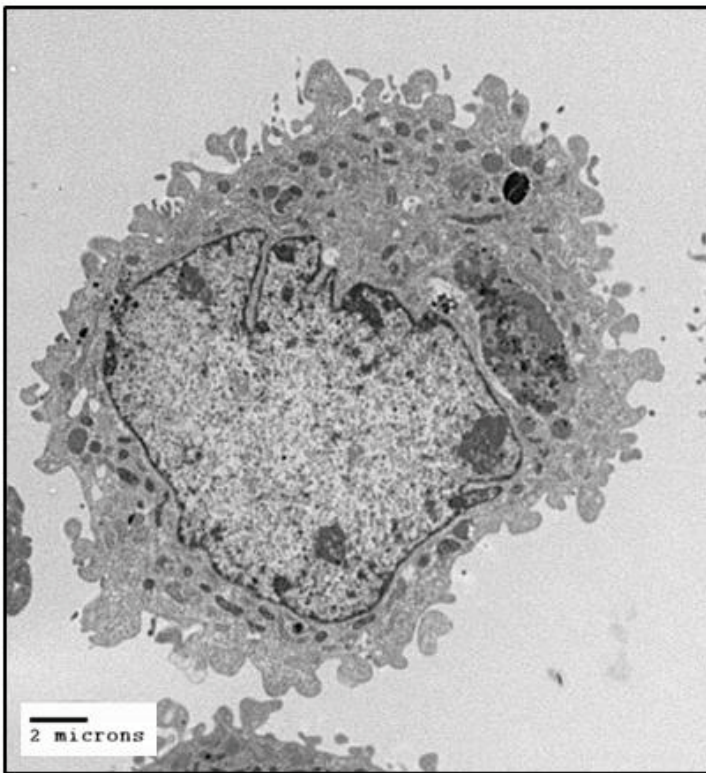


Figure 32: Ultrastructure Analysis Revealed a Lack of Autophagosome Induction After Virus Infection in GCN2 Knockout MEFs. A) GCN2 Wild-type MEFs, mock infected, 4000x Magnification. B) GCN2 Wild-type MEFs, Ad300 infected, 4000x Magnification. C) GCN2 Knockout MEFs, mock infected, 4000x Magnification. D) GCN2 Knockout MEFs, Ad300 infected, 4000x Magnification. Solid arrow: autolysosome.

#### 4.7 In vivo analysis of GCN2

It was important to not only understand the implications of GCN2 deficiency *in vitro* but we also wanted to analyze the role of GCN2 *in vivo*. We infected wild-type and GCN2 knockout mice with adenovirus and analyzed the difference in liver morphology and cytotoxicity. Adenovirus has a strong tropism for the liver and therefore is the most appropriate organ to examine for adenovirus toxicity. We found that the knockout mice had a strikingly different morphology compared to wild-type mice. The knockout mice had twice the amount of necrosis compared to wild-type mice. At high doses of viral infection which kill the mice in 3 days, wild-type pathology revealed acute coagulation periportal necrosis (figure 33A). However, in the knockout mice the necrosis was not confined solely to the periportal region anymore (figure 33B). The necrosis was diffused throughout the liver. The knockout mice also had hemorrhage in their liver. At three days there was no evidence of infiltration and the Kupffer cells were still inactive. This was probably due to the insufficient time for the

immune system to react. We were, however, able to detect E1A via immunohistochemistry in both of these livers (figure 34A and B). Therefore we can conclude that the E1A was responsible for the cell death in these livers. Mice that were infected with  $5 \times 10^9$  vp/mouse and euthanized on day 7 revealed a less severe pathology. Both groups had necrosis and the knockout mice had twice the amount of necrosis versus the wild-type group (figure 35 a) (student's t-test  $p < 0.05$ ). An interesting finding was that E1A expression seemed to be congruent with cell death (figure 35b). The knockout mouse livers had twice the amount of cell death and half the amount of E1A. At day 7, one can visualize the increased lymphocytic infiltration and Kupffer cell hyperplasia, although there was increased Kupffer cell hyperplasia in the knockout mice. Interestingly the knockout mice also had depletion of their bone marrow as revealed by microscopic analysis of their femur and sternum. In order to characterize autophagy in these animals we performed immunofluorescence for the autophagy protein p62 (figure 36). p62 punctuation in the cytoplasm was revealed in wild-type mice infected with adenovirus while the GCN2 knockout mice infected with virus did not have p62 foci in the cytoplasm; nor did the PBS controls. Therefore, we can conclude that the GCN2 null mouse livers *in vivo* do not undergo autophagy, similarly to the GCN2 null cells *in vitro*.



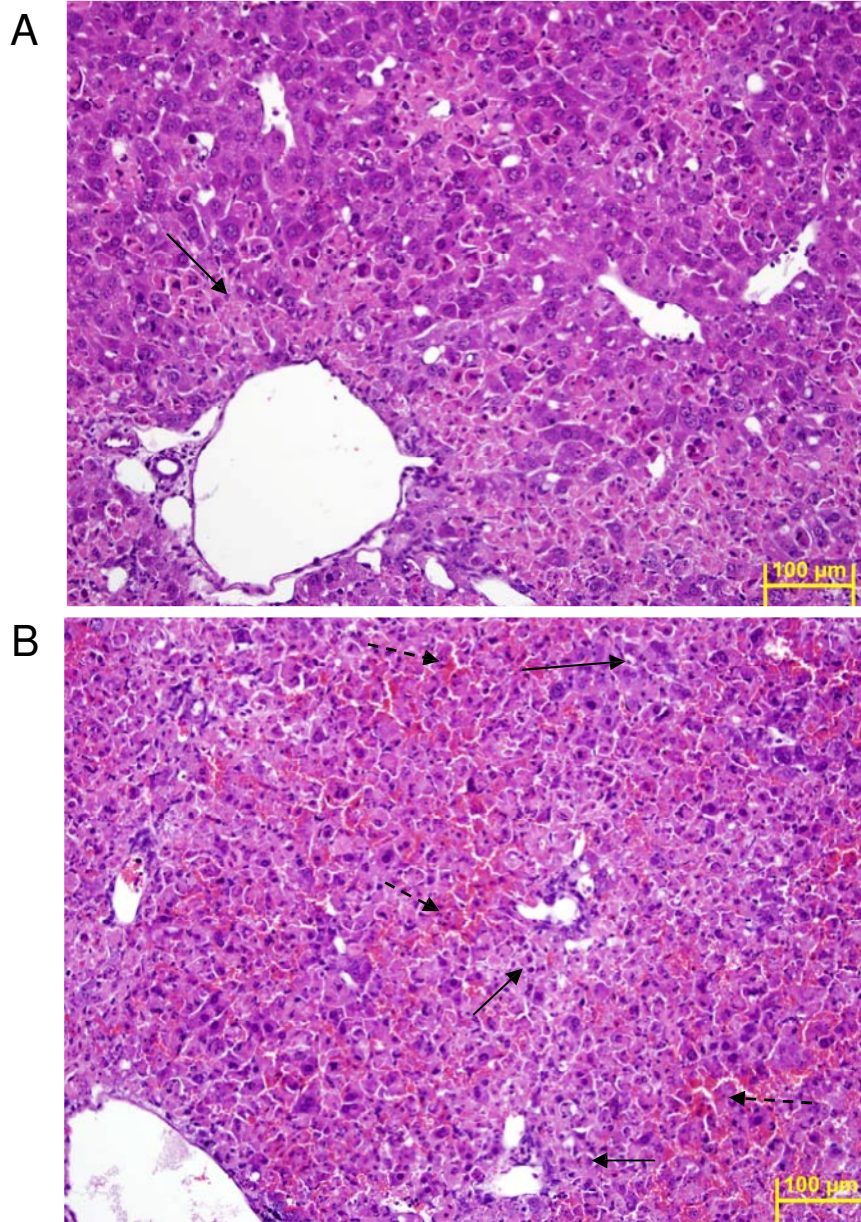


Figure 33: GCN2 Null Mice Undergo Large Amounts of Necrosis and Hemorrhage After Infection with Extremely High Viral Doses. GCN2 wild-type (A) and knockout mice (B) were injected with  $1 \times 10^{11}$  vp/mouse via tail vein injection. The mice were euthanized 3 days later. Solid arrow: necrosis. Dashed arrow: hemorrhage.



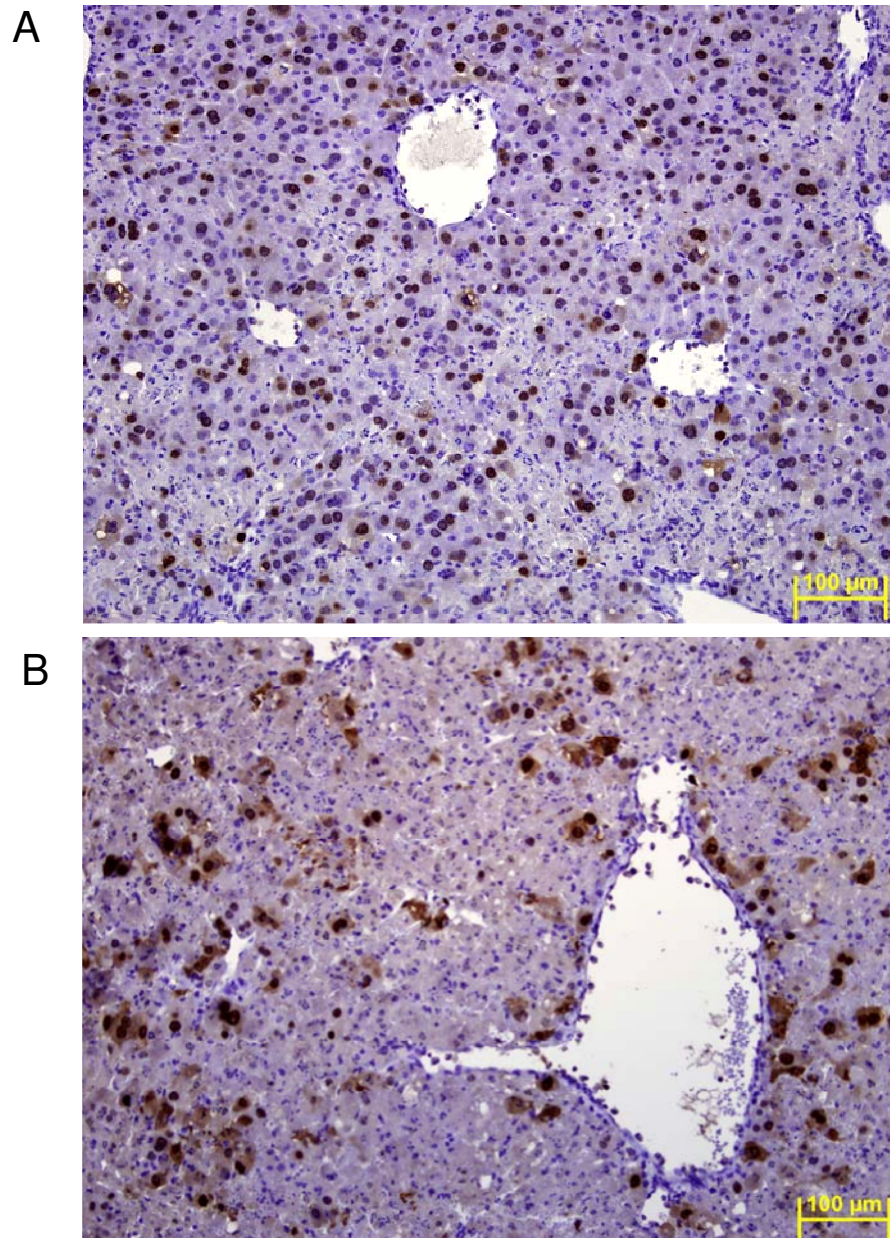


Figure 34: GCN2 Wild-type and Null Mice Both Express E1A. GCN2 wild-type (A) and knockout mice (B) were injected with  $1 \times 10^{11}$  vp/mouse via tail vein injection. The mice were euthanized 3 days later. Their livers were extracted, embedded in paraffin, and subjected to E1A immunohistochemistry.

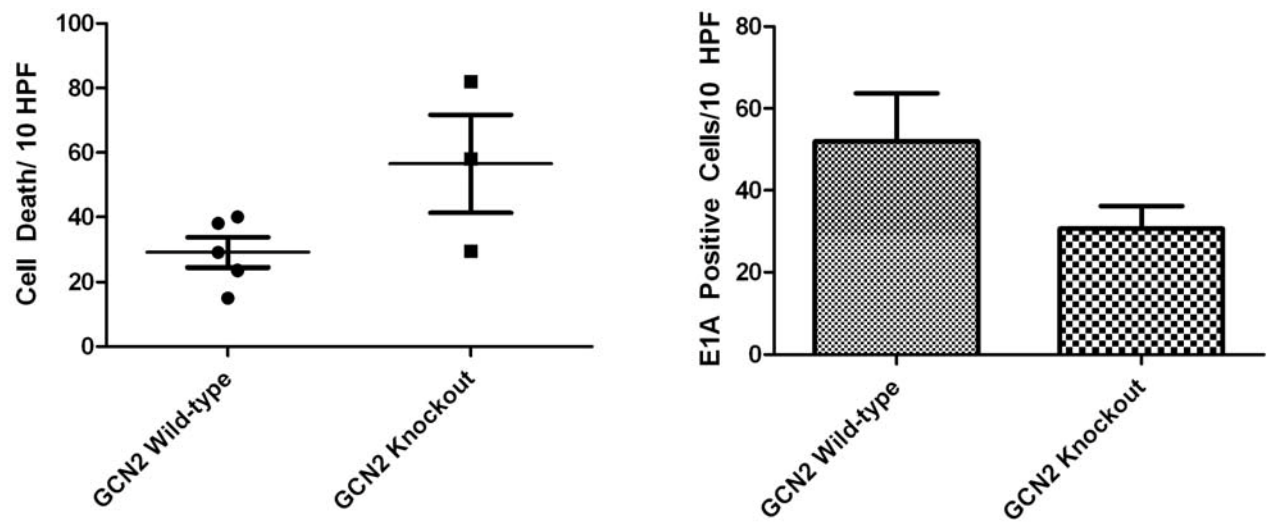


Figure 35: Cell Death in Mouse Livers is Congruent with E1A Expression. Mice were infected with  $5 \times 10^9$  virus particles per mouse and analyzed for E1A and cell death.

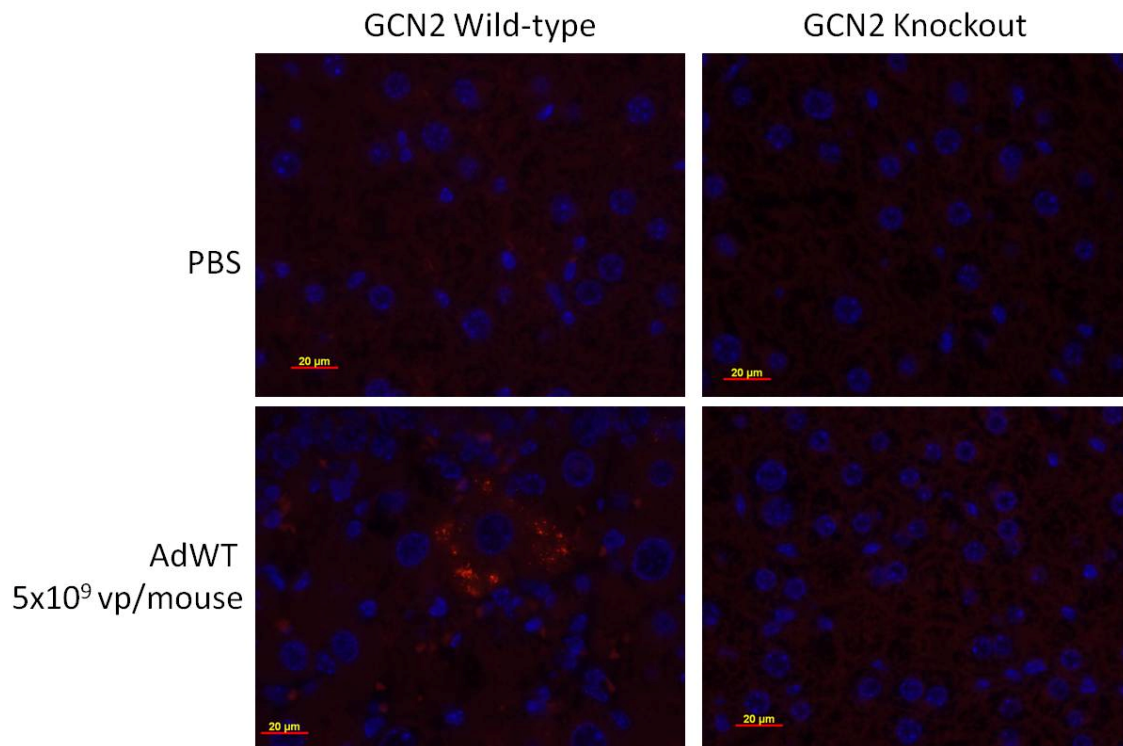


Figure 36: Autophagic Analysis of Livers from GCN2 Wild-type and Knockout Mice. Mice were infected with  $5 \times 10^9$  virus particles per mouse or PBS via tail vein injection. Mice were euthanized and their livers were fixed in formalin and analyzed for the autophagy protein p62.

## 5.0 Examination of Cell Lysis after Adenovirus Infection

To first examine the correlation between adenovirus replication and autophagy we treated cells with the late stage autophagy inhibitor Bafilomycin A1 (figure 37). The control cells had a continuous cytoplasm with no disturbances. Treatment with Bafilomycin alone did halt the basal autophagy process and vacuoles with undigested material were detected. Treatment with adenovirus

was visually drastically different than with Bafilomycin alone. Most of the vacuoles appeared white or empty and some had some remnants of digested cytoplasmic material. However, treatment with Bafilomycin and adenovirus revealed a substantial increase in the number of vacuoles suggesting a decrease in the turnover of vacuoles. The vacuoles were filled with undigested material. Treatment with Bafilomycin A1 did not increase cell lysis and viral particles were visible in the nucleus (figure 37). We wanted to analyze whether the inhibition of autophagy had any effect on replication and we confirmed that replication was still occurring through a replication assay (figure 38). There was no statistical significant difference between untreated and Bafilomycin treated cells.

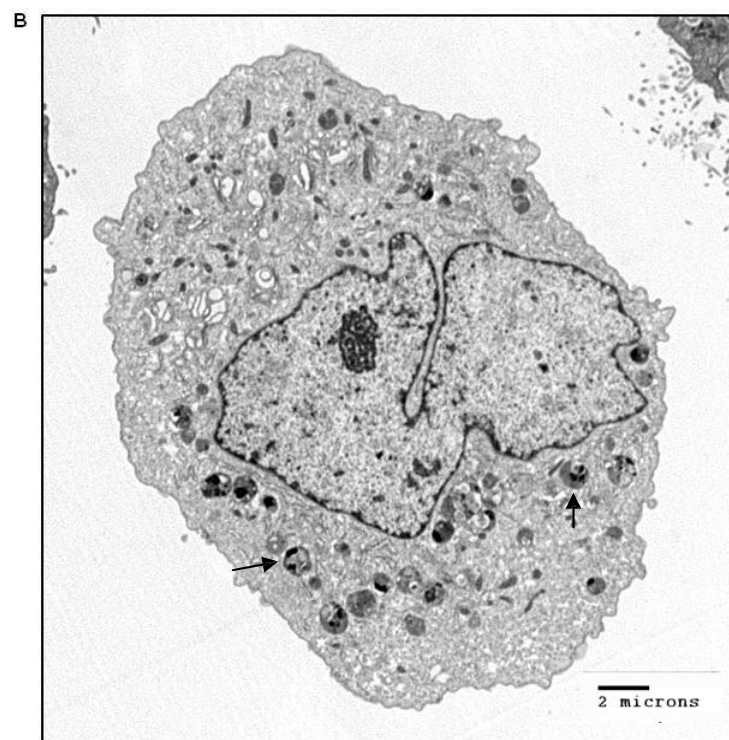
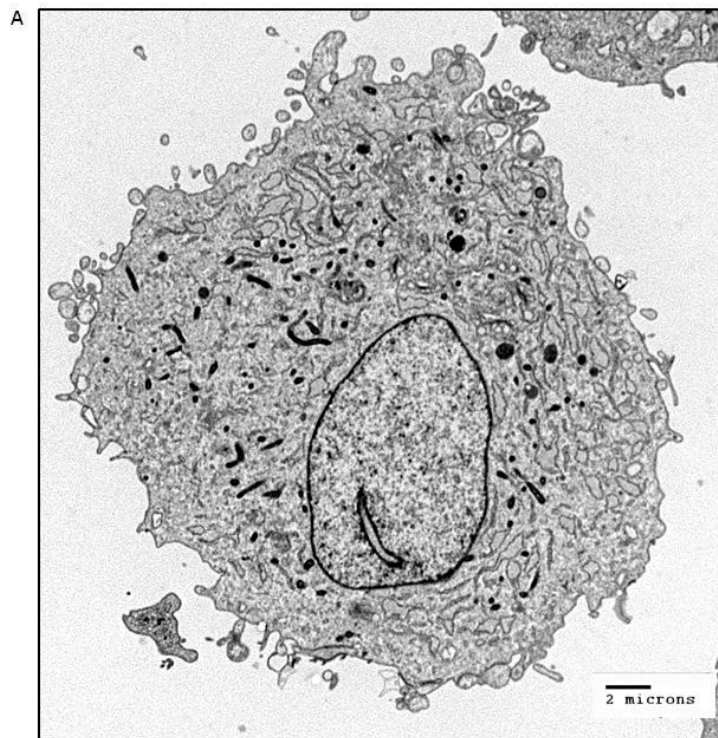
We believed that lysis may be a late event in viral replication. Therefore, we decided to visualize the process of lysis during adenovirus infected through time point experiments chronicling every 12 hours of virus infection from 0 hours to 120 hours (figure 39). We infected U251 cells with 100 MOI of wild-type adenovirus. Figure 39 shows 0 hours, 72 hours, 96 hours, and 108 hours. At 72 hours the membranes remained intact. There was a large quantity of virus in the nucleus and large vacuoles in the cytoplasm. However, there was still strong staining by osmium tetroxide. It was not until 96 hours when it was possible to see active breakage of the membrane. The cytoplasm was being degraded as evidenced by lack of osmium tetroxide staining. At 108 hours the nucleus and cytoplasm were completely degraded. The cells had no membrane integrity. The inset shows where the outer membrane was broken and released contents into the media. We can derive from this experiment that autophagy does

participate in degradation of the cytoplasm and membrane the can aid in cell lysis.

### **5.1 Autophagy induces and inhibitors regulate the viral plaque area**

One assay to asses viral spread and lysis is through a plaque forming assay. The media is replaced by agarose so the virions cannot passively move and infect the neighboring cells. We first examined, the autophagy inducer, rapamycin on its ability to increase viral lysis. We showed that there was a dose dependent increase in the total area of plaques (figure 40). From virus alone to virus plus 300nM of rapamycin there was a 1.88 fold increase in the area of plaques. 300nM to 500nM increase in rapamycin concentration increased the area of plaques by 1.38 folds. Therefore comparing 500nM rapamycin to virus alone there was an increase of 2.6 folds. We saw a slight increase in the number of plaques and wanted to further examine the effect on replication with hexon staining assays. U251 cells were infected at 30 MOI with wild-type adenovirus and the cells and supernatant were collected and examined for the presence of infectious virions (figure 41). There was a significant increase in the titer between virus alone and virus plus rapamycin ( $p=0.0052$ ). Therefore, we conclude that rapamycin does aid in viral lysis and increases replication.





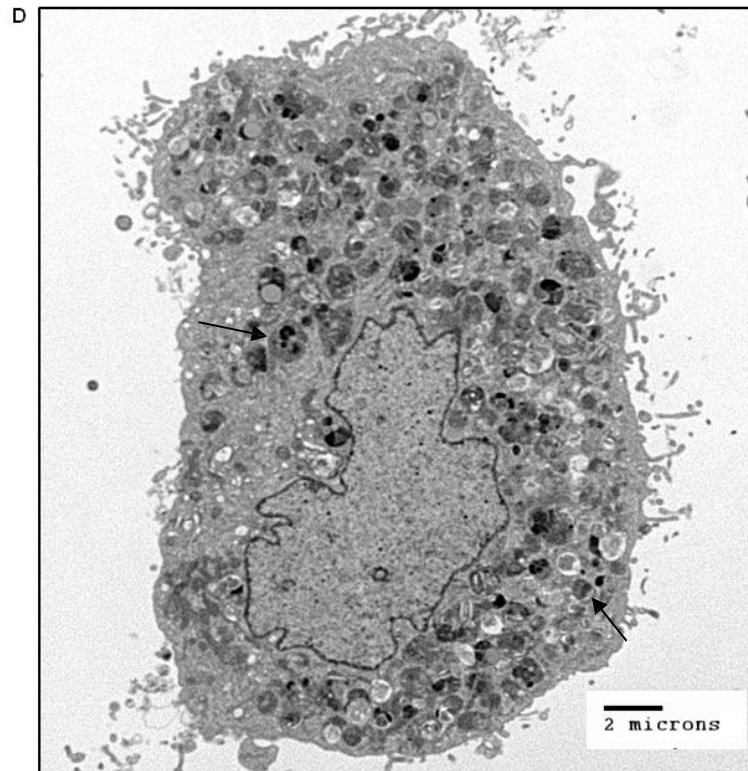
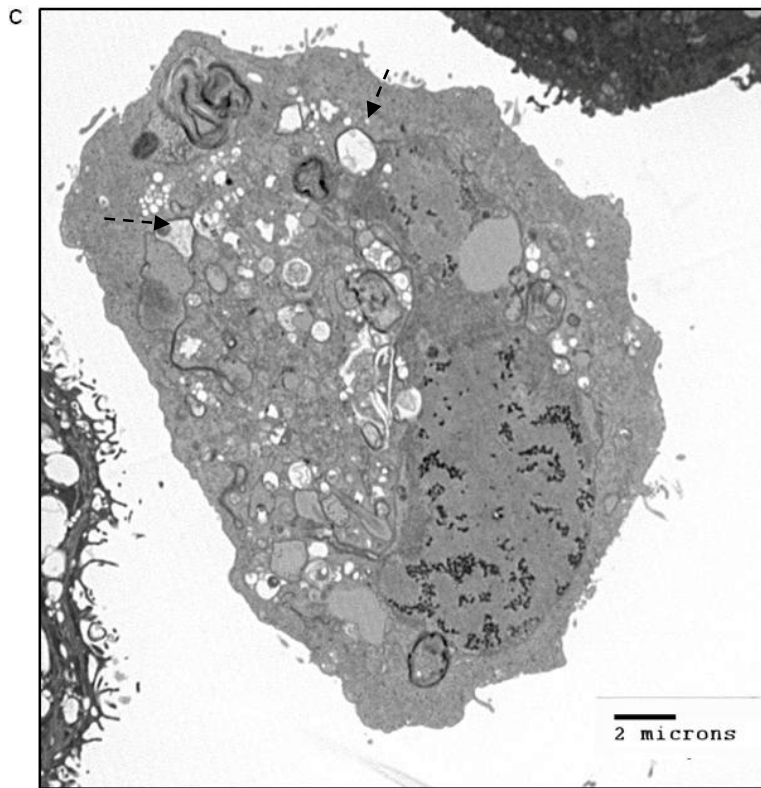


Figure 37: Bafilomycin Inhibits Autophagosomal Degradation During Adenovirus Infection. MRC5 cells were either mock infected (A), treated 150 $\mu$ M Bafilomycin A1 (B), infected at 100 MOI with Ad300 (C), or treated with 150 $\mu$ M Bafilomycin A1 and infected with Ad300 (D). Solid arrow: autophagosome. Dashed arrow: autolysosome.

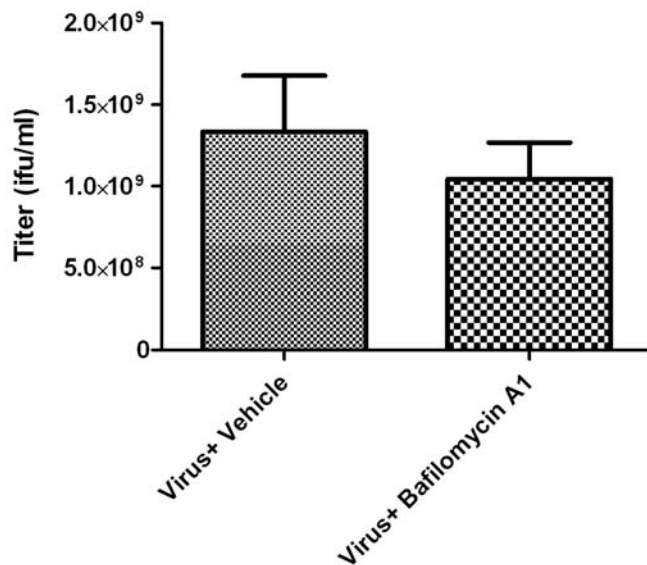
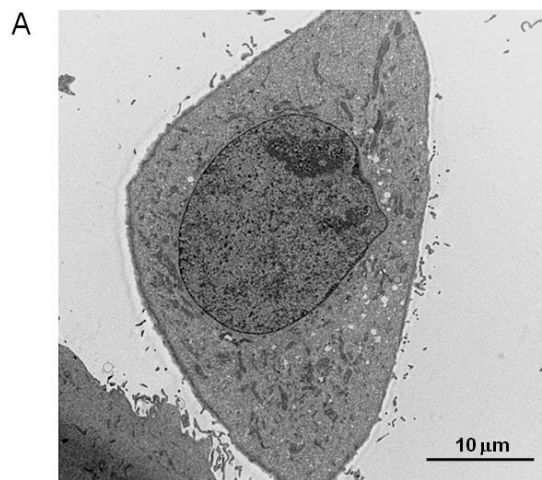
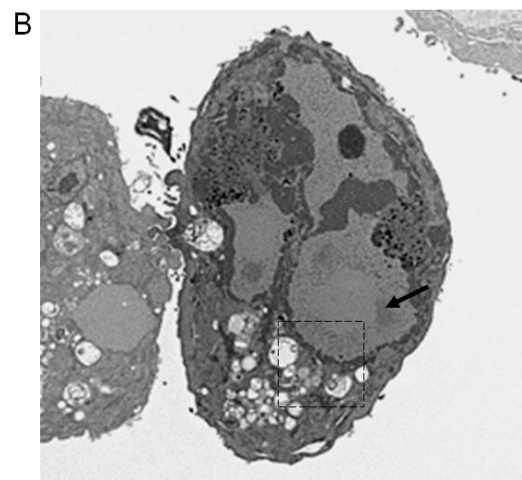


Figure 38: Treatment with Bafilomycin A1 Does Not Have an Effect on Viral Replication. MRC5 cells were treated with DMSO or Bafilomycin A1 at 150 $\mu$ M. They were infected at 100 MOI with Ad300. After 72 hours the supernatant and the cells were collected and subjected to 3 freeze thaw cycles. The virus containing media was used for a hexon staining replication assay.

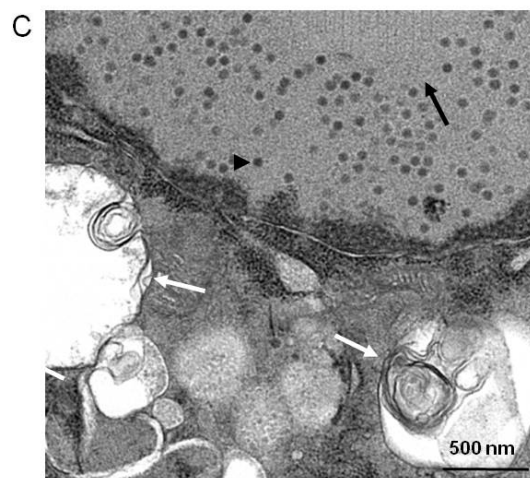




0 hours



72 hours



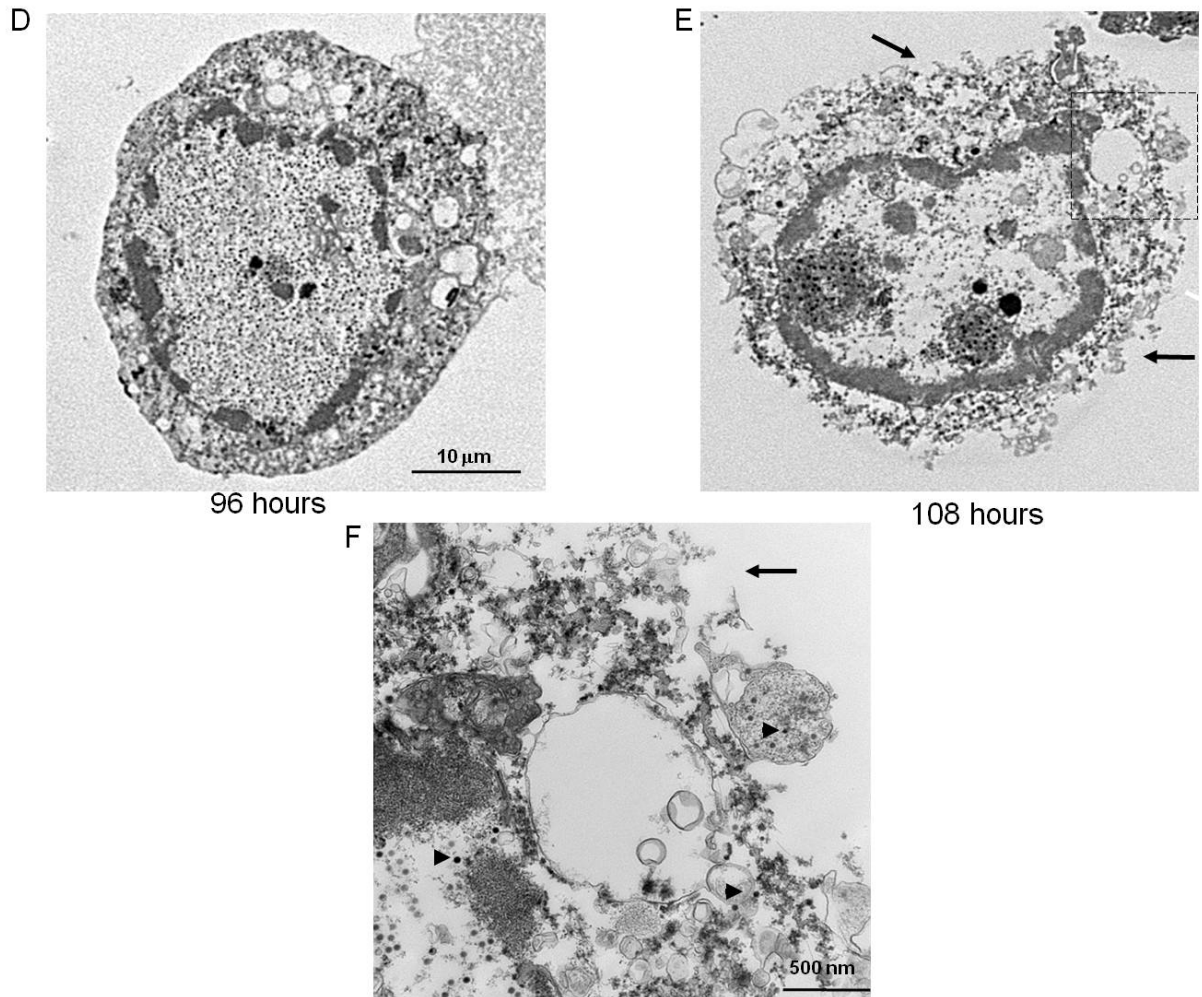


Figure 39: U251 Cells Infected with Ad300 Display Increased Membrane Degradation Over Time.  $1 \times 10^6$  U251 cells were plated in a 10cm dish and infected with 100 MOI. Cells were collected at the time point indicated and analyzed for cell lysis A) 0 hours B) 72 hours C) Inset of 72 hours. Long arrow indicates viral inclusion. White arrow shows double membrane. Small arrow indicated virus particle. D) 96 hours E) 108 Hours. Long arrow indicates membrane breakage. F) Inset of 108 hours. Small arrow indicates virus particle. Long arrow indicates membrane breakage.

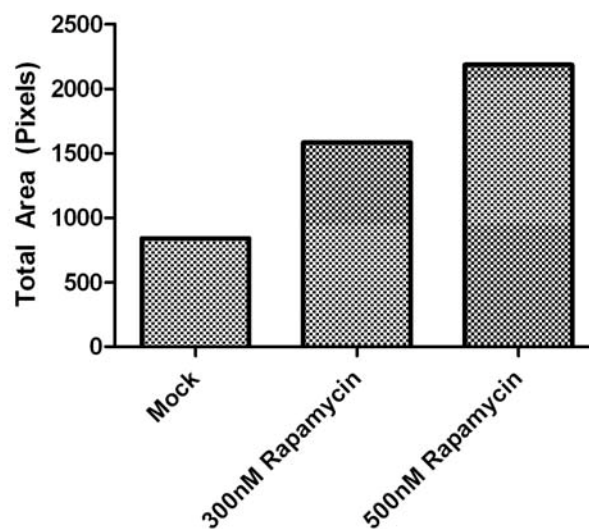
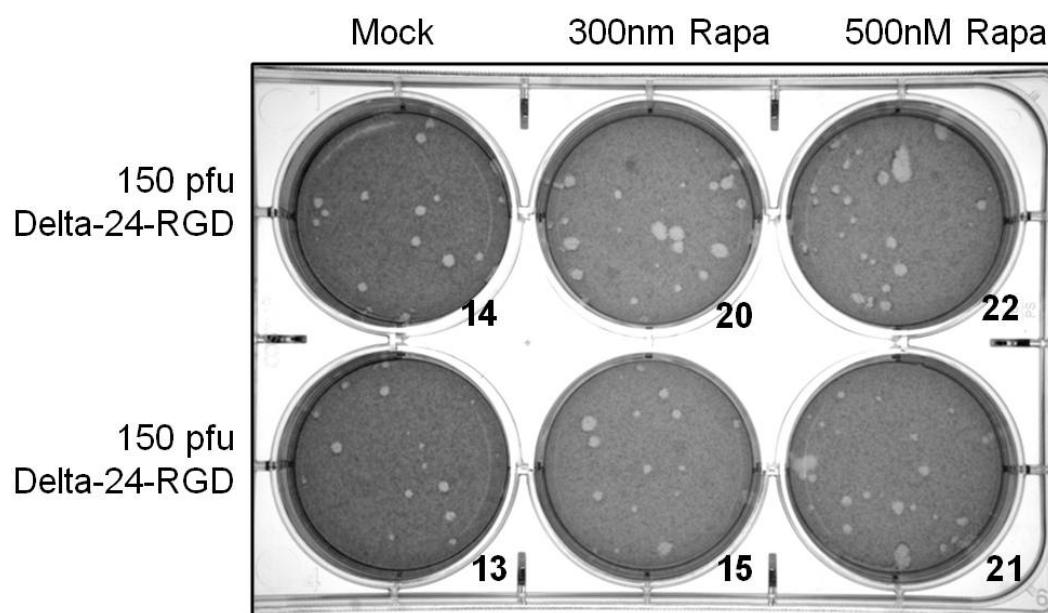


Figure 40: Rapamycin Increased the Number of Plaques and the Size. Cells were plated, infected as indicated, overlaid with agarose, and treated with Rapamycin as indicated. 7 days later the cells were stained with MTT and lysis was quantified.

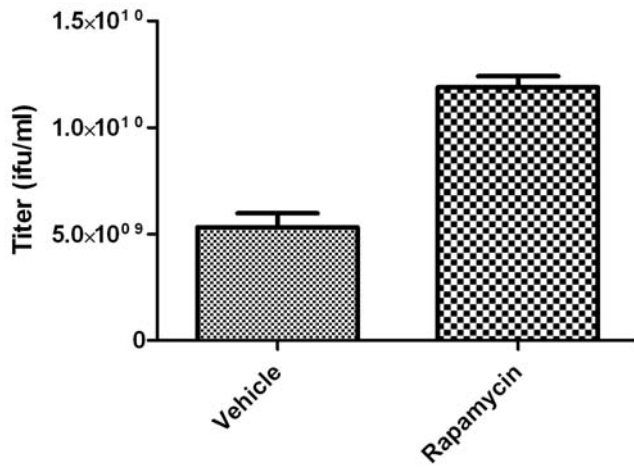


Figure 41: Rapamycin Increased Viral Titer. U251 cells were treated with DMSO or Rapamycin at 300nM. They were infected at 100 MOI with Ad300. After 96 hours the supernatant and the cells were collected and subjected two 3 freeze thaw cycles. The virus containing media was used for a hexon staining replication assay.  $p=0.0052$

We also wanted to further study the phenomenon of increased viral lysis with autophagy inducers and thus we chose 2-deoxyglucose (98). 2-deoxyglucose is a glucose analog that cannot be broken down and halts glycolysis (99). Treatment of U2-OS cells with virus alone at 200 and 400 PFU did not increase the total area of pixels (figure 41). There was a 2.9 fold increase in the total pixel area with 800 PFU. Looking at the same PFU but with treatment and without treatment with 2-DG showed a 1.28, 5.78, and 3.18 fold increase for 200, 400 and 800 PFU, respectively. The autophagy inducer 2-DG, similar to rapamycin, increases cell lysis.

Conversely, experiments with an autophagy inhibitor, 3-MA were undertaken to examine the effect of autophagy impairment on cell lysis. Cells were treated with 1mM and 3mM 3-MA and infected at 150 PFU (figure 42). There was a decrease in the total number of plaques after 3-MA treatment and there was also 3-fold decrease in the total read of plaques, however not in a dose dependent manner. Therefore, we can conclude that inhibition of autophagy with 3-MA decreases viral spread.

## **5.2 3-MA decreases cell lysis**

As a more direct assay for examining lysis, we used a dye, ethidium homodimer-1 that only stains dead (permeable) cells. We used 3-MA to inhibit autophagy during virus infection. As proof of principle, we stained the cells with acridine orange and there was a significant decrease in AVO positive cells after treatment with 3-MA (student's t-test  $p=0.001$ ) and there was a significant

increase in AVO positive cells after virus treatment with water as a control (student's t-test  $p=0.005$ ) (figure 44a). To examine the lysed cells we sorted the cells along with x-axis with forward scatter and along with y-axis with log FL-3. Treatment with the virus and water as a control led to a 25% increase in lysed cells (student's t-test  $p=0.001$ ), while treatment with virus and 3-MA leads to less than a 15% increase in lysed cells (student's t-test  $p=0.003$ ) (figure 44b).

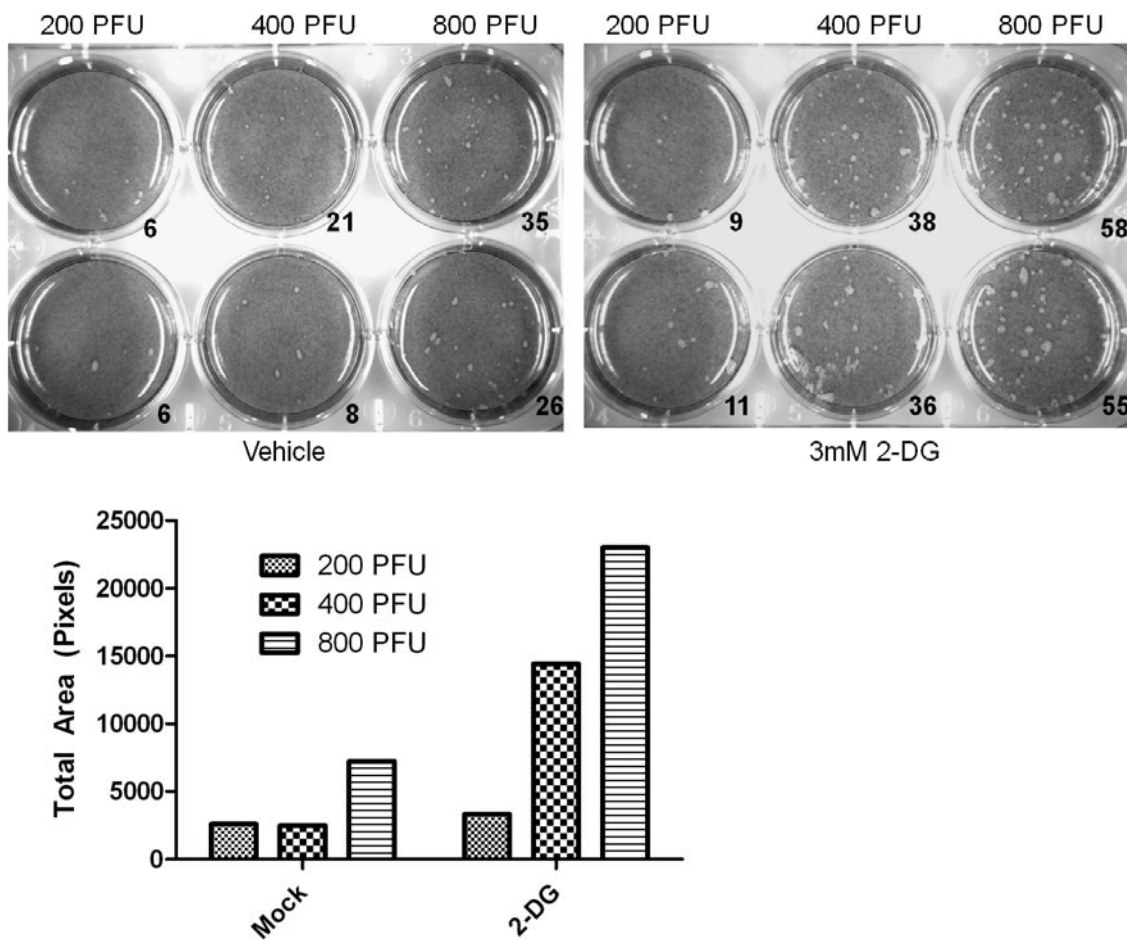


Figure 42: 2-Deoxyglucose Increased the Number of Plaques and the Size of Plaques. Cells were plated, infected as indicated, overlaid with agarose, and treated with 2-DG as indicated. 7 days later the cells were stained with MTT and lysis was quantified.

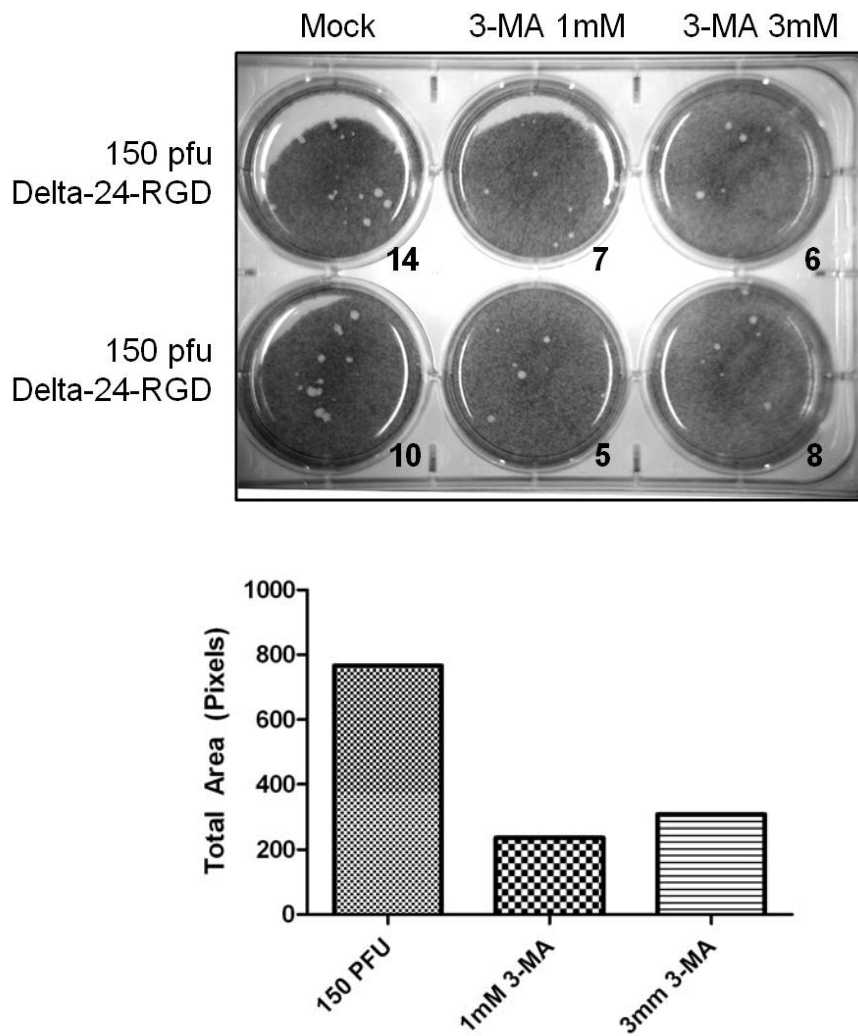


Figure 43: 3-Methyladenine Decreased Plaque Number and Overall Plaque Size. Cells were plated, infected as indicated, overlaid with agarose, and treated with 3-MA as indicated. 7 days later the cells were stained with MTT and lysis was quantified.

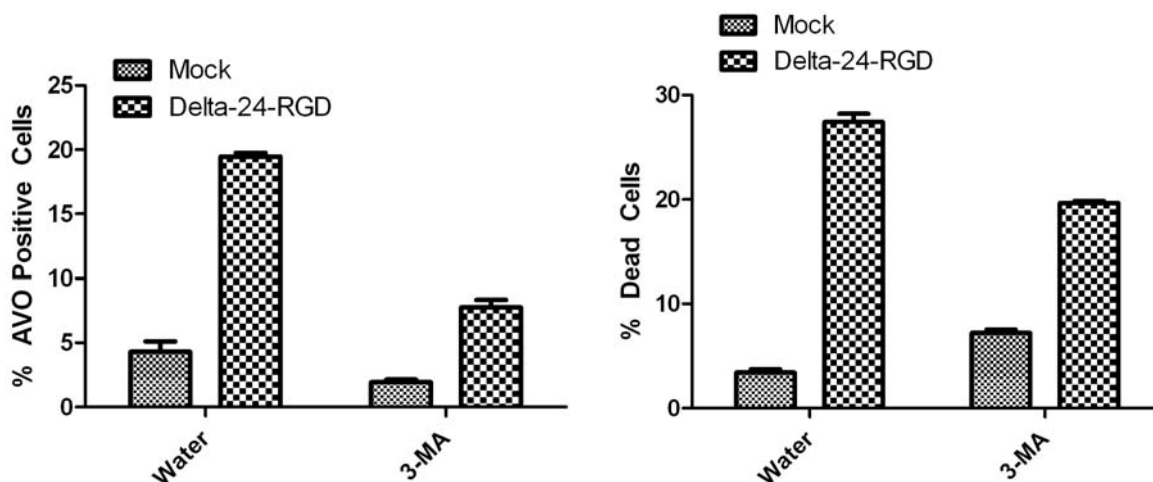


Figure 44. 3-MA Inhibits AVO formation and Cell Lysis. U-87 cells were treated with 3-MA and adenovirus and analyzed for AVO formation and cell lysis using ethidium homodimer 1.

### 5.3 Knockdown or downmodulation of ATG5 impairs cell lysis

We also used a cell biology approach to inhibit autophagy versus using chemical inhibition. Atg5 knockout mouse embryonic fibroblasts were a gift from Dr. Seiji Kondo (100). In order to understand the role autophagy plays during lysis we utilized autophagy-deficient ATG5 knockout MEFs to study lysis during viral infection. The first experiment was to study the morphological changes after virus infection. Electron microscopy revealed a complete difference in morphology between the wild-type and knockout cell lines (figure 45). The morphology was similar to the GCN2 deficient cells after infection with adenovirus. There was no rounding of the cells, no accumulation of autophagosomes or degradation of the cytoplasm in knockout cells compared to



wild-type cells. Cytoplasmic whorls were present in the wild-type infected cell line. We concluded that Atg5 null cells do not display a phenotype corresponding to autophagy after adenovirus infection. We decided to study this further using lysis assays.

Infection of wild type and ATG5 deficient cells led to a drastically different phenotype. Infection with the virus in autophagy deficient cells does not cause cytopathic effect. In a dose dependent experiment infection with 20, 50 and 100 MOI leads to a complete conversion of LC3-I to LC3-II at 100 MOI and no conversion at all in the ATG5 knockout MEFs (figure 46). Interestingly there is differential expression in fiber between the two cell lines. Fiber starts to accumulate at 20 MOI and it does not start to appear in the wild-type cells until 50 MOI. Wild-type mouse cells undergo autophagy and cells deficient for ATG5 do not undergo autophagy.

Next we examined the difference between cell lysis in these two cell lines. Application of ethidium homodimer-1 to the cells revealed a 3.5% cell death with mock, and 10.2, 37.9 and 69.8 for 20, 50 and 100 MOI respectively (figure 47). While in the ATG5 deficient cell lines the amount of cell lysis was 1.9, 2.6, 5.0 and 9.1 for mock, 20, 50, and 100 MOI respectively. While there was a slight increase in the number of lysed cells there was still a 7.7 fold increase in the number of lysed cells after 100 MOI between the two cell lines. This experiment showed that autophagy is important for cell lysis.

When we analyzed replication we found there was no difference between Bafilomycin A1 treated cells and vehicle treated cells. We opted to downregulate the autophagy protein ATG5 to inhibit autophagy (figure 48). We stably transfected U87 cells with shRNA against ATG5 and selected the two clones with the largest decrease of ATG5 and least functional autophagy pathway. Western blot analysis confirmed the decrease in ATG5 expression and we used 2 clones, #2 and #11 for our experiments. Upon infection of the cells with 10 MOI Delta-24-RGD for 72 hours there was complete conversion of LC3-I to LC3-II in the parental and shControl cell line (figure 47). However, in the shATG5 2 and 11 cell lines there was no conversion despite the presence of the viral protein fiber. Therefore, similar to the mouse cell lines, ATG5 does play a role in adenovirus-mediated autophagy and deletion or knocking down ATG5 impairs autophagy induction.

We subsequently analyzed lysis in these cell lines. Further analysis with acridine orange revealed there was a 30% decrease in AVO positive cells between shControl and shATG5 11 (student's t-test  $p=0.0005$ ) (figure 52). Application of ethidium homodimer-1 revealed a  $60.9\pm4.2\%$  decrease in the number of lysed shATG511 cells compared to the shControl cell line (student's t-test  $p=0.00326$ ) (figure 51). There  $21.6\pm1.1\%$  and  $25.7\pm1.7\%$  dead cells in the parental and shControl infected cells compared to  $2.6\pm0.0\%$  and  $3.3\pm0.4\%$  under mock conditions (student's t-test  $p=0.001$ ,  $p=0.0027$  respectively). Deletion of ATG5 plays a significant role in AVO formation and cell lysis.

We performed a burst cell assay on these clones to identify whether lack of replication was important to cell lysis (figure 50). Parental, shControl, and two shATG5 cell lines were infected at 100 MOI for one hour, the media was replaced and the supernatant was analyzed for E1A transcripts 24 hours later by quantitative-real time PCR. There was no statistical difference between the control and knockdown cell lines. We also analyzed production of infectious viral progeny. The two control and two knockdown cell lines were infected at 10 MOI and the cell lysates and supernatant were collected 72 hours post infection and analyzed for viral particle quantitation. There was no statistical difference between the control and knockdown cell lines, indicating replication was not compromised in these cells.

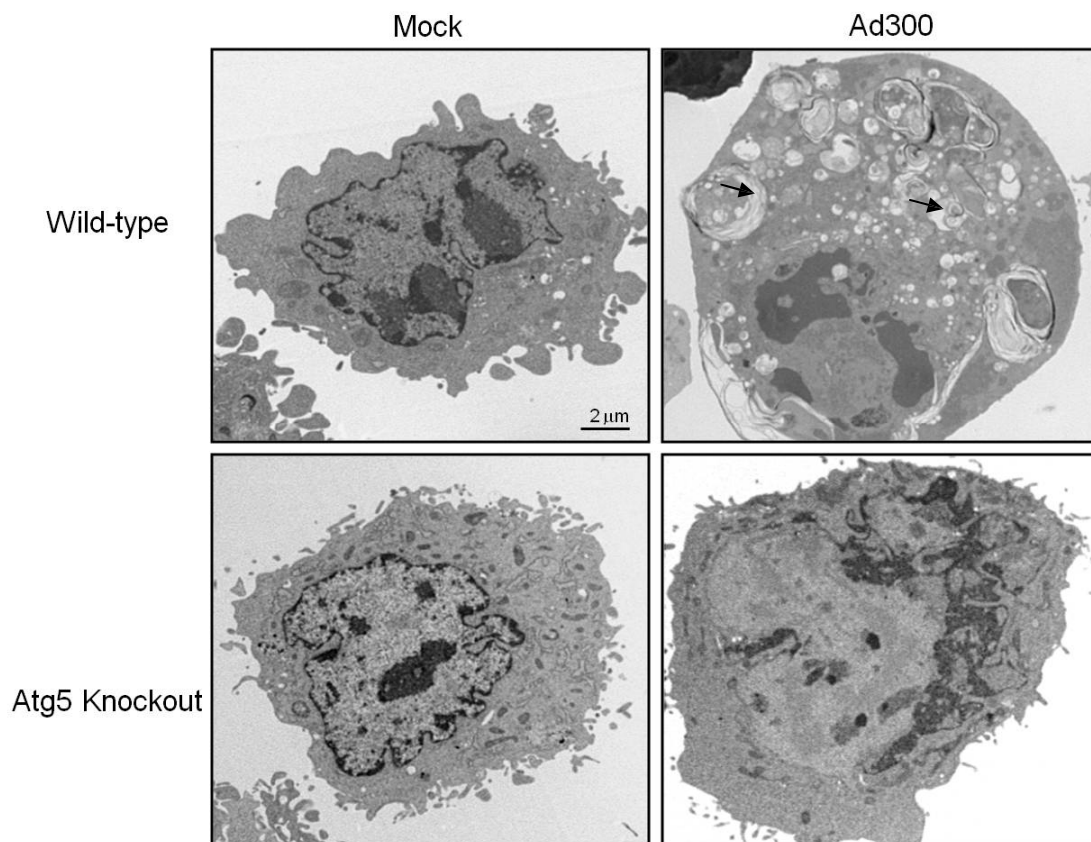


Figure 45: Infection of ATG5 Knockout MEFs Did Not Induce Autophagic Vacuole Formation. Atg5 wild-type and Atg5 knockout MEFs were infected at 100 MOI for 72 hours. There were fixed and subjected to processing for electron microscopy. Arrows indicate autophagosomes.

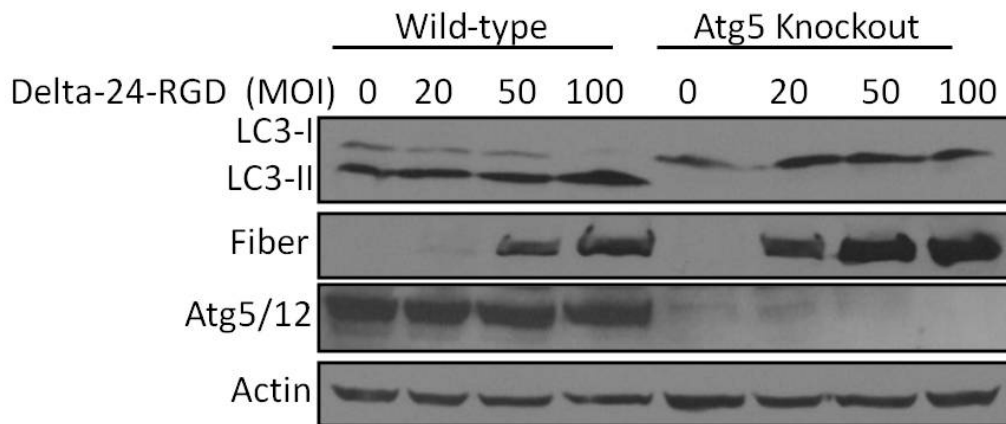


Figure 46: Infection of ATG5 Knockout MEFs Did Not Induce LC3 Cleavage.

ATG5 wild-type and ATG5 knockout cells were infected as indicated and after 72 hours the cells were subjected to Immunoblotting for virus and autophagy proteins.

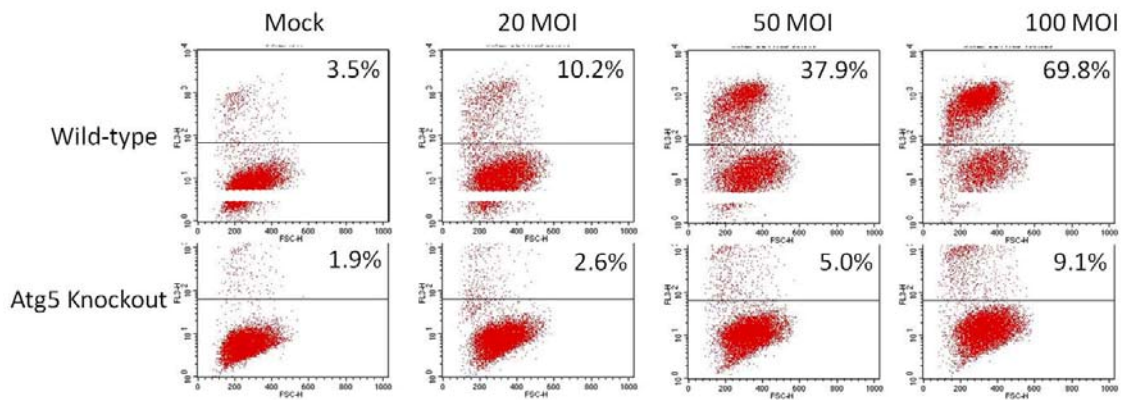


Figure 47: Membrane Degradation was Decreased in ATG5 Null Cells Compared to Wild-type. Atg5 wild-type and Atg5 knockout mouse embryonic fibroblasts were infected as indicated for 72 hours and incubated with 8 $\mu$ M Ethidium Homodimer 1 for 15 minutes and analyzed by flow cytometry for cell membrane permeability

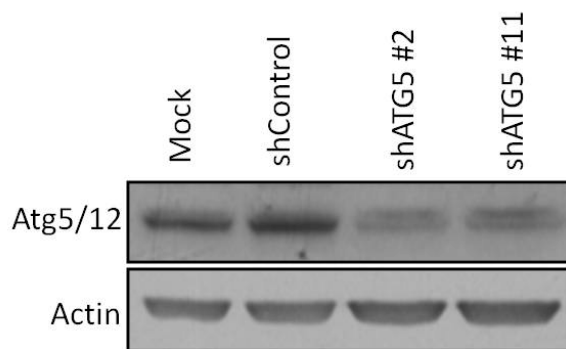


Figure 48: Generation of an ATG5 Downregulated Cell Line. U87 cells were transfected with an shATG5 plasmid. Clones were chosen and assayed for ATG5 expression.

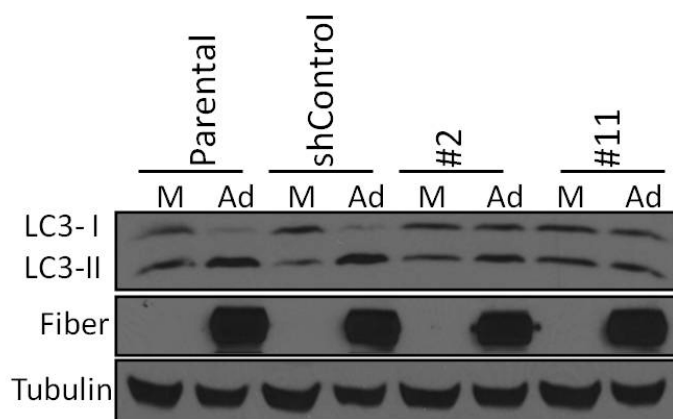


Figure 49: Cells with Downregulated ATG5 Failed to Cleave LC-3 After Adenovirus Infection. Cells were infected at 10 MOI for 72 hours and the protein was collected and assayed for LC-3 cleavage and the adenoviral structural protein fiber.

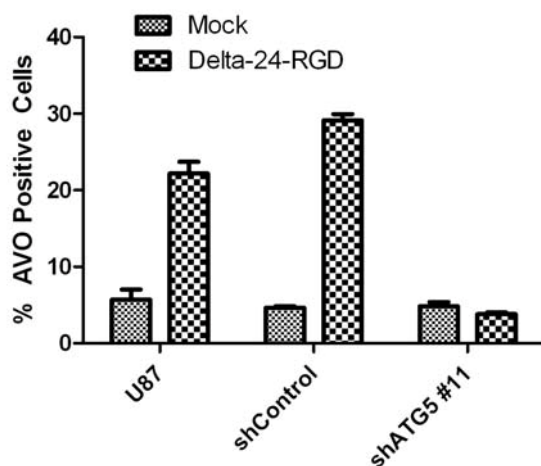


Figure 50: Downregulation of ATG5 Led to Decreased Acidic Compartment Volume. Cells were seeded in a 6-well plate and infected with Delta-24-RGD for 48 hours. Cells were analyzed by flow cytometry after acridine orange staining.

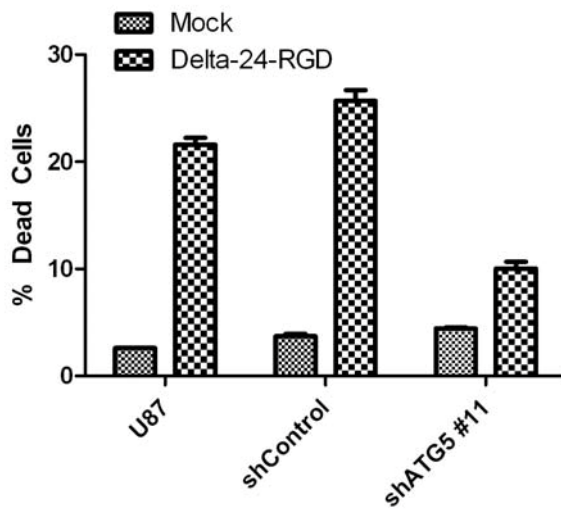


Figure 51: Downregulation of ATG5 Decreased Cell Lysis. U87 Parental, shControl and shATG5 cells were infected at 10 MOI for 72 hours and incubated with 8 $\mu$ M Ethidium Homodimer 1 for 15 minutes and analyzed by flow cytometry for cell membrane permeability.

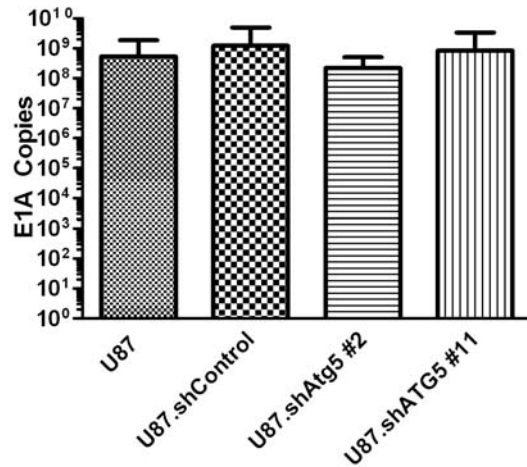


Figure 52: Downregulation of ATG5 Did Not Affect Viral Replication. The U87 parental, control, and shATG5 cells were infected with Delta-24-RGD at 100 MOI for 24 hours. A) The media was collected and used as a template for E1A PCR to determine the number of E1A copies. B) The supernatant and the cells were collected and subjected to 3 freeze thaw cycles. The virus containing media was used for a hexon staining replication assay.



## Chapter 4

### Conclusions

- 1) Infection with a replication-deficient virus failed to induce autophagosomes formation.
- 2) Replication deficient viruses, as opposed to replication competent, failed to induce cleavage of LC3 I to LC3 II and degradation of p62.
- 3) Cells infected with a replication competent adenovirus induced GFP-LC3 punctuation.
- 4) Cells infected with a replication competent adenovirus increased the acidic compartment of the cell, correlating with autophagy.
- 5) Transient, exogenous expression of E1A did not increase LC3 conversion or increase p62 degradation.
- 6) Electron Micrograph studies revealed E1B55K, E1B19K, E3, E4, and VARNA mutant adenoviruses induce autophagy.
- 7) E1B55K, E1B19K, E3, E4, and VARNA mutant adenoviruses induced GFP-LC3 punctuation, thus correlating with autophagy.

- 8) AKT was activated during virus infection.
- 9) Loss of AMPK had no effect on adenovirus-mediated autophagy.
- 10) eIF2 $\alpha$  phosphorylation correlated with p62 degradation after virus infection.
- 11) Adenovirus did not upregulate ER-stress proteins.
- 12) Loss of GCN2 rendered the cell resistant to adenovirus infection.
- 13) Loss of GCN2 correlated with resistance to autophagy after adenovirus infection.
- 14) *In vivo* infected wild-type mice underwent autophagy in the liver while GCN2 knockout mice failed to undergo autophagy.
- 15) Livers of GCN2 knockout mice displayed twice as much necrosis and cell death compared to wild-type mice.
- 16) Infection with adenoviruses increased the number of autophagic vacuoles and Bafilomycin decreased the turnover over autophagic vacuoles without impairing replication.
- 17) Lysis of the cell after adenoviral infection was a late process.

18) The use of autophagy inducers increased the size of viral plaques, while the autophagy inhibitor 3-MA reduced the size of plaques.

19) ATG5 null MEFs and shATG5 cells failed to undergo autophagy and have decreased cell lysis.

During this study we found that replication is not sufficient to induce autophagy and that only viruses that replicate can induce autophagy. We found that, of the early genes tested, there was not one single gene that was responsible for the induction of autophagy however, evidence showed that E1B19K does contribute to adenovirus-mediated autophagy by interacting with Beclin1 and excluding BCL-2 from the PI3K-CIII-Beclin 1 interactome. Examination of the cellular pathways proved more promising in understanding the regulation of autophagy during adenovirus mediated autophagy. The classical starvation pathway of autophagy induction, AKT/mTOR, does not seem to play a role in adenovirus-mediated autophagy. However, the intracellular amino acid sensing pathway, GCN2/eIF2 $\alpha$ , is required for adenovirus mediated autophagy. Cells lacking GCN2 fail to undergo autophagy after adenovirus infection and are more viable *in vitro*. On the other hand, in the *in vivo* setting GCN2 deficient mice are unable to cope with viral infection and their livers undergo more cell death. We used this idea of autophagy and cell death and examined the role of autophagic cell death and lysis. We found that cells unable to undergo autophagy through chemical inhibition or deletion

of crucial autophagy genes had impaired lysis; while cells that had increased autophagy flux through chemical manipulation underwent more autophagy.

## Chapter 5

### Discussion

The relationship between adenovirus and autophagy is relatively unexplored compared with that between other viruses and autophagy. Most papers have only reported that autophagy coexists in a cell infected with adenovirus or in conjunction with a therapeutic treatment (13, 27-30, 101). However, we believe that our results provide insight into the role of autophagy during adenovirus infections. Previous studies have shown that adenoviruses induce autophagy (13, 27-30, 101, 102); however, only LC3 conversion and increased Atg5/12 have been identified as biochemical markers. In this study, we validated the changes in p62 observed in other autophagy studies (18); these changes may be useful as biochemical markers for autophagy during adenoviral infections (69). This addition to the overall studies with adenovirus and autophagy are beneficial because p62 degradation and addition of Bafilomycin A (103) can be used to monitor autophagy flux (11). Therefore the functional output of autophagy can be studied.

We began our studies examining whether infection alone was sufficient to induce autophagy. We proposed that adenovirus replication induces a hyper anabolic state that consumes large amounts of ATP and amino acids (32). We found that infection alone was not sufficient to induce autophagy, therefore there must be a role for viral proteins or the act of replication itself that induces autophagy. To identify the specific role each early gene played we infected cells

deleted with each early gene. Of the early genes tested we were not able to definitively prove that loss of these proteins was responsible for autophagy induction. No virus was completely devoid of the induction of autophagy. Some viruses were attenuated, for example E1B19K, but the only virus that had a complete ablation of autophagy was the Delta-E1 virus, lacking E1A. The caveat is that a virus deleted for E1A is also replication deficient. Therefore we cannot separate the function of E1A for the cause of replication or its functions in inducing autophagy. Exogenous restoration of E1A failed to induce autophagy, however this is a very artificial way to attempt to replicate the role of E1A within the cell. It is possible that E1A corroborates with other viral proteins to exert its full function (47, 104). We believe further studies are needed that are able to examine the role E1A plays specifically in the context of autophagy induction.

Because of the attenuated autophagy induction we decided to delve into the viral protein-cellular protein interaction of E1B19K and Beclin 1. Yeast two hybrid screens had never shown E1B19K to interact with Beclin 1 (105). This is the first time that E1B19K has been shown to associate in a complex with Beclin 1. Beclin 1 is a positive regulator of autophagy. We found that Beclin 1, E1B19K, and PI3K CIII all associate in a complex and remove BCL2 to induce autophagy. It is possible that E1B19K stabilizes the complex to promote autophagy or E1B19K is involved in competitive binding with BCL2 to bind to Beclin 1.

Although no single early gene appears to be required for autophagy induction we cannot rule out the interplay of two or more early genes to exert a

cellular function (47, 106). Therefore further studies with the deletion of two or more viral proteins need to be done to fully examine the role viral proteins play in adenovirus-mediated autophagy.

We also monitored the intracellular status of the cells to identify any changes that were related to autophagy pathways. We proposed that the cells are in a hyperanabolic status during virus infection and we did, in fact, find a significant decrease in ATP. However, upon examination of the kinases that sense and regulate ATP levels we found no involvement in autophagy regulation during virus infection. The lack of involvement of LKB1 and AMPK in autophagy regulation could be because their function is regulating protein translation during virus infection.

The downstream effector in the AMPK pathway is mTOR (reviewed by (107)). mTOR is primarily known as a monitor of cell growth by controlling S6K1 and 4E-BP1, and by regulating autophagy through via interaction with ULK1 (69). mTOR is activated by growth factors, AKT, and AMPK (reviewed by (107)). Generally speaking, autophagy is primarily known to be triggered through the AKT/PDK1/mTOR pathway (3). We analyzed TSC2 within this pathway and did not find a requirement of TSC2 in adenovirus-mediated autophagy. We also did not find the mTOR was inhibited during virus infection. We found that AKT was only fully activated at 48 hours post infection. Carloni *et al* reported an mTOR feedback loop activation of AKT in the presence of growth factor receptor stimulation(108) which is relevant to virus infection because O'Shea *et al* 2005 reported that adenovirus mimics growth factor signals to activate mTOR (53,

109, 110). We also found that p70S6K was phosphorylated throughout the experiment and this contradicts the phosphorylation status of mTOR. Nonetheless, it has been reported that E1A regulates phosphorylation of S6K1 and 4E-BP1 independently of mTOR to facilitate viral replication (53, 111). Therefore more information is needed to clarify the role of mTOR by coupling or uncoupling the downstream substrates and identify their participation in protein translation inhibition and autophagy induction. We believe that AKT pathway activation is more involved in protein translation for productive viral replication (53), however, these studies do not provide evidence for a role in the induction of autophagy. Further studies are warranted to understand the role of AKT activation during adenovirus infection and the possibility of an mTOR independent mechanism.

Basal levels of eIF2 $\alpha$  phosphorylation under normal conditions is around 5-10% (82-84). 25% of eIF2 $\alpha$  was phosphorylated in the late stage of adenovirus infection (85). eIF2 $\alpha$  activation, upon adenovirus infection, has historically been attributed to PKR activation, despite the fact adenovirus employs VA RNA against PKR, 25% of eIF2 $\alpha$  remains phosphorylated. We propose that the adenovirus neutralized PKR to inhibit an immune response, not to control translation. In vitro phosphorylation assays revealed that activation of PKR and subsequent phosphorylation of PKR are not sufficient to halt protein translation, suggesting another alternative motive (85). We too saw an increase in eIF2 $\alpha$  phosphorylation and hypothesize that the purpose is to regulate autophagy.



Previous studies have described the relationship between herpes viruses and the regulation of autophagy through eIF2 $\alpha$  pathway (66). Tallóczy et al reported the GCN2 and PKR play roles in starvation and virus induced autophagy, respectively (66). Since PKR does not play a role in eIF2 $\alpha$  regulation during adenovirus infection we chose not to examine PKR in autophagy induction. Kouroku et al in 2006 identified that polyQ overexpression lead to increase of LC3 conversion and was ablated in eIF2 $\alpha$  S51A Mefs and Atg5 KO MEFs along with an increase in ATG5/12 (67). We also saw similar increase in LC3 conversion and ATG5/12 increase during adenovirus infection (13). However, we saw an unexpected decrease in the PERK-regulated chaperone folding proteins, if the cell were under ER stress we would expect the levels of expression to increase. Therefore GCN2 seemed to be the prime candidate of examination.

We noted that cells lacking GCN2 were rendered resistant to the cytopathic effect of the virus and these cells were unable to undergo autophagy. We believed that the cells infected with adenovirus consumed large amounts of amino acids and the cell was able to activate GCN2 to respond to the decline in free amino acids, however when GCN2 is ablated, the cell has an impaired ability to sense the amino acids and fails to induce autophagy therefore impairing viral production. Mice deficient for GCN2 fail to undergo autophagy in the liver suggesting that GCN2 does play a role in autophagy regulation during *in vivo* viral life cycle. We were surprised to see that the livers in GCN2 null mice underwent twice the amount of cell death *in vivo* and correlated with decreased

viability. We believe that autophagy is a protective mechanism and when the cells were not able to undergo autophagy in the *in vivo* niche the hepatocytes died by necrosis.

Neither our studies, nor Tallóczy *et al* and Kouroku *et al*, identified a complete mechanism of the role eIF2 $\alpha$  plays in the induction of autophagy (66, 67). A complete study of the eIF2 $\alpha$  pathway is needed to isolate its involvement in adenovirus-mediated autophagy. We believe the experiments here provide evidence for a role of GCN2 during adenovirus infection. However, more experiments are needed to identify the interplay between GCN2 and the autophagy pathway. GCN2 has been implicated during infection with Sindbis virus where GCN2 serves as an inhibitory molecule of viral replication by blocking viral translation during infection (86). They attributed this to the increased phosphorylation of eIF2 $\alpha$ , however no downstream effectors were analyzed. Ryzmski *et al* 2010 reported that bortezomib induces ER-stress and induces autophagy through an eIF2 $\alpha$ /ATF4 dependent mechanism (87). Activating transcription factor 4 (ATF4) binds the cyclic AMP response element binding domain of LC3, leading to transcriptional upregulation (87, 88). The ATF4 binding partner CHOP has been shown to bind and upregulate ATG5 (88). However, our transcriptional activation studies have not shown any increase in ATG5 or LC3 after virus infection (data not shown). We postulate this could be due to the short turnover of the mRNAs, therefore an accumulation of mRNA is difficult to identify.

The relationship between autophagy and adenovirus-mediated cell lysis has yet to be fully examined. We speculate that the generation of vacuoles in the cytoplasm destroys the intracellular and membrane integrity of the cell facilitating breakage of the membrane to aid in viral lysis. Here, for the first time, we show that autophagy plays an essential role in the process of cell lysis induced by adenovirus.

In the past there are three main viral proteins that have been the focus of mediating viral cell lysis. The L3 viral protease cleaves cytokeratin K18 and promoting lysis . There are a few reports suggesting that viral proteins regulate the cell lysis process (112). The E3 11.6-kD adenovirus death protein (ADP), aids in the destruction of the nuclear membrane and release of progeny virions (50, 51). Overexpression of ADP was shown to increase oncolysis by adenoviruses (113). It is unknown whether these two proteins play a role in the regulation of autophagy.

Nevertheless, our data clearly demonstrate that autophagy plays an essential role in adenovirus-mediated cell lysis. Treatment of cells with autophagy inducers increases the size of plaques which one can attribute to cell lysis, while treatment with 3-MA, an autophagy inhibitor, decreases the area of plaques. Consistent with the above observations, knockout or downmodulation of the key autophagy gene *ATG5* substantially impairs the ability of the virus to induce lysis of host cells. Thus, there is a cause-and-effect relationship between autophagy and cell lysis. This suggests that autophagy, a highly genetically

programmed cellular process, is a candidate target whose manipulation might improve the efficiency of oncolytic adenovirus to induce lysis in cancer cells.

Our results here also provide a mechanistic rationale for our previous reports showing that rapamycin has a synergistic effect with oncolytic adenoviruses and strongly suggest that rapamycin-enhanced oncolytic potency is due to facilitation of autophagy (28). These findings offer a rationale for the combination of autophagy inducing drugs and oncolytic adenoviruses to enhance glioma treatment. In this regard, the gold standard for glioma treatment, temozolomide, induces autophagy and has synergistic effects with oncolytic adenoviruses (27).

In summary, we demonstrate here that GCN2 plays a significant role in the regulation of adenovirus-mediated autophagy and that autophagy plays an indispensable role in adenovirus-mediated cell lysis. Our study provides a new mechanism for adenovirus-induced cell lysis through which strategies can be imposed to improve oncolytic adenoviral potency in cancer therapy.

## References

1. Furnari, F. B., T. Fenton, R. M. Bachoo, A. Mukasa, J. M. Stommel, A. Stegh, W. C. Hahn, K. L. Ligon, D. N. Louis, C. Brennan, L. Chin, R. A. DePinho, and W. K. Cavenee. 2007. Malignant astrocytic glioma: genetics, biology, and paths to treatment. *Genes & Development* 21:2683-2710.
2. Stupp, R., W. P. Mason, M. J. van den Bent, M. Weller, B. Fisher, M. J. Taphoorn, K. Belanger, A. A. Brandes, C. Marosi, U. Bogdahn, J. Curschmann, R. C. Janzer, S. K. Ludwin, T. Gorlia, A. Allgeier, D. Lacombe, J. G. Cairncross, E. Eisenhauer, and R. O. Mirimanoff. 2005. Radiotherapy plus concomitant and adjuvant temozolomide for glioblastoma. *N Engl J Med* 352:987-996.
3. Levine, B., and D. J. Klionsky. 2004. Development by Self-Digestion: Molecular Mechanisms and Biological Functions of Autophagy. *Developmental Cell* 6:463-477.
4. Tsukada, M., and Y. Ohsumi. 1993. Isolation and characterization of autophagy-defective mutants of *Saccharomyces cerevisiae*. *FEBS Letters* 333:169-174.
5. Otto, G. P., M. Y. Wu, N. Kazgan, O. R. Anderson, and R. H. Kessin. 2003. Macroautophagy Is Required for Multicellular Development of the Social Amoeba *Dictyostelium discoideum*. *Journal of Biological Chemistry* 278:17636-17645.

6. Juhász, G., G. Csikós, R. Sinka, M. Erdélyi, and M. Sass. 2003. The *Drosophila* homolog of Aut1 is essential for autophagy and development. *FEBS Letters* 543:154-158.
7. Scott, R. C., O. Schuldiner, and T. P. Neufeld. 2004. Role and Regulation of Starvation-Induced Autophagy in the *Drosophila* Fat Body. *Developmental Cell* 7:167-178.
8. Melendez, A., Z. Talloczy, M. Seaman, E.-L. Eskelinen, D. H. Hall, and B. Levine. 2003. Autophagy Genes Are Essential for Dauer Development and Life-Span Extension in *C. elegans*. *Science* 301:1387-1391.
9. Kuma, A., M. Hatano, M. Matsui, A. Yamamoto, H. Nakaya, T. Yoshimori, Y. Ohsumi, T. Tokuhiisa, and N. Mizushima. 2004. The role of autophagy during the early neonatal starvation period. *Nature* 432:1032-1036.
10. Yue, Z., S. Jin, C. Yang, A. J. Levine, and N. Heintz. 2003. Beclin 1, an autophagy gene essential for early embryonic development, is a haploinsufficient tumor suppressor. *Proceedings of the National Academy of Sciences of the United States of America* 100:15077-15082.
11. Klionsky, D. J., H. Abeliovich, P. Agostinis, D. K. Agrawal, G. Aliev, D. S. Askew, M. Baba, E. H. Baehrecke, B. A. Bahr, A. Ballabio, B. A. Bamber, D. C. Bassham, E. Bergamini, X. Bi, M. Biard-Piechaczyk, J. S. Blum, D. E. Bredesen, J. L. Brodsky, J. H. Brumell, U. T. Brunk, W. Bursch, N. Camougrand, E. Cebollero, F. Cecconi, Y. Chen, L. S. Chin, A. Choi, C. T. Chu, J. Chung, P. G. Clarke, R. S. Clark, S. G. Clarke, C. Clave, J. L. Cleveland, P. Codogno, M. I. Colombo, A. Coto-Montes, J. M. Cregg, A.

M. Cuervo, J. Debnath, F. Demarchi, P. B. Dennis, P. A. Dennis, V. Deretic, R. J. Devenish, F. Di Sano, J. F. Dice, M. Difiglia, S. Dinesh-Kumar, C. W. Distelhorst, M. Djavaheri-Mergny, F. C. Dorsey, W. Droge, M. Dron, W. A. Dunn, Jr., M. Duszenko, N. T. Eissa, Z. Elazar, A. Esclatine, E. L. Eskelinen, L. Fesus, K. D. Finley, J. M. Fuentes, J. Fueyo, K. Fujisaki, B. Galliot, F. B. Gao, D. A. Gewirtz, S. B. Gibson, A. Gohla, A. L. Goldberg, R. Gonzalez, C. Gonzalez-Estevez, S. Gorski, R. A. Gottlieb, D. Haussinger, Y. W. He, K. Heidenreich, J. A. Hill, M. Hoyer-Hansen, X. Hu, W. P. Huang, A. Iwasaki, M. Jaattela, W. T. Jackson, X. Jiang, S. Jin, T. Johansen, J. U. Jung, M. Kadowaki, C. Kang, A. Kelekar, D. H. Kessel, J. A. Kiel, H. P. Kim, A. Kimchi, T. J. Kinsella, K. Kiselyov, K. Kitamoto, E. Knecht, M. Komatsu, E. Kominami, S. Kondo, A. L. Kovacs, G. Kroemer, C. Y. Kuan, R. Kumar, M. Kundu, J. Landry, M. Laporte, W. Le, H. Y. Lei, M. J. Lenardo, B. Levine, A. Lieberman, K. L. Lim, F. C. Lin, W. Liou, L. F. Liu, G. Lopez-Berestein, C. Lopez-Otin, B. Lu, K. F. Macleod, W. Malorni, W. Martinet, K. Matsuoka, J. Mautner, A. J. Meijer, A. Melendez, P. Michels, G. Miotto, W. P. Mistiaen, N. Mizushima, B. Mograbi, I. Monastyrska, M. N. Moore, P. I. Moreira, Y. Moriyasu, T. Motyl, C. Munz, L. O. Murphy, N. I. Naqvi, T. P. Neufeld, I. Nishino, R. A. Nixon, T. Noda, B. Nurnberg, M. Ogawa, N. L. Oleinick, L. J. Olsen, B. Ozpolat, S. Paglin, G. E. Palmer, I. Papassideri, M. Parkes, D. H. Perlmutter, G. Perry, M. Piacentini, R. Pinkas-Kramarski, M. Prescott, T. Proikas-Cezanne, N. Raben, A. Rami, F. Reggiori, B. Rohrer, D. C. Rubinsztein, K. M. Ryan, J.

- Sadoshima, H. Sakagami, Y. Sakai, M. Sandri, C. Sasakawa, M. Sass, C. Schneider, P. O. Seglen, O. Seleverstov, J. Settleman, J. J. Shacka, I. M. Shapiro, A. Sibirny, E. C. Silva-Zacarin, H. U. Simon, C. Simone, A. Simonsen, M. A. Smith, K. Spaniel-Borowski, V. Srinivas, M. Steeves, H. Stenmark, P. E. Stromhaug, C. S. Subauste, S. Sugimoto, D. Sulzer, T. Suzuki, M. S. Swanson, I. Tabas, F. Takeshita, N. J. Talbot, Z. Talloczy, K. Tanaka, I. Tanida, G. S. Taylor, J. P. Taylor, A. Terman, G. Tettamanti, C. B. Thompson, M. Thumm, A. M. Tolkovsky, S. A. Tooze, R. Truant, L. V. Tumanovska, Y. Uchiyama, T. Ueno, N. L. Uzcategui, I. van der Klei, E. C. Vaquero, T. Vellai, M. W. Vogel, H. G. Wang, P. Webster, J. W. Wiley, Z. Xi, G. Xiao, J. Yahalom, J. M. Yang, G. Yap, X. M. Yin, T. Yoshimori, L. Yu, Z. Yue, M. Yuzaki, O. Zabirnyk, X. Zheng, X. Zhu, and R. L. Deter. 2008. Guidelines for the use and interpretation of assays for monitoring autophagy in higher eukaryotes. *Autophagy* 4:151-175.
12. Mizushima, N., and T. Yoshimori. 2007. How to interpret LC3 immunoblotting. *Autophagy* 3:542-545.
  13. Jiang, H., C. Gomez-Manzano, H. Aoki, M. M. Alonso, S. Kondo, F. McCormick, J. Xu, Y. Kondo, B. N. Bekele, H. Colman, F. F. Lang, and J. Fueyo. 2007. Examination of the Therapeutic Potential of Delta-24-RGD in Brain Tumor Stem Cells: Role of Autophagic Cell Death. *J. Natl. Cancer Inst.* 99:1410-1414.



14. Mizushima, N., T. Noda, T. Yoshimori, Y. Tanaka, T. Ishii, M. D. George, D. J. Klionsky, M. Ohsumi, and Y. Ohsumi. 1998. A protein conjugation system essential for autophagy. *Nature* 395:395-398.
15. Shintani, T., N. Mizushima, Y. Ogawa, A. Matsuura, T. Noda, and Y. Ohsumi. 1999. Apg10p, a novel protein-conjugating enzyme essential for autophagy in yeast. *EMBO J* 18:5234-5241.
16. Mizushima, N., T. Noda, and Y. Ohsumi. 1999. Apg16p is required for the function of the Apg12p-Apg5p conjugate in the yeast autophagy pathway. *EMBO J* 18:3888-3896.
17. Kabeya, Y., N. Mizushima, T. Ueno, A. Yamamoto, T. Kirisako, T. Noda, E. Kominami, Y. Ohsumi, and T. Yoshimori. 2000. LC3, a mammalian homologue of yeast Apg8p, is localized in autophagosome membranes after processing. *EMBO J* 19:5720-5728.
18. Bjorkoy, G., T. Lamark, A. Brech, H. Outzen, M. Perander, A. Årsvatn, H. Stenmark, and T. Johansen. 2005. p62/SQSTM1 forms protein aggregates degraded by autophagy and has a protective effect on huntingtin-induced cell death. *The Journal of Cell Biology* 171:603-614.
19. Pankiv, S., T. H. Clausen, T. Lamark, A. Brech, J. A. Bruun, H. Outzen, A. Overvatn, G. Bjorkoy, and T. Johansen. 2007. p62/SQSTM1 binds directly to Atg8/LC3 to facilitate degradation of ubiquitinated protein aggregates by autophagy. *J Biol Chem* 282:24131-24145.
20. Orvedahl, A., and Levine, B. 2008. Viral Evasion of Autophagy. *Autophagy* 4:280-285.

21. Wileman, T. 2006. Aggresomes and Autophagy Generate Sites for Virus Replication. *Science* 312:875-878.
22. Gosert, R., A. Kanjanahaluethai, D. Egger, K. Bienz, and S. C. Baker. 2002. RNA Replication of Mouse Hepatitis Virus Takes Place at Double-Membrane Vesicles. *J. Virol.* 76:3697-3708.
23. Prentice, E., W. G. Jerome, T. Yoshimori, N. Mizushima, and M. R. Denison. 2004. Coronavirus Replication Complex Formation Utilizes Components of Cellular Autophagy. *Journal of Biological Chemistry* 279:10136-10141.
24. Jackson, W. T., T. H. Giddings, Jr., M. P. Taylor, S. Mulinyawe, M. Rabinovitch, R. R. Kopito, and K. Kirkegaard. 2005. Subversion of Cellular Autophagosomal Machinery by RNA Viruses. *PLoS Biol* 3:e156.
25. Chaumorcet, M., Souquère, S., Pierron, G., Codogno, P., Esclatine, A. 2008. Human cytomegalovirus controls a new autophagy-dependent cellular antiviral defense mechanism. *Autophagy* 4:46-53.
26. Zhou, D., and S. A. Spector. 2008. Human immunodeficiency virus type-1 infection inhibits autophagy. *AIDS* 22:695-699  
610.1097/QAD.1090b1013e3282f1094a1836.
27. Yokoyama, T., E. Iwado, Y. Kondo, H. Aoki, Y. Hayashi, M. M. Georgescu, R. Sawaya, K. R. Hess, G. B. Mills, H. Kawamura, Y. Hashimoto, Y. Urata, T. Fujiwara, and S. Kondo. 2008. Autophagy-inducing agents augment the antitumor effect of telomerase-sense oncolytic adenovirus OBP-405 on glioblastoma cells. *Gene Ther* 15:1233-1239.

28. Alonso, M. M., H. Jiang, T. Yokoyama, J. Xu, N. B. Bekele, F. F. Lang, S. Kondo, C. Gomez-Manzano, and J. Fueyo. 2008. Delta-24-RGD in combination with RAD001 induces enhanced anti-glioma effect via autophagic cell death. *Mol Ther* 16:487-493.
29. Ito, H., H. Aoki, F. Kuhnel, Y. Kondo, S. Kubicka, T. Wirth, E. Iwado, A. Iwamaru, K. Fujiwara, K. R. Hess, F. F. Lang, R. Sawaya, and S. Kondo. 2006. Autophagic Cell Death of Malignant Glioma Cells Induced by a Conditionally Replicating Adenovirus. *J. Natl. Cancer Inst.* 98:625-636.
30. Baird, S. K., J. L. Aerts, A. Eddaoudi, M. Lockley, N. R. Lemoine, and I. A. McNeish. 2007. Oncolytic adenoviral mutants induce a novel mode of programmed cell death in ovarian cancer. *Oncogene* 27:3081-3090.
31. Lamfers, M. L. M., J. Grill, C. M. F. Dirven, V. W. van Beusechem, B. Georger, J. van den Berg, R. Alemany, J. Fueyo, D. T. Curiel, G. Vassal, H. M. Pinedo, W. P. Vandertop, and W. R. Gerritsen. 2002. Potential of the Conditionally Replicative Adenovirus Ad5-{Delta}24RGD in the Treatment of Malignant Gliomas and Its Enhanced Effect with Radiotherapy. *Cancer Res* 62:5736-5742.
32. Jiang, H., E. J. White, C. Gomez-Manzano, and J. Fueyo. 2008. Adenovirus's last trick: you say lysis, we say autophagy. *Autophagy* 4:118-120.
33. Hilleman, M., Werner, J. 1954. Recovery of new agent from patients with acute respiratory illness. *Proc Soc Exp Biol Med* 85:183-188.
34. Jawetz, E. 1959. The story of shipyard eye. *Br Med J* 15:873-876.

35. Rowe, W., Heubner, R., Gilmore, et al. 1953. Isolation of a cytopathogenic agent from human adenoids undergoing spontaneous degeneration of tissue culture. *Proc Soc Exp Biol Med* 84:570-573.
36. De Jong, J. C., A. G. Wermenbol, M. W. Verweij-Uijterwaal, K. W. Slaterus, P. Wertheim-Van Dillen, G. J. J. Van Doornum, S. H. Khoo, and J. C. Hierholzer. 1999. Adenoviruses from Human Immunodeficiency Virus-Infected Individuals, Including Two Strains That Represent New Candidate Serotypes Ad50 and Ad51 of Species B1 and D, Respectively. *J. Clin. Microbiol.* 37:3940-3945.
37. Hierholzer, J. C., Y. O. Stone, and J. R. Broderson. 1991. Antigenic relationships among the 47 human adenoviruses determined in reference horse antisera. *Archives of Virology* 121:179-197.
38. Fields, B. N., D. M. Knipe, and P. M. Howley. 2007. *Fields' virology*. Wolters Kluwer Health/Lippincott Williams & Wilkins, Philadelphia.
39. Fueyo, J., C. Gomez-Manzano, R. Alemany, P. S. Lee, T. J. McDonnell, P. Mitlianga, Y. X. Shi, V. A. Levin, W. K. Yung, and A. P. Kyritsis. 2000. A mutant oncolytic adenovirus targeting the Rb pathway produces anti-glioma effect in vivo. *Oncogene* 19:2-12.
40. Fueyo, J., R. Alemany, C. Gomez-Manzano, G. N. Fuller, A. Khan, C. A. Conrad, T.-J. Liu, H. Jiang, M. G. Lemoine, K. Suzuki, R. Sawaya, D. T. Curiel, W. K. A. Yung, and F. F. Lang. 2003. Preclinical Characterization of the Antiglioma Activity of a Tropism-Enhanced Adenovirus Targeted to the Retinoblastoma Pathway. *J. Natl. Cancer Inst.* 95:652-660.

41. Witlox, A. M., V. W. van Beusechem, B. Molenaar, H. Bras, G. R. Schaap, R. Alemany, D. T. Curiel, H. M. Pinedo, P. I. J. M. Wuisman, and W. R. Gerritsen. 2004. Conditionally Replicative Adenovirus with Tropism Expanded towards Integrins Inhibits Osteosarcoma Tumor Growth in Vitro and in Vivo. *Clinical Cancer Research* 10:61-67.
42. Suzuki, K., J. Fueyo, V. Krasnykh, P. N. Reynolds, D. T. Curiel, and R. Alemany. 2001. A Conditionally Replicative Adenovirus with Enhanced Infectivity Shows Improved Oncolytic Potency. *Clinical Cancer Research* 7:120-126.
43. Bauerschmitz, G. J., J. T. Lam, A. Kanerva, K. Suzuki, D. M. Nettelbeck, I. Dmitriev, V. Krasnykh, G. V. Mikheeva, M. N. Barnes, R. D. Alvarez, P. Dall, R. Alemany, D. T. Curiel, and A. Hemminki. 2002. Treatment of Ovarian Cancer with a Tropism Modified Oncolytic Adenovirus. *Cancer Res* 62:1266-1270.
44. Bauerschmitz, G. J., A. Kanerva, M. Wang, I. Herrmann, D. R. Shaw, T. V. Strong, R. Desmond, D. T. Rein, P. Dall, D. T. Curiel, and A. Hemminki. 2004. Evaluation of a selectively oncolytic adenovirus for local and systemic treatment of cervical cancer. *International Journal of Cancer* 111:303-309.
45. Page, J., B. Tian, K. Schweikart, T. Tomaszewski, R. Harris, T. Broadt, J. Polley-Nelson, P. Noker, M. Wang, S. Makhija, R. Aurigemma, D. Curiel, and R. Alvarez. 2007. Identifying the safety profile of a novel infectivity-enhanced conditionally replicative adenovirus, Ad5-24-RGD, in

- anticipation of a phase I trial for recurrent ovarian cancer. *American journal of obstetrics and gynecology* 196:389.e381-389.e310.
46. Bandara, L. R., and N. B. La Thangue. 1991. Adenovirus E1a prevents the retinoblastoma gene product from complexing with a cellular transcription factor. *Nature* 351:494-497.
  47. Rao, L., Debbas, M., Sabbatini, P., Hockenberry, D., Korsmeyer, S., White, E. 1992. The Adenovirus E1A Proteins Induce Apoptosis, Which is Inhibited by the E1B 19-kDa and Bcl-2 Proteins. *Proc Natl Acad Sci U S A* 89:7742-7746.
  48. Yew, P. R., and A. J. Berk. 1992. Inhibition of p53 transactivation required for transformation by adenovirus early 1B protein. *Nature* 357:82-85.
  49. Crighton, D., S. Wilkinson, J. O'Prey, N. Syed, P. Smith, P. R. Harrison, M. Gasco, O. Garrone, T. Crook, and K. M. Ryan. 2006. DRAM, a p53-induced modulator of autophagy, is critical for apoptosis. *Cell* 126:121-134.
  50. Tollefson, A. E., A. Scaria, T. W. Hermiston, J. S. Ryerse, L. J. Wold, and W. S. Wold. 1996. The adenovirus death protein (E3-11.6K) is required at very late stages of infection for efficient cell lysis and release of adenovirus from infected cells. *J Virol* 70:2296-2306.
  51. Tollefson, A. E., J. S. Ryerse, A. Scaria, T. W. Hermiston, and W. S. Wold. 1996. The E3-11.6-kDa adenovirus death protein (ADP) is required for efficient cell death: characterization of cells infected with adp mutants. *Virology* 220:152-162.

52. Halbert, D. N., J. R. Cutt, and T. Shen. 1985. Adenovirus early region 4 encodes functions required for efficient DNA replication, late gene expression, and host cell shutoff. *J Virol* 56:250-257.
53. O'Shea, C., K. Klupsch, S. Choi, B. Bagus, C. Soria, J. Shen, F. McCormick, and D. Stokoe. 2005. Adenoviral proteins mimic nutrient/growth signals to activate the mTOR pathway for viral replication. *EMBO J* 24:1211-1221.
54. Kostura, M., and M. B. Mathews. 1989. Purification and activation of the double-stranded RNA-dependent eIF-2 kinase DAI. *Mol Cell Biol* 9:1576-1586.
55. Talloczy, Z., W. Jiang, H. W. Virgin, D. A. Leib, D. Scheuner, R. J. Kaufman, E.-L. Eskelinen, and B. Levine. 2002. Regulation of starvation- and virus-induced autophagy by the eIF2a kinase signaling pathway. *Proceedings of the National Academy of Sciences of the United States of America* 99:190-195.
56. Shackelford, D. B., D. S. Vasquez, J. Corbeil, S. Wu, M. Leblanc, C. L. Wu, D. R. Vera, and R. J. Shaw. 2009. mTOR and HIF-1alpha-mediated tumor metabolism in an LKB1 mouse model of Peutz-Jeghers syndrome. *Proc Natl Acad Sci U S A* 106:11137-11142.
57. Kimura, N., C. Tokunaga, S. Dalal, C. Richardson, K. Yoshino, K. Hara, B. E. Kemp, L. A. Witters, O. Mimura, and K. Yonezawa. 2003. A possible linkage between AMP-activated protein kinase (AMPK) and mammalian target of rapamycin (mTOR) signalling pathway. *Genes Cells* 8:65-79.

58. Hezel, A. F., and N. Bardeesy. 2008. LKB1; linking cell structure and tumor suppression. *Oncogene* 27:6908-6919.
59. Hemminki, A., D. Markie, I. Tomlinson, E. Avizienyte, S. Roth, A. Loukola, G. Bignell, W. Warren, M. Aminoff, P. Hoglund, H. Jarvinen, P. Kristo, K. Pelin, M. Ridanpaa, R. Salovaara, T. Toro, W. Bodmer, S. Olschwang, A. S. Olsen, M. R. Stratton, A. de la Chapelle, and L. A. Aaltonen. 1998. A serine/threonine kinase gene defective in Peutz-Jeghers syndrome. *Nature* 391:184-187.
60. Woods, A., S. R. Johnstone, K. Dickerson, F. C. Leiper, L. G. Fryer, D. Neumann, U. Schlattner, T. Wallimann, M. Carlson, and D. Carling. 2003. LKB1 is the upstream kinase in the AMP-activated protein kinase cascade. *Curr Biol* 13:2004-2008.
61. Lizcano, J. M., O. Goransson, R. Toth, M. Deak, N. A. Morrice, J. Boudeau, S. A. Hawley, L. Udd, T. P. Makela, D. G. Hardie, and D. R. Alessi. 2004. LKB1 is a master kinase that activates 13 kinases of the AMPK subfamily, including MARK/PAR-1. *EMBO J* 23:833-843.
62. Fay, J. R., V. Steele, and J. A. Crowell. 2009. Energy homeostasis and cancer prevention: the AMP-activated protein kinase. *Cancer Prev Res (Phila)* 2:301-309.
63. Carling, D. 2004. The AMP-activated protein kinase cascade - a unifying system for energy control. *Trends in Biochemical Sciences* 29:18-24.
64. Adams, J., Z. P. Chen, B. J. Van Denderen, C. J. Morton, M. W. Parker, L. A. Witters, D. Stapleton, and B. E. Kemp. 2004. Intracellular control of



- AMPK via the gamma1 subunit AMP allosteric regulatory site. *Protein Sci* 13:155-165.
65. Huang, J., and B. D. Manning. 2008. The TSC1-TSC2 complex: a molecular switchboard controlling cell growth. *Biochem J* 412:179-190.
  66. Inoki, K., T. Zhu, and K.-L. Guan. 2003. TSC2 Mediates Cellular Energy Response to Control Cell Growth and Survival. *Cell* 115:577-590.
  67. Martin, D. E., and M. N. Hall. 2005. The expanding TOR signaling network. *Curr Opin Cell Biol* 17:158-166.
  68. Memmott, R. M., and P. A. Dennis. 2009. Akt-dependent and -independent mechanisms of mTOR regulation in cancer. *Cell Signal* 21:656-664.
  69. Ganley, I. G., D. H. Lam, J. Wang, X. Ding, S. Chen, and X. Jiang. 2009. ULK1·ATG13·FIP200 Complex Mediates mTOR Signaling and Is Essential for Autophagy. *Journal of Biological Chemistry* 284:12297-12305.
  70. Harding, H. P., Y. Zhang, A. Bertolotti, H. Zeng, and D. Ron. 2000. Perk Is Essential for Translational Regulation and Cell Survival during the Unfolded Protein Response. *Molecular Cell* 5:897-904.
  71. Deng, J., H. P. Harding, B. Raught, A.-C. Gingras, J. J. Berlanga, D. Scheuner, R. J. Kaufman, D. Ron, and N. Sonenberg. 2002. Activation of GCN2 in UV-Irradiated Cells Inhibits Translation. *Current Biology* 12:1279-1286.
  72. Zhang, P. R., B. Olsen, D. Lei, L. Gill, S. Wek, S. Vattam, K. Wek, R. Kimball, S. Jefferson, L. Cavener, D. 2002. The GCN2 eIF2α Kinase is

- Required for Adaptation to Amino Acid Deprivation in Mice. *Mol Cell Biol* 22:6681-6688.
73. Lu, L., A.-P. Han, and J.-J. Chen. 2001. Translation Initiation Control by Heme-Regulated Eukaryotic Initiation Factor 2 $\alpha$  Kinase in Erythroid Cells under Cytoplasmic Stresses. *Mol. Cell. Biol.* 21:7971-7980.
74. Srivastava, S., Davies, M., Kaufman, R. 1995. Calcium Depletion from the Endoplasmic Reticulum Activates the Double-stranded RNA-dependent Protein Kinase (PKR) to Inhibit Protein Synthesis. *The Journal of Biological Chemistry* 270:16619-16624.
75. de Haro, C., R. Mendez, and J. Santoyo. 1996. The eIF-2 $\alpha$  kinases and the control of protein synthesis. *FASEB J.* 10:1378-1387.
76. Dever, T. E. 2002. Gene-Specific Regulation by General Translation Factors. *Cell* 108:545-556.
77. Pal, J. K., J. J. Chen, and I. M. London. 1991. Tissue distribution and immunoreactivity of heme-regulated eIF-2  $\alpha$  kinase determined by monoclonal antibodies. *Biochemistry* 30:2555-2562.
78. Katze, M., DeCorato, G., Safer, B., Galabru, J., Hovanessian, A. 1987. Adenovirus VAI RNA complexes with the 68 000 Mr protein kinase to regulate its autophosphorylation and activity. *EMBO J* 6:689-697.
79. Harding, H. P., Y. Zhang, H. Zeng, I. Novoa, P. D. Lu, M. Calfon, N. Sadri, C. Yun, B. Popko, R. Paules, D. F. Stojdl, J. C. Bell, T. Hettmann, J. M. Leiden, and D. Ron. 2003. An Integrated Stress Response Regulates

Amino Acid Metabolism and Resistance to Oxidative Stress. *Molecular Cell* 11:619-633.

80. Karpinski, B. A., G. D. Morle, J. Huggenvik, M. D. Uhler, and J. M. Leiden. 1992. Molecular cloning of human CREB-2: an ATF/CREB transcription factor that can negatively regulate transcription from the cAMP response element. *Proceedings of the National Academy of Sciences of the United States of America* 89:4820-4824.
81. Harding, H. P., Y. Zhang, and D. Ron. 1999. Protein translation and folding are coupled by an endoplasmic-reticulum-resident kinase. *Nature* 397:271-274.
82. Koumenis, C., C. Naczki, M. Koritzinsky, S. Rastani, A. Diehl, N. Sonenberg, A. Koromilas, and B. G. Wouters. 2002. Regulation of Protein Synthesis by Hypoxia via Activation of the Endoplasmic Reticulum Kinase PERK and Phosphorylation of the Translation Initiation Factor eIF2{alpha}. *Mol. Cell. Biol.* 22:7405-7416.
83. Ameri, K., C. E. Lewis, M. Raida, H. Sowter, T. Hai, and A. L. Harris. 2004. Anoxic induction of ATF-4 through HIF-1-independent pathways of protein stabilization in human cancer cells. *Blood* 103:1876-1882.
84. Yorimitsu, T., U. Nair, Z. Yang, and D. J. Klionsky. 2006. Endoplasmic reticulum stress triggers autophagy. *J Biol Chem* 281:30299-30304.
85. Ding, W. X., H. M. Ni, W. Gao, Y. F. Hou, M. A. Melan, X. Chen, D. B. Stolz, Z. M. Shao, and X. M. Yin. 2007. Differential effects of endoplasmic

- reticulum stress-induced autophagy on cell survival. *J Biol Chem* 282:4702-4710.
86. Juan, J. B., S. Javier, and H. César de. 1999. Characterization of a mammalian homolog of the GCN2 eukaryotic initiation factor 2alpha kinase. *European Journal of Biochemistry* 265:754-762.
  87. Guo, F., and D. R. Cavener. 2007. The GCN2 eIF2 $\pm$  Kinase Regulates Fatty-Acid Homeostasis in the Liver during Deprivation of an Essential Amino Acid. 5:103-114.
  88. Wek, S. A., S. Zhu, and R. C. Wek. 1995. The histidyl-tRNA synthetase-related sequence in the eIF-2 alpha protein kinase GCN2 interacts with tRNA and is required for activation in response to starvation for different amino acids. *Mol. Cell. Biol.* 15:4497-4506.
  89. Wek, R., Jackson, B., Hinnebusch, A. 1989. Juxtaposition of domains homologous to protein kinases and histidyl-tRNA synthetases in GCN2 protein suggests a mechanism for coupling GCN4 expression to amino acid availability. *Proc Natl Acad Sci U S A* 86:4579-4583.
  90. Zhu, S., Sobolev, A., Wek, R. 1996. Histidyl-tRNA Synthetase-related Sequences in GCN2 Protein Kinase Regulate in Vitro Phosphorylation of eIF-2. *Journal of Biological Chemistry* 271:24989-24994.
  91. Bischoff, J. R., D. H. Kirn, A. Williams, C. Heise, S. Horn, M. Muna, L. Ng, J. A. Nye, A. Sampson-Johannes, A. Fattaey, and F. McCormick. 1996. An Adenovirus Mutant That Replicates Selectively in p53- Deficient Human Tumor Cells. *Science* 274:373-376.

92. Halbert, D., Cutt, J., Shenk, T. 1985. Adenovirus Early Region 4 Encodes Functions Required for Efficient DNA Replication, Late Gene Expression, and Host Cell Shutoff. *Journal of Virology* 56:250-257.
93. Cascallo, M., A. Gros, N. Bayo, T. Serrano, G. Capella, and R. Alemany. 2006. Deletion of VAI and VAIL RNA Genes in the Design of Oncolytic Adenoviruses. *Human Gene Therapy* 17:929-940.
94. Levine, B., and V. Deretic. 2007. Unveiling the roles of autophagy in innate and adaptive immunity. *Nat Rev Immunol* 7:767-777.
95. Espert, L., P. Codogno, and M. Biard-Piechaczyk. 2007. Involvement of autophagy in viral infections: antiviral function and subversion by viruses. *Journal of Molecular Medicine* 85:811-823.
96. Mizushima, N., A. Yamamoto, M. Matsui, T. Yoshimori, and Y. Ohsumi. 2004. In Vivo Analysis of Autophagy in Response to Nutrient Starvation Using Transgenic Mice Expressing a Fluorescent Autophagosome Marker. *Mol. Biol. Cell* 15:1101-1111.
97. Toker, A., and A. C. Newton. 2000. Akt/protein kinase B is regulated by autophosphorylation at the hypothetical PDK-2 site. *J Biol Chem* 275:8271-8274.
98. Matsuda, F., J. Fujii, and S. Yoshida. 2009. Autophagy induced by 2-deoxy-D-glucose suppresses intracellular multiplication of *Legionella pneumophila* in A/J mouse macrophages. *Autophagy* 5:484-493.

99. Wick, A. N., D. R. Drury, H. I. Nakada, and J. B. Wolfe. 1957. Localization of the primary metabolic block produced by 2-deoxyglucose. *J Biol Chem* 224:963-969.
100. Mizushima, N., A. Yamamoto, M. Hatano, Y. Kobayashi, Y. Kabeya, K. Suzuki, T. Tokuhi, Y. Ohsumi, and T. Yoshimori. 2001. Dissection of Autophagosome Formation Using Apg5-Deficient Mouse Embryonic Stem Cells. *The Journal of Cell Biology* 152:657-668.
101. Ulasov, I. V., A. M. Sonabend, S. Nandi, A. Khramtsov, Y. Han, and M. S. Lesniak. 2009. Combination of adenoviral virotherapy and temozolomide chemotherapy eradicates malignant glioma through autophagic and apoptotic cell death in vivo. *Br J Cancer* 100:1154-1164.
102. Maria, R., H. Taija af, H. Tanja, N. Petri, H. Sampsa, I. N. Anni, T. Mikko, R. Ville, A. D. Reneé, C. Dung-Tsa, G. Kilian, S. Ulf-Håkan, G. Ricardo, K. Mika, K. Juha, K. Anna, P. Sari, A. Laura, and H. Akseli. 2009. Mre11 inhibition by oncolytic adenovirus associates with autophagy and underlies synergy with ionizing radiation. *International Journal of Cancer* 125:2441-2449.
103. Yamamoto, A., Tagawa, Y., Yoshimori, T., Moriyama, Y., Masaki, R., and Tashiro, Y. 1998. Bafilomycin A1 Prevents Maturation of Autophagic Vacuoles by Inhibiting Fusion between Autophagosomes and Lysosomes in Rat Hepatoma Cell Line, H-4-II-E Cells. *Cell Structure and Function* 23:33-42.

104. Debbas, M., and E. White. 1993. Wild-type p53 mediates apoptosis by E1A, which is inhibited by E1B. *Genes & Development* 7:546-554.
105. Rao, L., D. Modha, and E. White. 1997. The E1B 19K protein associates with lamins in vivo and its proper localization is required for inhibition of apoptosis. *Oncogene* 15:1587-1597.
106. Cathomen, T., and M. D. Weitzman. 2000. A functional complex of adenovirus proteins E1B-55kDa and E4orf6 is necessary to modulate the expression level of p53 but not its transcriptional activity. *J Virol* 74:11407-11412.
107. Lian, J., X.-H. Yan, J. Peng, and S.-W. Jiang. 2008. The mammalian target of rapamycin pathway and its role in molecular nutrition regulation. *Molecular Nutrition & Food Research* 52:393-399.
108. Carloni, S., Girelli, S., Scopa, C., Buonocore, G., Longini, M., Balduini, W. 2010. Activation of autophagy and Akt/CREB signaling play an equivalent role in the neuroprotective effect of rapamycin in neonatal hypoxia-ischemia. *Autophagy* 6:366-377.
109. Bhaskar, P. T., and N. Hay. 2007. The Two TORCs and Akt. *Developmental Cell* 12:487-502.
110. O'Reilly, K. E., F. Rojo, Q.-B. She, D. Solit, G. B. Mills, D. Smith, H. Lane, F. Hofmann, D. J. Hicklin, D. L. Ludwig, J. Baselga, and N. Rosen. 2006. mTOR Inhibition Induces Upstream Receptor Tyrosine Kinase Signaling and Activates Akt. *Cancer Research* 66:1500-1508.

111. Feigenblum, D., and R. J. Schneider. 1996. Cap-binding protein (eukaryotic initiation factor 4E) and 4E-inactivating protein BP-1 independently regulate cap-dependent translation. *Mol Cell Biol* 16:5450-5457.
112. Chen, P. H., D. A. Ornelles, and T. Shenk. 1993. The adenovirus L3 23-kilodalton proteinase cleaves the amino-terminal head domain from cytokeratin 18 and disrupts the cytokeratin network of HeLa cells. *J Virol* 67:3507-3514.
113. Doronin, K., K. Toth, M. Kuppuswamy, P. Ward, A. E. Tollefson, and W. S. Wold. 2000. Tumor-specific, replication-competent adenovirus vectors overexpressing the adenovirus death protein. *J Virol* 74:6147-6155.



## Vita

Erin White was born in Lawton, Oklahoma on June 20, 1984 to Janet Jordan and James Ronald White. At the age of 17, Erin became fascinated with Genetics after attending a Genetics Seminar at Lamar University in Beaumont, TX. After graduating from the top 11% of her class at Little Cypress-Mauriceville high School in May of 2002 she attended Texas Tech University where her mother was offered an Assistant Professor Position in Educational Psychology. There she graduated in three and a half years with a Bachelors of Biology and Minor in Chemistry, with a 3.3 GPA. During her the summer of her sophomore year, she spent a month doing undergraduate research at the Louisiana State University Health Sciences Center with Dr. Nathan Davis and Dr. Shari Meyers. While attending Tech she was accepted into the prestigious Texas Tech University/ Howard Hughes Medical Institute Undergraduate Research Scholars Program. There she worked with Dr. Maurizio Chiriva-Internati at the Texas Tech Health Sciences Center. Her work focused on vaccine strategies with Adeno-associated virus. She continued to work for Dr. Chiriva-Internati for after graduation until she enrolled in graduate school at the University of Texas Health Science Center Graduate School of Biomedical Sciences. She fulfilled 3 rotations with Dr. Jagannahada Sastry, Dr. Lu-Yu Hwang, and Dr. Juan Fueyo. She continued in Dr. Fueyo's laboratory with her project focusing on the budding adenovirus and autophagy studies in his laboratory.

Permanent Address:

1793 North Lapis Drive

Prescott, Arizona 86301